ESPOO 2007 VTT PUBLICATIONS 634

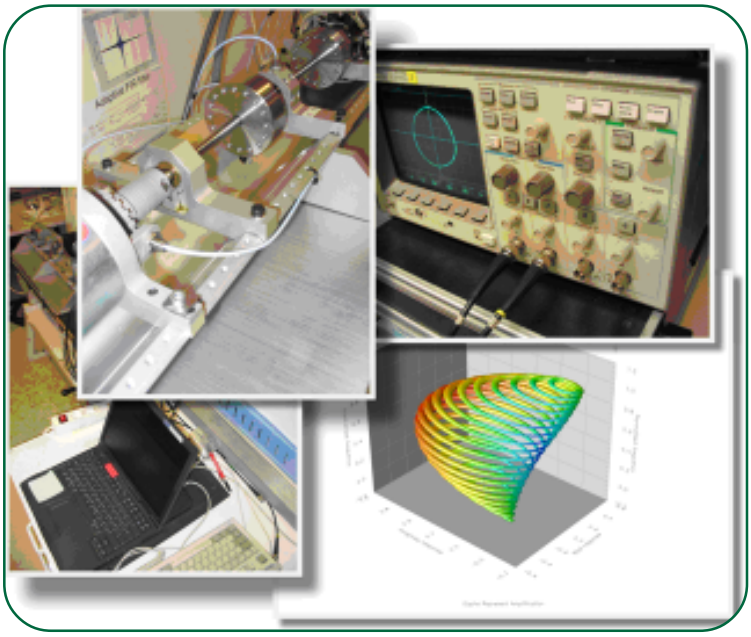

Kari Tammi

Active control of radial rotor vibrations

Identification, feedback, feedforward, and repetitive control methods

VTT PUBLICATIONS 634

Active control of radial rotor vibrations

Identification, feedback, feedforward, and repetitive control methods

Kari Tammi

Dissertation for the degree of Doctor of Science in Technology to be presented with due permission of the Department of Automation and Systems Technology, for public examination and debate in Auditorium AS1 at the Helsinki University of Technology (Espoo, Finland) on the 4th of May, 2007, at 12 noon.

ISBN 978-951-38-7007-2 (soft back ed.)
ISSN 1235-0621 (soft back ed.)

ISBN 978-951-38-7008-9 (URL: http://www.vtt.fi/publications/index.jsp)
ISSN 1455-0849 (URL: http://www.vtt.fi/publications/index.jsp)

JULKAISIJA – UTGIVARE – PUBLISHER

VTT, Vuorimiehentie 5, PL 2000, 02044 VTT
puh. vaihde 020 722 111, faksi 020 722 4374

VTT, Bergsmansvägen 5, PB 2000, 02044 VTT
tel. växel 020 722 111, fax 020 722 4374

VTT Technical Research Centre of Finland, Vuorimiehentie 5, P.O.Box 2000, FI–02044 VTT, Finland
phone internat. +358 20 722 111, fax + 358 20 722 4374

VTT, Otakaari 7 B, PL 1000, 02044 VTT
puh. vaihde 020 722 111, faksi 020 722 5888

VTT, Otsvängen 7 B, PB 1000, 02044 VTT
tel. växel 020 722 111, fax 020 722 5888

VTT Technical Research Centre of Finland, Otakaari 7 B, P.O. Box 1000, FI-02044 VTT, Finland
phone internat. +358 20 722 111, fax +358 20 722 5888

Technical editing Leena Ukskoski

Edita Prima Oy, Helsinki 2007

Tammi, Kari. Active control of radial rotor vibrations. Identification, feedback, feedforward, and repetitive control methods [Roottorin radiaalivärähtelyjen aktiivinen hallinta]. Espoo 2007. VTT Publications 634. 151 p. + app. 5 p.

Keywords dynamic rotor systems, radial vibrations, rotors, control methods, active control, vibrations, identification, feedback control, feedforward control, repetitive control

Abstract

Active vibration control methods for rotors were studied in order to develop solutions to enhance machines' dynamic behaviour, durability, and operating range. The aim of the thesis was to develop identification and control methods for active vibration control of a rotor. The identification method developed in the thesis improved run-time rotor identification by compensating rotation-related disturbances before the actual identification procedure. The control system design comprised an inner feedback loop and an outer loop for compensation for harmonic excitations due to mass unbalance and other rotation-related excitations. The feedback loop was shown to be essential in terms of providing favourable conditions for the other compensation algorithm in the outer loop. For the outer loop, three algorithms were tested: two feedforward control methods and a repetitive control method. The algorithms were validated and compared using an experimental set-up. Concerning the feedforward methods, the Convergent Control algorithm was found to be a more effective and simpler algorithm for the purpose than the adaptive FIR filter with the LMS algorithm. The adaptive gradient-based repetitive control, developed in this thesis, was found to have a poorer performance than the feedforward control methods, but to provide benefits for applications where excitation frequencies are not as predictable as in the current application.

Tammi, Kari. Active control of radial rotor vibrations. Identification, feedback, feedforward, and repetitive control methods [Roottorin radiaalivärähtelyjen aktiivinen hallinta]. Espoo 2007. VTT Publications 634. 151 s. + liitt. 5 s.

Avainsanat dynamic rotor systems, radial vibrations, rotors, control methods, active control, vibrations, identification, feedback control, feedforward control, repetitive control

Tiivistelmä

Aktiivisia roottoriväräht elyjen hallintamenetelmiä tutkittiin koneiden dynaamisen käyttäytymisen ja kestävyyden parantamiseksi sekä käyttöalueen laajentamiseksi. Väitöskirjan tavoite oli kehittää identifiointi- ja säätömenetelmiä roottorin aktiivisen värähtelynhallinnan tarkoituksiin. Kehitetty identifiointimenetelmä paransi roottorin käynninaikaista mallinnusta kompensoimalla pyörimisestä johtuvat häiriöt ennen varsinaista identifiointia. Kehitetty säätöjärjestelmä perustui sisempään takaisinkytkentäsilmukkaan ja ulompaan silmukkaan. Takaisinkytkentäsilmukalla osoitettiin olevan merkittävä rooli systeemin muokkaamisessa suotuisaksi ulomman silmukan säätöä silmällä pitäen. Ulommassa silmukassa testattiin kahta myötäkytkettyä säätömenetelmää ja yhtä oppivaa säätömenetelmää. Algoritmien toimivuutta vertailtiin koelaitteistolla. Myötäkytketyistä menetelmistä taajuustason algoritmi todettiin tehokkaammaksi ja yksinkertaisemmaksi kuin adaptiiviseen FIR-suotimeen perustuva LMS-algoritmi. Työssä kehitetty adaptiivinen oppiva algoritmi todettiin suorituskyvyltään huonommaksi kuin myötäkytketyt algoritmit. Toisaalta kyseisestä oppivasta algoritmista löydettiin etuja sovelluksiin, joissa herätetaajuudet eivät ole yhtä ennustettavia kuin tutkitussa tapauksessa.

Preface

I wish to thank my supervisor Professor Heikki Koivo and instructor Dr Kai Zenger for their excellent support. I am also grateful to Dr Jari Hätönen, Dr Erkki Lantto, Professor Steve Daley, and Dr Seppo Aatola for good advice and kind help during the thesis work.

To Mr Pekka Koskinen and Mr Ismo Vessonen I owe the interesting opportunity to work on the subject at VTT. I am also grateful to other colleagues in VTT who have contributed to the work, or just made our daily life pleasant. Particularly, I wish to mention Mr Antti Laiho, Mr Markku Järviluoma, Mr Antti Hynninen, Mr Juha Kortelainen, and Mr Kalle Vehviläinen. I also wish to thank the language consultant Mr Paavo Anttila for his kind advice.

Equally, I wish to thank my friends with whom we run, ski, bike, hike, climb, and have all kinds of fun. These activities give positive energy and "good vibrations" that are not to be attenuated as rotor vibrations are in this thesis.

I am greatly thankful to my parents Ritva and Martti and to my dear wife (Dr) Katja for their love, support and understanding. They always encourage and help me in my undertakings. I also wish to welcome our new family member Matilda.

This thesis has been examined by Professor Gregory D. Buckner and Dr Erkki Lantto. Professor André Preumont and Dr Erkki Lantto acted as the opponents. The author wishes to thank the examiners and the opponents for their contribution. The work was started within VTT's strategic research theme called *Intelligent Products and Systems* and completed in the project called *Active Control of Rotor Vibrations in Electrical Machines* funded by the Academy of Finland and VTT. The funding parties are gratefully acknowledged.

Raleigh, March 19, 2007

Kari Tammi

Contents

Nomenclature

ABBREVIATIONS

AMB	Active Magnetic Bearings
FEM	Finite Element Method
FIR	Finite Impulse Response filter or non-recursive filter
FRF	Frequency Response Function
IIR	Infinite Impulse Response filter or recursive filter
LMS	Least Mean Squares
MIMO	Multiple Input Multiple Output
PD	Proportional-Derivative
PDD	Proportional-Derivative-Derivative
rms	root-mean-square
rpm	revolutions per minute
rps	revolutions per second
SDOF	Single Degree of Freedom
SISO	Single Input Single Output

OPERATORS

∂	Partial derivative

$\overline{U}, \overline{A}$	Complex conjugate operator (of U, A, for example)
floor	Largest integer number, truncation downwards
Im	Imaginary part
Re	Real part
sup	Least upper bound

SYMBOLS

α	Convergence coefficient, learning gain
γ	Leakage coefficient (integrator leak) in adaptive update law
δ	Positive number to prevent division by zero in normalised law
ε	Eccentricity of rotor
θ	System parameter estimates
λ	Real and imaginary part of system pole, eigenvalue
μ	Convergence coefficient
ξ	Relative damping
Φ	Regression vector matrix
ϕ	Natural mode matrix, phase of filtered reference signal
$\varphi(n)$	Regression variable vector
ψ	Modal coordinate of a mechanical system
Ω	Eigenvalue matrix

ω	Angular frequency, or rotational speed (rad/s)
ω'	Normalised angular frequency, between [0, 2 π]
ω_{cr}	Critical speed in radians per second (rad/s)
A	System matrix
A_F	Fourier coefficients of system inverse
[a_{n-1}, ... , a_0]	Polynomial coefficients in pulse transfer function denominator
B	Input matrix
[b_m, ..., b_0]	Polynomial coefficients in pulse transfer function numerator
C, c	Damping matrix, output matrix, damping constant
$D(q)$	Annihilator polynomial
D_{AMB}	Diameter of active magnetic bearing
$D_F(n)$	Fourier coefficients of disturbance
$d(t)$, $d(n)$	Disturbance signal
E	Vector of error signals
$E_F(n)$	Fourier coefficients of error signal
E_{ind}	Phase error indicator
e	Neper number
$e(t)$, $e(n)$	Error signal, defined as $e(t) = y(t) + d(t)$
f	Frequency

f_{ac}	Active force
$G(q)$	Pulse transfer function of plant
$G_F(n)$	Fourier coefficients of plant
$G_m(q)$	Pulse transfer function of plant model
$H(n)$	Vector of FIR coefficients
$H(s)$	Continuous time transfer function
$H(q)$	Discrete time pulse transfer function
$H_{JR}(\mathrm{i}\omega)$	Frequency response of Jeffcott rotor in one direction
h_i	Coefficient of FIR filter
i	Imaginary unit
i	Phase shift in pulse queue
I	Unity matrix, FIR filter order
J	Cost function
K, k	Stiffness matrix, spring constant, index of Fourier coefficient
$K(q)$	Filter in repetitive control
K, K_D, K_P	General, derivative and proportional feedback gains
L_{AMB}	Length of active magnetic bearing
l_e	Delay filter length error
M, m	Mass matrix, mass, order of numerator in pulse transfer function

M	Order of truncated FIR filter in repetitive control
m_u	Mass unbalance in Jeffcott rotor
N	Integer number, delay order in repetitive control,
n	Index in pulse queue, order of denominator, integer number
p	Pole of system
P	Mass matrix decomposition matrix, such that $M = P^T P$
P	Order of *Q filter* in repetitive control
$P(q)$	Characteristic polynomial
$Q(q)$	Control signal filter in repetitive control (*i.e.* the *Q filter*)
q	Forward shift operator
$R(n)$	Vector of reference signal samples
$r(t)$, $r(n)$	Radial complex displacement of the rotor, reference signal
r_a	Amplitude of reference signal
r_u	Radius of mass unbalance in Jeffcott rotor
$S(f)$	Spectrum
s	Laplace variable
T	Time delay in repetitive control
T_S	Sampling time
t	Time

$U_F(n)$	Fourier coefficients of controller output
$u(t)$, $u(n)$	Controller output, plant input
v	Trial solution vector for eigenvalue problem
V_G	Quality grade for static mass unbalance
$W(n)$	Coefficients in unified adaptive law
X, x	Coordinate direction in horizontal plane, system state vector
Y, y	Coordinate direction in vertical plane, rotor displacement (Final)
Z	Coordinate parallel to rotor shaft

1. Introduction

1.1 Background

The term *active vibration control* generally refers to the attenuation of vibration or to shifting of the vibration to a different frequency band. However, in some applications an amplification of vibrations may be desired. In this work, active vibration control always refers to attenuation of vibrations.

Active vibration control of structures is usually divided into active and semi-active control (Preumont 2002). In active vibration control, a dynamic force is applied against the vibration to be attenuated. For example, a force-producing member in a structure may compensate vibrations by inducing forces in the structure. In semi-active vibration control, the characteristics of a structure are adjusted in such a way that the vibration response is optimised. For example, a component with controllable stiffness or damping may be used. A vibration control system usually consists of one or several actuators, sensors and control units. The sensors provide information about the vibration to be controlled. The control unit is used to realise an algorithm and the actuator is used to apply the control action. Today, one trend is integrating all these functions into the structure, constituting an embedded system. Another trend is to develop control systems that can even cope with unexpected operating conditions.

Generally, vibration control in rotating machines is linked to a *critical speed*, to an excitation at rotation harmonics or to rotordynamic instability. The dynamics of structures are characterised by natural modes. Structures have a tendency to vibrate at their natural frequencies when excited. A rotating object is subjected to excitation due to gravity, asymmetry, bearings *etc*. The strongest excitation components caused by rotation often occur at frequencies equal to the rotational speed and its sub-multiples and multiples. In this work, the term *critical speed* refers to the speed at which the rotational frequency is equal to a natural frequency of the rotor. As indicated by its name, the critical speed is an issue of great importance for a rotor system. This is because excitation at the natural frequency may cause an excessive response in the rotor. Theoretically, with zero damping, the response could increase infinitely. However, damping and non-linearity restrict the response in practice. Some rotor systems can be run at the

critical speed, while others cannot. Usually, heavy rotors (*e.g.* largest electrical machines, paper machine rolls) are operated below the critical speed, in sub-critical conditions. Lighter high-speed rotors can be run in super-critical conditions. However, there are exceptions; for example, heavy turbo-generators in power plants work are designed for super-critical operation. As mentioned above, excitation at rotation harmonics might also cause a problem. For example, the second multiple of rotational speed is know to excite the rotor at half the critical speed (Vance 1987). One possible cause for a strong excitation component at the second multiple is axial asymmetry in the stiffness of a loaded rotor. Rotordynamic instability is usually associated with the variation of some fluid dynamic pressure around the circumference of the rotor (Vance 1987). This variation can be caused by an interaction between the rotor and its bearings, for example.

The most common active vibration control solution used in rotating machines is achieved through the use of AMBs[1]. A rotor is levitated in an air gap by actively controlled magnetic forces. Levitating a rotor provides advantages such as low friction and almost maintenance-free operation. AMBs have been used in a variety of high-speed applications, from magnetically levitating trains to small electrical machines. AMBs have changed rotor applications remarkably by pushing up the maximum speeds of rotating machines. Today, the fastest industrial rotors operate at a speed of 6 kHz, and the speed is then limited by the rotor's material strength rather than by the resonance behaviour. (Schweitzer *et al.* 1994)

Active magnetic bearings have also made it possible to build "smart" rotor systems where active magnetic bearings have several other functions besides the basic supporting function. They may be used for identification of wear or faults, compensation of process deviations, optimisation of machine life, *etc*. (Schweitzer 2002, Hirschmanner *et al.* 2002, Nordmann & Aenis 2004). AMB solutions are rarer in low-speed applications or in applications where a rotor has to carry large loads or has strong interactions with its environment. For example, a pair of rolls in a nip contact needs to be supported by strong conventional bearings. However, active vibration control is making its debut also in heavy machine design.

[1] Active Magnetic Bearing

The main purpose of this work was to study how to control vibrations of a rotor supported by conventional bearings by using a supplementary non-contacting electromagnetic actuator. In particular, the work was focused on applications that were not potential AMB applications. This was prompted by the importance of heavy rotating machine manufacturers in Finnish industry. An electromagnetic actuator was chosen because the use of electronics is prevalent in contemporary actuators, sensors, and control systems. The test environment designed was simple and small in scale. This was found important because basic rotordynamic phenomena could be studied and control systems implemented quickly and safely in a laboratory environment. Implementing the design methods and control algorithms in a large-scale system will require more effort and further research.

The work was started in a project included in the "ÄLYMARA – Smart Materials and Structures" research programme. The work was then continued within the VTT research theme 'Intelligent Products and Systems'. A goal in both research programmes was to introduce intelligent features into conventional machine design. The completion of this work was carried out within the project called "Active Control of Rotor Vibrations in Electrical Machines (ACRVEM)" funded by the Academy of Finland. The ACRVEM project is aimed at intelligent control of internal radial forces in electrical machines. The results presented here are to be applied further in the project.

1.2 General literature review

An introductory literature review is given below. More specific references, related to the chapter's specific topics, are given in the forthcoming chapters.

1.2.1 Textbooks

Rotordynamics is discussed thoroughly, for example, in textbooks by Vance (1987), Childs (1993), Krämer (1993), Genta (1999, 2005), and Gasch *et al.* (2002). The analysis of mechanical dynamic systems can be found in Meirovitch (1997). The modal analysis, numerical and experimental, is dealt by Ewins (2000) and Heylen *et al.* (1999). The principles of active control of mechanical

vibrations can be found, for example, in Gawronski (1996), Fuller *et al.* (1996), or Preumont (2002).

The aspects of digital control are presented by Åström & Wittenmark (1990). This book provides important knowledge on the sampling of continuous-time systems and the related digital control. Optimal control is presented by Glad & Ljung (2000). This book discusses the optimality of several control methods. Textbooks on adaptive control have been written by Åström & Wittenmark (1995) and Ioannou & Sun (1996). Repetitive control, being a relatively new method, has not yet made its way to textbooks. Albertos & Sala (2002), however, present principles of iterative control and identification that are close to the methods of repetitive control.

Active vibration control with magnetic bearings has been studied widely by the control engineering community. AMBs are also related to the subject of the present work, since the actuator and the control unit were modified from an active magnetic bearing system. A general description of active magnetic bearings can be found in the textbook by Schweitzer *et al.* (1994); and their application, for example, in Lantto (1999).

1.2.2 Active vibration control of rotors

This section gives an overview of the industrial applications of active rotor vibration control and on similar test-benches for research. As already explained, active magnetic bearing applications were outside the scope. Test benches consisting of a rotor supported by conventional bearings and an active (or semi-active) vibration control system were of interest. Different actuating methods, actuator placements and scales were used in the test benches reported. Different control principles are also used; some systems used a reference signal to compensate the disturbances at the frequency of rotation, while others do not.

One example of an industrial application is the active control of barring in a paper calender. It was first tested in a smaller-scale test calender (Fehren *et al.* 2000), and later applied to full-scale paper machinery (Siebald *et al.* 2005). The compensator used was an adaptive feedforward controller that decreased the relative movement between the calender rolls and thus reduced deformation in

the roll surfaces. In terms of paper-making process quality, the objective was to regulate the nip pressure variations and thus improve the paper quality and extend the life-time of the roll surface material.

Rotor vibrations were controlled with a magnetic actuator by Cheung *et al.* (1994) at the University of Bath. In a test set-up, the rotor was supported by journal bearings and the control force was applied with a magnetic actuator located at a point within the bearing span. The sliding-mode control method was applied to minimise vibrations due to mass unbalance. The study also included comparative tests between a fixed-gain PD[2] control and the sliding mode method. The performance of both methods was tested on a test bench with a 2 358-mm-long rotor, 100 mm in diameter. Overhanging disks were attached to the ends of the rotor. The results indicated that the sliding-mode control had better performance than the fixed-gain PD controller (not necessarily an optimally tuned controller). Both control methods gave large reductions in the response around the critical speed.

An electromagnetic actuator located between the load-carrying bearings was also used by Ishimatsu *et al.* (1991) at the Nagasaki University. The approach was to use an analogue PDD[3] controller to control the transients and a digital controller to control the synchronous whirl motion. The two control systems worked in parallel in a similar manner to those that will be presented in this thesis: one system for wideband damping and another for mass unbalance compensation. Two different strategies were tested in the digital controller: a heuristic approach and a neural network approach. The heuristic approach was termed the Gain-Phase Modification Method. The method used a reference signal derived from speed measurements and generated a compensation signal by using the displacement error in the output signal. In the neural network approach, the model of the damper was replaced with a learning neural network. The test set-up consisted of a 460-mm-long rotor, 6 mm in diameter. The use of the unbalance compensation system provided large reductions in synchronous rotor responses.

---

[2] Proportional-Derivative.
[3] Proportional-Derivative-Derivative.

A multivariable adaptive self-tuning controller was used to control forced vibrations in a rotor by Sun L. *et al.* (1998) at the University of Melbourne. The researchers used an active hydrodynamic bearing as a third bearing to add damping to the system. The self-tuning regulator was implemented to control oil-film thickness in the third bearing located between the load-carrying ball bearings. The system was designed to cope with non-linear fluid-film bearing characteristics, parameter variations and parameter uncertainty. The simulations indicated that the self-tuning regulator was suitable for forced vibration compensation. The inclusion of a reference signal in the cost function improved the results.

Sliding-mode control and magnetic actuators were also used to damp vibrations in circular saws (Sun J.C. *et al.* 2000). The objective was to reduce vibrations in the saw blade, *i.e.* the vibrations in the axial direction of a rotor. The tests showed a significant reduction in the cut width. The system was realised in a sawmill and is working in a production line. The study is slightly off focus for the present work, being concerned with axial rather than radial vibrations.

Rotor vibrations have been compensated with feedforward control using the *Convergent Control* method (Järviluoma & Valkonen 2001, 2002). The study was conducted by VTT and the Helsinki University of Technology. The reference signal used for control was derived from the rotational speed measurement. The test bench consisted of a large and heavy rotor (diameter 320 mm, length 4 000 mm, weight 800 kg) supported by roller bearings at the ends. The actuating forces, generated by hydraulic cylinders, were applied to the rotor through a third roller bearing located within the bearing span, close to one end of the rotor. The control objective was to minimise the response at the centre of the rotor. The response at the frequency of rotation and its second multiple were successfully attenuated.

The studies presented above used a third point in the rotor for controlling the vibrations. Another approach is to integrate an actuator with a load-carrying bearing. This was done by Ehmann *et al.* (2003) at the Technical University of Darmstadt. A piezo-actuator was integrated inside one of two roller bearings in a rotor. Two disks were attached to the shaft. Two different controllers were considered: an integral-force-feedback controller and a robust controller designed with μ-synthesis (Ehmann *et al.* 2003). The use of active control

significantly reduced the response of the rotor. Przybyłowicz (2004) presented another study of an integrated bearing-piezo-actuator device. The piezo actuators acted on the body of a journal bearing. The advantage of these integrated bearing-actuator devices is their compact construction: no significant extra space is required. The challenges lie in achieving a sufficient force, if the rotor is heavy, and also in achieving good controllability if the bearings are located close to nodal points.

Finally, as an example of semi-active control, a magneto-rheological (MR) fluid damper was introduced into a rotor system in (Wang & Meng 2002) of Shanghai Jiao Tong University. A rotor, 500 mm in length, 9.5 mm in diameter, was supported by two bearings, one of them integrated with the magneto-rheological damper. An overhanging disk was attached to the non-drive end of the rotor. The damper was controlled by changing the electrical current through the damper manually. The experiments showed that the damper had an effect on the stability of the rotor. In this author's view, this was due to the follower forces exerted on the rotor by the damper. Forte *et al.* (2004) used MR fluids to design a squeezed film damper to control rotor vibrations. The experiments, with a test rig similar to that used in this author's work, were carried out to show the benefits of adjustable damping control when exceeding the critical speed. A third MR damping device, also integrated with the bearing, was explored by Zhu *et al.* (2002). The researchers demonstrated how the unbalance response of an overhanging rotor can be controlled by the MR device.

1.3 Goal & scope

The goal of this work was to shed light on the design and application of active vibration control systems for rotors. The aim was to cover the complete design path from understanding the dynamics of rotor systems to their identification, controller synthesis, and finally the implementation of controllers. At the start of the work, there were general research questions such as:

- What can be achieved with active control?
- What are the boundary conditions and restrictions?
- How should a control system be realised and algorithms implemented?

The main focus of the thesis was on mass unbalance compensation algorithms. Feedforward and repetitive control methods were developed and validated for this purpose. To cover the complete design path, identification methods, suitable feedback control, and implementation issues were also studied. The research questions became more focused:

- What has to be known about the controlled rotor system and what is the accuracy required?
- What algorithms should be used? What directs the choice between the three algorithms examined?
- What are the benefits (mainly in terms of performance, but also reliability) of the different algorithms?
- What are the requirements for the control system (with regard to the computational power, the bandwidth, and the force required)?

Technically, the aim of this work was to construct a test environment for the active vibration control of rotors, to identify it, and to design and test active vibration control systems. The systems would have to reduce the displacement response in the rotor and extend the operating range of the test system beyond its critical speed. Adaptation to rotor speed changes was a central property required of the control system to be designed.

The test environment was envisaged as a rotor supported by conventional bearings, with control forces generated by a non-contacting auxiliary actuator. This work was designed to be a step towards the final goal of developing a generic intelligent control system for heavy rotating machines. Therefore, the plan was to study the applicability of the test environment, to relate the results to practice, and to point the way for further research.

The work was focused on the vibrations in the rotor. The objective was to minimise the displacement in the radial direction in the neighbourhood of the displacement transducers. The actuator was able to produce forces in the radial direction only.

As explained, the concept studied was different from active magnetic bearings; a support function was unwanted as the rotor was supported by its bearings. The

generation of low-frequency (near DC) forces was avoided in the controller design to prevent the actuator from bending the rotor and to study what can be achieved with the small (or practical) actuation forces. Also, in the current test environment, the actuator would have been able to virtually eliminate the critical speed if pushing it up to higher frequencies by using an aggressive proportional position control. Pushing the critical speed up to high frequencies would have meant an unfruitful set-up for any research: a rotor without restrictions due to its critical speed.

1.4 Organisation of the thesis

This thesis first presents the rotor vibration control problem and the general principles involved in attenuating the vibrations. Secondly, identification, feedback and feedforward control systems are presented and validated using the test environment in Chapters 3 and 4. Thirdly, a newer method called repetitive control is presented in Chapter 5 as a challenger to the methods previously studied. Finally, a comparison of the methods is presented.

In Chapter 2, the dynamic models of rotor systems are presented, beginning with the Jeffcott rotor and ending in a more general formulation. The characteristics of rotor systems and the nature of excitations are discussed. The chapter also contains a motivating discussion of the benefits of active vibration control of rotors.

The identification method and the feedback and feedforward control methods, to be validated in the following chapter, are presented in Chapter 3. The principle of the identification method, applicable to rotating systems, is presented first. The use of a relatively simple feedback method to tune the plant characteristics suitable for feedforward systems is then presented. Finally, two feedforward methods for compensating periodic signals are presented.

Chapter 4 comprises the validation of the methods presented. The test environment used and two different utilised layouts are presented and the results of the validating tests are shown. The results comprise the rotor responses with and without the controllers. The choices for algorithm parameters in terms of practical implementation are also discussed. This chapter forms a benchmark for the repetitive control concept introduced in the next chapter.

Chapter 5 presents the repetitive control method, and the gradient-based repetitive control law is developed further for variable speed rotor vibration control. The chapter contains validating experiments in the test environment. The theory and the experimental work concerning the repetitive control are reported in the same chapter because of the novelty and the differences of the method with respect the other method.

Chapter 6 is a summarising chapter pointing out the similarities and differences of the algorithms, together with a comparison of the algorithms. Performance and implementation issues of all the algorithms in question are discussed. Lastly, the results achieved are discussed in Chapter 7.

Appendix A presents quality grades for rotor balancing. Appendix B describes shortly positive real systems and Appendix C present the system models and filters used in the experimental part of this thesis.

1.5 Scientific contribution

This work provides new information about the identification of rotor systems and active control systems for rotor vibration control. The work covers the full path from identification to controller synthesis and validation. The following points are original contributions of this work:

- A new identification procedure for run-time rotor identification was formulated such that load disturbances were taken into account. This was done by using a model augmentation technique and a reference signal. (Tammi 2005).

- The different roles of the feedback and feedforward controllers were pointed out (Tammi 2003a, Tammi 2003b). The work led to the design of some tools applicable to the construction of the new algorithms. (Tammi 2005).

- The derivation of the discrete-time feedback equivalent for the frequency-domain feedforward algorithm with an instantaneous coefficient update (called *Convergent Control* or *Higher Harmonic Control*) was presented

(Hätönen *et al.* 2006, Daley *et al.* 2006). The author participated in the derivation and carried out the implementation of the algorithm and its validation on the rotor test environment.

- The repetitive control algorithm was extended so as to be applicable to variable speed rotors. A novel algorithm consisted of a filter with adaptive delay time and two combined filters manipulating the control signal. The algorithm was implemented and validated in the rotor test environment and its stability analysis was presented. Differences of repetitive control with respect to the other two algorithms studied were also pointed out. (Tammi *et al.* 2006a, 2006b). The author's contribution was the modification of the basic algorithm for a variable speed rotor together with its implementation and validation in the test environment. The author also carried out the stability analysis for the new algorithm presented in Chapter 5.

- As an important contribution to connecting the theoretical and experimental domains, all the algorithms presented have been validated by experiments. The experimental work with the desktop test environment confirmed the effectiveness of the algorithms, facilitated their comparison, and helped in gaining knowledge about their implementation issues. All the algorithm implementations and the experimental work were carried out by the author.

2. Dynamic rotor systems

This chapter presents the rotor models, starting with the Jeffcott rotor and ending with more complex rotor system models. At the end of the chapter, the importance of the current research topic is argued in the light of two motivating examples.

2.1 Jeffcott rotor

According to a historical overview by Nelson (2002), experts discussed the significance of the critical speed and the possibility of super-critical operation at the end of the 19th century. Some studies indicated that the rotor response would increase without limit beyond a certain speed. Other studies predicted that a resonance-like phenomenon would occur at a certain speed. This speed was called the critical speed by Dunkerey. Some studies indicated that the critical speed was the maximum achievable speed of a rotor until Foppl's analysis and Kerr's experiments showed that the critical speed can be exceeded. (Nelson 2002).

Jeffcott (1919) published a paper confirming Foppl's theory and the simplest rotor model got the name the *Jeffcott rotor*. The rotor consists of a flexible shaft, with zero mass, supported at its ends (Figure 1). The supports are rigid and allow rotation around the centre axis of the shaft. The mass is concentrated in a disk, fixed at the midpoint of the shaft. The rotor system is geometrically symmetric with respect to its rotational axis, except for a mass unbalance attached to the disk. When rotating, the mass unbalance provides excitation to the system. Hence, the excitation is sinusoidal, occurring only at the speed of rotation.

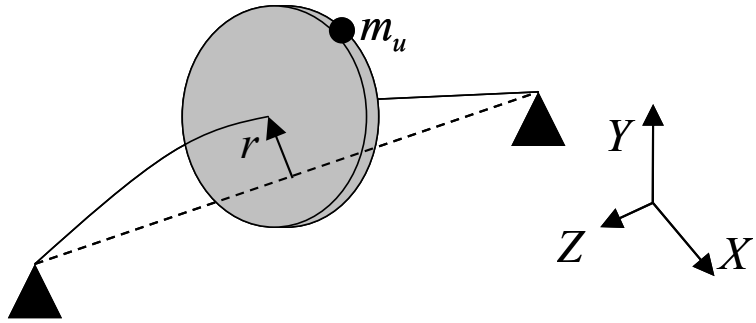

Figure 1. The Jeffcott rotor consists of a shaft, a disk, and a mass unbalance. The coordinate directions shown are used in this work.

A complex variable can be adopted to describe the displacement of the disk centre in the Jeffcott rotor. The displacement in the Cartesian coordinate system is then

$$\begin{aligned} y_X &= \mathrm{Re}(r) \\ y_Y &= \mathrm{Im}(r) \end{aligned} \tag{1}$$

where r is the complex radial displacement of the disk in the XY plane. The equation of motion at a constant speed of rotation is described by

$$m\ddot{r} + c\dot{r} + kr = m_u r_u \omega^2 e^{\mathrm{i}\omega t} \tag{2}$$

where m is the mass of the disk, c is the damping constant representing an external source of damping, k is the spring constant, equivalent to the stiffness of the shaft. $\ddot{r}$ and $\dot{r}$ are the second and first time derivatives of radial position. On the right-hand side, m_u is equal to the unbalancing mass, r_u is the distance of the unbalance from the geometrical centre of the rotor, ω is the rotational speed, i is the imaginary unit, and t is the time variable. The real part and the imaginary part of r can be understood as perpendicular coordinate values of the position of the disk. The excitation is a sinusoidal, rotating, force at the angular frequency ω.

The critical speed is equal to the undamped natural frequency of the Jeffcott rotor[4]. The undamped critical speed in radians per second and relative damping can be expressed as

$$\omega_{cr} = \sqrt{\frac{k}{m}}, \quad \xi = \frac{c}{2\sqrt{km}} \tag{3}$$

The mass unbalance can alternatively be accounted for as the eccentricity, which describes the relative distance between the centre of gravity and the geometrical centre of rotation

[4] In the literature, the critical speed may be defined as the undamped or damped natural frequency. Sometimes it is defined as the speed at which the maximum response occurs.

$$\varepsilon = \frac{m_u r_u}{m} \tag{4}$$

With these definitions, Equation (2) can be written

$$\ddot{r} + 2\xi\omega_{cr}\dot{r} + \omega_{cr}^2 r = \varepsilon\omega^2 e^{\mathrm{i}\omega t} \tag{5}$$

The Jeffcott rotor is originally modelled as two separate one-degree-of-freedom oscillator systems. Both oscillators have equal mass, damping and spring constants. The system still has its place as an analysis tool and a simple model of rotor systems. This thesis uses the Jeffcott rotor to justify the use of active control and to study what can be achieved control and what requirements are imposed by an active vibration control system.

The unbalance response of an oscillator can be expressed as a function of the frequency of rotation

$$H_{JR}(\mathrm{i}\omega) = \frac{\varepsilon\omega^2}{\omega_{cr}^2 - \omega^2 + \mathrm{i}2\xi\omega_{cr}\omega} \tag{6}$$

The excitation and the response are equal to zero at zero frequency; in the resonance region the magnitude of the response is defined by the relative damping. At frequencies above resonance, the displacement response approaches a constant value defined by the eccentricity

$$H_{JR}(\mathrm{i}\omega) \xrightarrow[\omega\to\infty]{} = -\varepsilon \tag{7}$$

Figure 2 shows the response as a function of frequency, scaled to the critical speed, with different values of relative damping. The analysis also shows that the response is in phase with the excitation at zero frequency. At resonance, the phase lag of the response is 90° with respect to the excitation. At high speeds, *i.e.* speeds significantly higher than the critical speed, the phase lag is 180°. In other words, the Jeffcott rotor rotates around its centre of gravity at high frequencies; the transition from rotational movement around the geometrical centre to rotational movement around the centre of gravity is called *critical speed inversion* (Vance 1987).

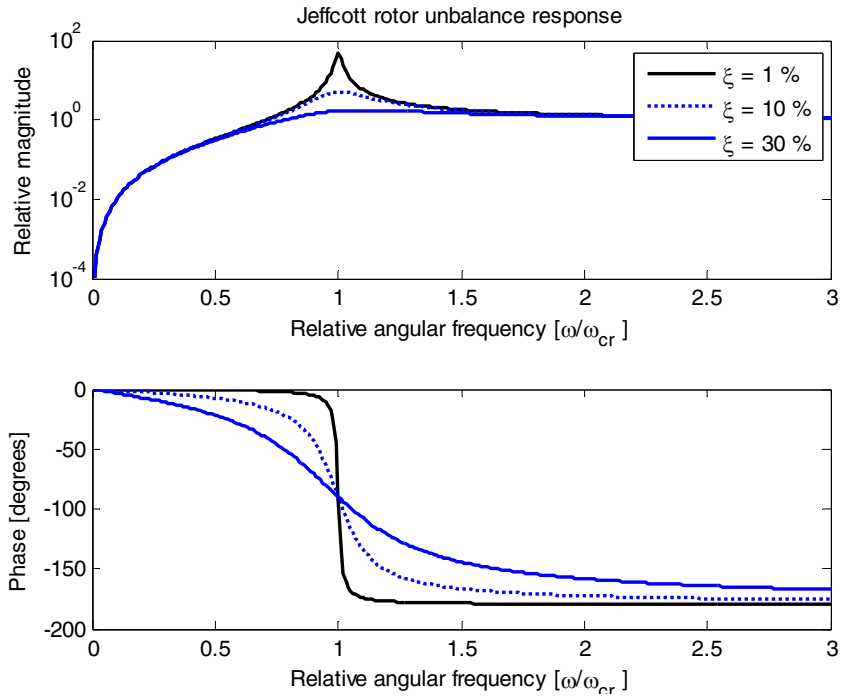

Figure 2. The response of a one-degree-of-freedom oscillator with excitation proportional to the square of the rotational speed plotted for a relative damping of 1 %, 10 %, and 30 %.

2.2 General mechanical models

The Jeffcott rotor does not take into account more complicated mechanics, flexible bearings, nor speed dependency due to gyroscopic effects. Therefore, more complicated modelling methods have been developed. This section presents some basic concepts in dynamic mechanical models and presents an overview of rotor modelling and typical excitations. Also, a brief introduction to natural modes and natural frequencies is shown, because this thesis later refers to those concepts and experimental modal analysis. In case of further interest in mechanical models, see the textbooks of Meirovitch (1997) and Genta (2005), for instance.

Assume a mechanical system, described by differential equations motion

$$M\ddot{y} + C\dot{y} + Ky = u \tag{8}$$

where M, C and K are respectively mass, damping, and stiffness matrices; y is now a real-valued displacement vector. The matrices are square, with the dimensions equal to the number of degrees-of-freedom. M and K are real symmetric matrices, and moreover, M is positive definite. The equation of motion may be obtained, for instance, by combining a set of lumped-parameter equations, or by modelling a structure using FEM[5], which is the standard way to model mechanical systems.

The mechanical systems are usually characterised by natural modes and natural frequencies. They are obtained by solving a free vibration problem. Damping is often disregarded to make the forthcoming eigenvalue problem simpler. Assuming $C = 0$ and $u = 0$ the equation of motion becomes

$$M\ddot{y} + Ky = 0 \tag{9}$$

Remark 1

The approximation C = 0 is relatively accurate for ordinary mechanical systems that have low damping. For gyroscopic systems, rotor systems with fluid film bearings, etc. this assumption is less accurate (Genta 2005). However, it is common practise to characterise dynamic mechanical systems in this way.

The equation may be solved using a trial

$$y(t) = e^{\omega t}v \tag{10}$$

where ω is a scalar and v is a vector length equal to the number of degrees of freedom. The natural modes and the natural frequencies of the system appear as non-trivial solutions of

$$(K - \lambda M)v = 0,\ \lambda = -\omega^2 \tag{11}$$

[5] Finite Element Method

Because M is positive definite and a symmetric matrix with real elements, it can be decomposed into two matrices

$$M = P^T P \tag{12}$$

where P a real non-singular matrix (Meirovitch 1997). The decomposition is always possible if M is positive definite. A coordinate transformation is performed using matrix P

$$v = P^{-1}\psi \tag{13}$$

where ψ is a vector and where P^{-1} exists, because P is non-singular. Manipulation of the first eigenvalue problem leads to another eigenvalue problem

$$\begin{aligned} (K - \lambda P^T P)P^{-1}\psi &= 0 \\ (P^{-1})^T K P^{-1}\psi - \lambda (P^{-1})^T P^T P P^{-1}\psi &= 0 \\ (P^{-1})^T K P^{-1}\psi - \lambda\psi &= 0 \end{aligned} \tag{14}$$

where $(P^{-1})^T K P^{-1}\psi - \lambda\psi = 0$ is the equivalent eigenvalue problem to the problem $Kv - \lambda Mv = 0$ (Meirovitch 1997). The solutions for the eigenvalue problems described can be written in a compact form

$$K\phi = M\phi\Omega \tag{15}$$

where ϕ is the orthogonal eigenvector (natural mode) matrix and Ω contains the eigenvalues (squares of natural frequencies) in its diagonal. The eigenvectors and modes are real valued for a symmetric M and K (Meirovitch 1997). The symmetry is a common feature for ordinary mechanical systems. Here, the ordinary mechanical systems do not contain significant interactions with rotating components, fluids, electro-mechanical systems, *etc.* From the orthogonality relations, it follows

$$\begin{aligned} \phi^T M \phi &= I \\ \phi^T K \phi &= \Omega \end{aligned} \tag{16}$$

Finally, the equation of motion in (8) becomes

$$\begin{aligned} \phi^T M\phi\ddot{\psi} + \phi^T C\phi\dot{\psi} + \phi^T K\phi\psi &= \phi^T u \\ I\ddot{\psi} + \phi^T C\phi\dot{\psi} + \Omega\psi &= \phi^T u \end{aligned} \tag{17}$$

If the damping matrix C is presented as a linear combination of M and K, the equations are completely decoupled by the transformation $y = \phi\psi$ between the modal coordinates and the physical coordinates. This is a common way to approximate damping when modelling mechanical systems. However, for rotor systems the matrices are not generally symmetric. The effects of rotation (gyroscopic and Coriolis forces), non-symmetric bearings, and interactions with the environment make the rotor model asymmetric (Vance 1987, Genta 2005, Hynninen 2002). Later in this work, matrices ϕ and Ω will be determined experimentally to characterise the dynamics of the test environment used.

The present work deals with Equation (8) without assuming symmetry in the matrices. In the experimental work, the rotor system is identified at different speeds of rotation. The results show that the set-ups used in the work are somewhat speed dependent, but not drastically so. The equation of motion can be expressed in the state-space form

$$\begin{aligned} \dot{x}(t) &= \begin{bmatrix} 0 & I \\ -M^{-1}K & -M^{-1}C \end{bmatrix} x(t) + \begin{bmatrix} 0 \\ -M^{-1} \end{bmatrix} u(t) \\ y(t) &= \begin{bmatrix} I & 0 \end{bmatrix} x(t) \end{aligned} \tag{18}$$

where x contains the states of the system, the first half of the vector representing displacements of each degree of freedom and the second half representing velocities of these degrees of freedom. As noted before, matrix M is positive definite and thus invertible. Mechanical systems are typically modelled with FEM and thus have a large number of degrees of freedom. For control synthesis point of view, such models are impractically large and require the use of a model reduction technique. For instance, Tammi *et al.* (2004) showed a modular compression procedure for mechanical systems based on the method by Craig & Bampton (1968). The advantage of this method is the modular approach and the possibility to model the rotor as a separate component exhibiting the phenomena due to rotation (Klinge 2002).

The Jeffcott rotor model assumed that mass unbalance is a significant source of excitation. This is also the case with more general rotor systems. In addition, excitations are generated at harmonic frequencies. For instance, misalignment of bearings, or non-isotropic stiffness distribution with a loading force, generates an excitation at twice the rotation frequency (Vance 1987). The phenomenon can be understood by considering modulation of signals; any interaction force between the rotor and its surroundings is modulated by the frequency of rotation. If the interaction forces do not rotate together at the same frequency with the rotor, the modulated force is spread over harmonic frequencies.

2.3 Motivating examples

The motivation for the work came from the tightening requirements on performance and durability. Improved control of the resonance behaviour in the critical speed region can help in meeting the requirements. An active control method for reducing rotor responses provides a possibility to increase the machine speed (capacity) and still meet the specifications. On the other hand, active control may also allow a lighter design or cheaper components. Mechanical systems have an inherently low damping, often 0.1 % to 5 %. This implies that means to increase the damping, or to compensate an excitation, may reduce responses significantly in the resonance region. For the same reason, the forces required remain in an achievable region, even for heavy rotors.

2.3.1 Active control of Jeffcott rotor

The Jeffcott rotor model is further analysed in order to clarify what can be achieved with active control. If controlled actively, Equation (5) becomes

$$\ddot{r} + 2\xi\omega_{cr}\dot{r} + \omega_{cr}^2 r = \varepsilon\omega^2 e^{\mathrm{i}\omega t} + \frac{u_{ac}(t)}{m} \tag{19}$$

where $u_{ac}(t)$ is the complex valued active force determined by a control algorithm. The optimal way to control the vibrations would be to cancel the excitation completely in such a way that

$$u_{ac}(t) = -m\varepsilon\omega^2 e^{i\omega t} \tag{20}$$

In practice, this active control force is difficult to realise on the basis of Equation (20), because the unbalance and its position are typically unknown. This is the reason to study different adaptive compensation algorithms as it is done in this thesis.

The following example shows that active control reduces the response or allows a larger unbalance in the rotor compared with the situation without active control. The standards (*e.g.* ISO 1940) give quality grades for balancing a rotor. The typical quality grades can be found in Appendix A. The grades, also referred to as *G-values*, define a measure of static unbalance as

$$V_G = \varepsilon_{max}\omega_{max} \tag{21}$$

where ω_{max} is the maximum allowable angular velocity and ε_{max} is the maximum eccentricity.

As an example, let us consider the Jeffcott rotor as a component in a machine. The disk has a weight of 1 000 kg and rotates at a maximum of 3 000 rpm. The maximum eccentricity of the rotor is limited because the response due to mass unbalance is limited to a certain level for functional reasons in the machine. The disk has to be manufactured to a quality grade of 6.3 mm/s in order to meet the requirement. Let us then assume that an active dynamic force can be applied to the disk. The sinusoidal force can be controlled in the radial direction and it has an amplitude of 1 500 N. This force is controlled in such a way that the net force acting on the disk is minimised. In this case, the compensation of the excitation reduces the response of the rotor as if it were balanced to a quality grade of 1.5 mm/s. On the other hand, the manufacturing tolerances of an actively controlled rotor can be relaxed. The use of active control allows balancing to a quality grade of 11 mm/s while maintaining a response corresponding to a quality grade of 6.3 mm/s in a passive system. The relaxation in the quality grade can mean a significant reduction in rotor manufacturing cost.

The example assumed a sinusoidal radial force with an amplitude of 1 500 N. In the case of active magnetic bearings with traditional silicon steel laminates, the

maximum force can approximately be derived from the bearing dimensions (Lantto 1999)

$$u_{max} = L_{AMB} D_{AMB} \cdot 20 \frac{\mathrm{N}}{\mathrm{cm}^2} \tag{22}$$

where L_{AMB} is the length of the magnetic bearing and D_{AMB} is the diameter of the rotor at the bearing. This indicates that the required dimensions are realistic for a 1 000 kg rotor; the force can be realised with the bearing dimensions L_{AMB} = 75 mm and D_{AMB} = 100 mm.

As a conclusion, larger unbalance values can be allowed in a rotor if active control is used. Active control may be used to achieve lower production costs, to improve the working process, to increase the operating range, or to extend the service life of the machine. However, supplementary components are always required for active vibration control. These components cause additional cost, require design and need maintenance. Hence, the use of active control is a trade-off between the benefits and the required extra effort.

2.3.2 Benefits in design and in product line

This section briefly explains the motivation for the work. The explanation presented is the author's view on the design of industrial rotors, with arguments for implementing active control systems in industrial applications.

Today's variable-speed rotors with conventional journal or rolling element bearings are often designed to work in the sub-critical range. Their maximum speed of operation may be limited to less than one third or one half of the critical speed. This is common for variable-speed rotors found in industrial machinery. The reason for limiting the speed is the avoidance of an excessive dynamic response that can reduce the process quality, shorten the life of machine components, or cause disturbances in the environment of the machine. A relatively simple specification is to restrict the speed of operation such that rotation harmonics do not coincide with the bending resonance. Restricting the speed of rotation is an effective way to avoid resonant responses, because the mass unbalance excitations are proportional to the rotation speed squared. This

design philosophy leads to relatively heavy structures but robust machines with a restricted operating range.

Constant-speed rotors with conventional bearings can be designed to be super-critical in order to achieve a higher speed and thus a higher power. The critical speed is usually crossed rapidly, but continuous operation at the critical speed is not allowed. This is the case with turbo machinery, large power generators and high speed pumps, for instance. Such a design leads to a higher power density with respect to machine mass than for sub-critical machines, but also to a restricted operating range.

The choice between a variable-speed and a constant-speed machine and the choice between lower and higher power output face the designer with trade-offs. Today, the trade-off problem is often solved by offering different products for each purpose: heavy sub-critical products with a wider operating range, and lighter super-critical machines with a restricted operating range. Figure 3 presents a classification of rotating machines: the restrictions lead the design to flexible variable-speed machines with a lower power output, or constant speed machines with a higher power output. For heavy industrial machines, a tailored product must be designed for each purpose.

The AMB technology has offered one solution for this problem. The technology is rapidly gaining ground in high-speed pumps and compressors. The active vibration control concept studied in this thesis aims to offer a similar solution for heavy industrial rotors on conventional bearings where AMBs are not necessarily applicable. The concept is believed to offer a solution for the problems explained. It is designed to be an add-on device that may be applied to virtually any rotating machine. The benefits of application are found in performance (see the Jeffcott rotor example), process quality, life-cycle of components, but also in a wider product line based on the same basic product.

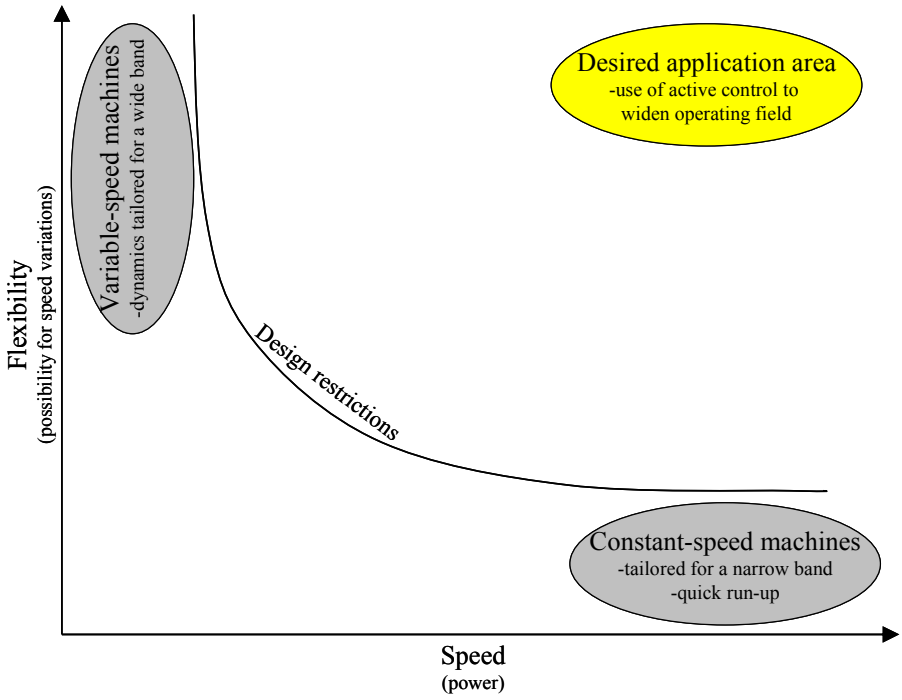

Figure 3. Active vibration control solutions are designed to help in covering new operating areas.

3. Identification, feedback and feedforward methods

The theoretical framework of the identification, feedback and feedforward methods used are presented in this chapter. These methods have been applied in a test environment and results are presented in Chapter 4. The results are to be compared with the results achieved with repetitive control.

An identification procedure is developed to enhance the estimation of rotor system parameters in order to identify a dynamic system under external load disturbances. The system model achieved is then utilised for active control of vibrations. The feedback control method is applied to tune the system characteristics favourable for the other control methods applied. The feedforward methods (and the repetitive control method in Chapter 5) are designed to compensate periodic excitations due to rotation. These methods are applied to work together with the feedback control system.

3.1 New method for identification

Run-time identification of a rotor system is often desirable, because the dynamic behaviour of a rotor may be dependent on its rotation speed and operating conditions. The accuracy of an ordinary identification procedure based on input-output measurements and a standard FRF[6] estimation method can be degraded by excitations that are not measurable at the system input. In rotordynamics, rotation harmonics cause excitations of this kind. These rotation harmonics appear at the frequency of rotation and its multiples (or sometimes submultiples), being caused by rotor unbalance, alignment errors, asymmetry in the rotor or its bearings, etc. (Vance 1987, Genta 2005). Such excitations may be estimated from a machine's geometry, but they are not accessible to direct measurement. Dealing with deleterious excitations during identification usually requires judgment of an operator. For example, the operator can exclude the harmonics before carrying out the modal analysis, or filter the corresponding

[6] Frequency Response Function

peaks out during the frequency response function measurement. This thesis presents a simple method for compensating such peaks that assumes a suitable reference signal is available. The method is developed in order to reduce the need for human intervention in identification, and thereby making the identification procedure automatic. Automatic identification is considered important in order to develop adaptive vibration control systems for rotors.

Recently, Moore *et al.* (2005) addressed the automatic identification problem in modal parameter estimation; the non-measured periodic excitations affect the estimated damping values and the mode shapes. Similar solutions for the problem have been developed for secondary-path estimation in active noise control (Kuo & Morgan 1996 and Hansen & Snyder 1997). These estimation methods take the periodic signal fed into the system into account in a manner similar to that presented here. Eriksson *et al.* (1999) compared off-line and on-line estimation methods; on-line estimation was found to be complex and computationally expensive. Meurers & Veres (2002) considered the implementation issues of a computationally light on-line secondary-path estimation method. In their study, the computationally light method meant avoiding spectral analysis in the disturbance estimation. Bao *et al.* (1993) compared identification and excitation methods that minimally perturb the plant to be controlled. The identification method presented in this work is also a computationally light method that compensates load disturbances due to rotation before the actual identification. The method presented uses a reference signal in a similar way as it is used in feedforward control.

The new identification scheme studied is visualised in Figure 4: a system to be identified is excited by measurable excitations, $u(n)$, and unknown disturbances (non-measurable excitations), $d(n)$. The response, $e(n)$, is a sum response of these two excitation components. Carrying out the identification from $u(n)$ to $e(n)$ can result in the dynamic system having a spurious resonance peak at the frequencies of $d(n)$; this is the problem to be overcome by the present work. In order to accomplish this, the rotor system is considered as two coupled systems to be identified: 1) the dynamic system from measurable excitations to the output, and 2) the dynamic system from the reference signal to the output. The former describes the dynamics of the actual plant. The latter describes the transfer of the forced vibrations due to rotation. Since the forced vibrations cannot be measured for use as the input signal, they are replaced by a signal

correlating with the forced vibrations. The replacing signal used is a sinusoidal reference signal, $r(n)$, derived from the rotation speed measurement (actually, the rotation speed is estimated from the revolution pulse measurement).

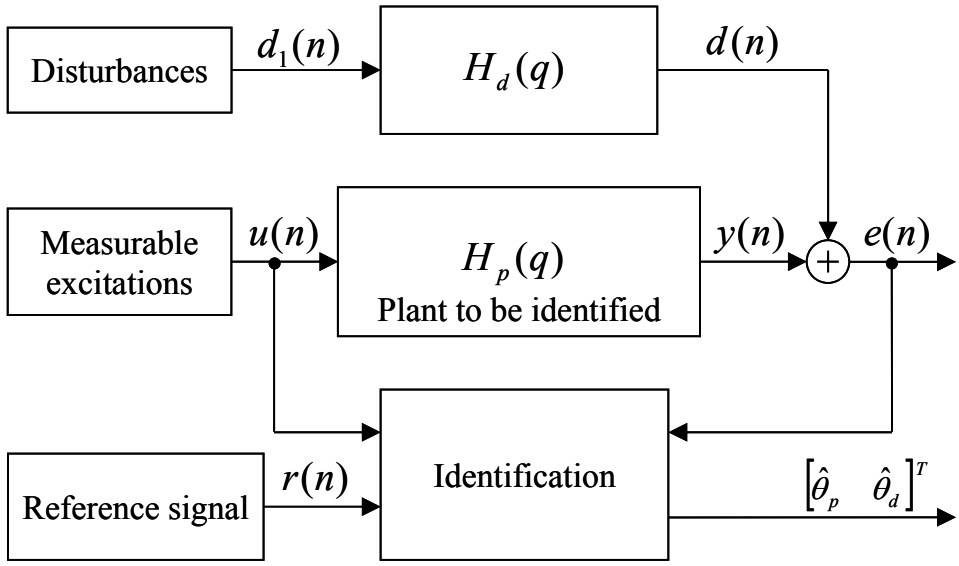

Figure 4. The rotor system to be identified with the disturbance.

In identification terminology, the rotation harmonics described above were interpreted as load disturbances unobservable in the input of the system (Hjalmarsson & Ljung 1993). This thesis investigates a simple idea for taking these disturbances into account and mitigating their influence on the identification result. The idea originates from the textbook of Maciejowski (2002), where an example of predictive control showed how to compensate the constant load disturbance in the output of a system.

Consider the equation of motion in Equation (18). Discretising results in

$$\begin{aligned} x(n+1) &= A_p x(n) + B_p u(n) \\ y(n) &= C_p x(n) \end{aligned} \tag{23}$$

where $x(n)$ is the system state vector at the time instant $t = nT_s$ where T_s is a constant sampling time and n = {0, 1, … , }. Matrices A_p, B_p, and C_p with dimensions described in Section 2.2 represent the plant dynamics (*i.e.* the

dynamic system to be identified). $y(n)$ contains the system displacements as usual. Note that matrix $C_p = [I\ 0]$ in Equation (18) and Equation (23).

The Internal Model Principle by Francis & Wonham (1975) states that a control system must have a model, or some information, of a disturbance in order to compensate the disturbance perfectly. In the present work, this means modelling the oscillating disturbance within the process or using an external signal correlated with the disturbance. The use of the reference signal was seen as a natural solution for a rotor system, since the speed of rotation is often measured and the disturbances occur at the rotation frequency and its multiples. Furthermore, the same reference signal is also being used for the feedforward compensation methods. The augmented system with supplementary input for the reference signal

$$\begin{aligned} \begin{bmatrix} x(n+1) \\ d(n+1) \end{bmatrix} &= \begin{bmatrix} A_p & 0 \\ 0 & A_d \end{bmatrix} \begin{bmatrix} x(n) \\ d(n) \end{bmatrix} + \begin{bmatrix} B_p & 0 \\ 0 & B_d \end{bmatrix} \begin{bmatrix} u(n) \\ r(n) \end{bmatrix} \\ e(n) &= \begin{bmatrix} C_p & I \end{bmatrix} \begin{bmatrix} x(n) \\ d(n) \end{bmatrix} \end{aligned} \tag{24}$$

where $r(n)$ is the sinusoidal reference signal that is correlated with the disturbance. Matrices A_d, and B_d filter the reference signal in such a way that it represents the disturbance in the system output. In Figure 4, the pulse transfer function of the disturbance is visualised from $d_1(n)$ to $d(n)$. In Equation (24), however, the transfer of the disturbance is considered as a transfer function from $r(n)$ to $d(n)$. Hence, the reference signal $r(n)$ acts as a proxy for the disturbance $d_1(n)$.

Remark 2

The reference signal must correlate with the forced vibrations to be able to compensate that particular frequency at the output.

For the experimental work, the plant model is required in the form of a pulse transfer function from the actuator $u(n)$ to the rotor displacement $y(n)$

$$H_p(q) = \frac{b^p_{m_p} q^{m_p} + b^p_{m_p-1} q^{m_p-1} + \cdots + b^p_0}{q^{n_p} + a^p_{n_p-1} q^{n_p-1} + a^p_{n_p-2} q^{n_p-2} + \cdots + a^p_0} \tag{25}$$

The choice of the polynomial degrees (model order) is discussed below together with experimental identification. A pulse transfer function from the reference signal $r(n)$ to the disturbance $d(n)$ is

$$H_d(q) = \frac{b^d_{m_d} q^{m_d} + b^d_{m_d-1} q^{m_d-1} + \cdots + b^d_0}{q^{n_d} + a^d_{n_d-1} q^{n_d-1} + a^d_{n_d-2} q^{n_d-2} + \cdots + a^d_0} \tag{26}$$

The order of $H_d(q)$ should be based on the number of spectral components in the reference signal. Two model parameters per sinusoid in the reference signal is the maximum amount of parameters to have *a persistently excited system*; the persistent excitation conditions can be found in (Åstrom & Wittenmark 1995). The same conditions are also dealt later in Section 3.4.1.

The identification problem was modified into the form of the standard least squares identification. The estimated output of the system is the sum of the outputs of two sub-systems

$$\begin{aligned} \hat{e}(n) &= H_p(q)u(n) + H_d(q)r(n) \\ \hat{e}(n) &= \varphi^T(n)\theta \end{aligned} \tag{27}$$

where $\varphi(n)$ contains the regression variables and θ contains the parameters to be identified (Åstrom & Wittenmark 1995). Since signals $y(n)$ and $d(n)$ are not directly measurable, but only their sum $e(n)$, the denominator polynomials of $H_p(q)$ and $H_d(q)$ cannot be chosen independently. An IIR[7] filter from $u(n)$ and $r(n)$ to $e(n)$ is expressed as

[7] Infinite Impulse Response

$$\varphi(n)=\begin{bmatrix} -e(n-1) \\ -e(n-2) \\ \vdots \\ -e(n-n_p) \\ u(n+m_p-n_p) \\ u(n+m_p-n_p-1) \\ \vdots \\ u(n-n_p) \\ r(n+m_d-n_p) \\ r(n+m_d-n_p-1) \\ \vdots \\ r(n-n_p) \end{bmatrix}, \theta=\begin{bmatrix} a^p{}_{n_p-1} \\ a^p{}_{n_p-2} \\ \vdots \\ a^p{}_0 \\ b^p{}_{m_p} \\ b^p{}_{m_p-1} \\ \vdots \\ b^p{}_0 \\ b^d{}_{m_d} \\ b^p{}_{m_d-1} \\ \vdots \\ b^d{}_0 \end{bmatrix} \tag{28}$$

Hence, the dynamic system to be identified has been augmented, similarly to Equation (24), by splitting it into two parts. As noticed, the systems are coupled by the common denominators. This may, however, be avoided by using a FIR representation for the transfer function filtering the disturbance, as was done in the experimental work. Standard least-squares identification shown in Åström & Wittenmark (1995) gives estimates for the coefficients

$$\hat{\theta}=(\Phi^T\Phi)^{-1}\Phi^T E \tag{29}$$

where

$$\Phi=\begin{bmatrix} \varphi^T(1) \\ \vdots \\ \varphi^T(n) \end{bmatrix}, \quad E=\begin{bmatrix} e(1) \\ \vdots \\ e(n) \end{bmatrix} \tag{30}$$

where $e(n)$ is the measured output of the plant to be identified comprising the actual plant output component $y(n)$ and the disturbance component $d(n)$. The identification procedure presented is used for the rotor system identification before the experimental validation of control algorithms. The identification results are presented in Section 4.3.

3.2 Outline of control systems

The active control systems used in this work are in a cascaded configuration with an inner loop feedback controller and an outer loop "feedforward" controller. Figure 5 shows the rotor system controlled by the feedback and the feedforward controller. Notice that the systems in this section are presented as continuous-time systems, contrary to the previous section.

The control force $u_{ac}(t) = u_{fb}(t) + u_{ff}(t)$ is a sum output of the feedback and feedforward controllers. The excitation $d(t)$ is considered as a forced displacement added to the rotor system output $y(t)$. The measured displacement is $e(t) = y(t) + d(t)$. The feedforward controllers use the system output and the reference signal $r(t)$. The reference signal is composed of a sinusoid or a sum of sinusoids corresponding to the disturbance frequencies to be compensated. The purpose of active control methods is to drive the measured displacement $e(t)$ to zero.

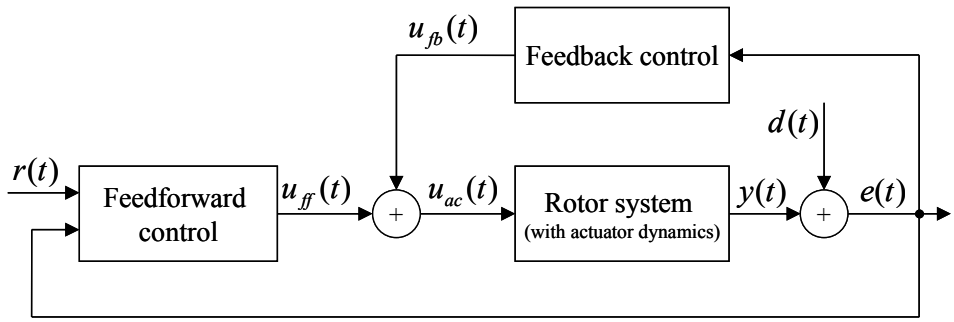

Figure 5. The feedback and feedforward controllers with the rotor system.

3.3 Feedback control

Velocity feedback control has been a popular method for collocated active control. The idea of the collocated velocity feedback is to measure vibration velocity at a sensor that is collocated with a corresponding actuator and to derive a control force for the actuator by using that particular velocity measurement only. It is a relatively simple method and stability can be guaranteed in the ideal case.

The statement on the guaranteed stability can be understood by considering the dynamics of a collocated system. The phase of the frequency response measured from the actuating force to the displacement at the same point varies between 0° and –180°. Introducing a phase lead by the velocity feedback method causes the phase of the system loop gain to vary from +90° to –90° (Preumont 2002). The argument of the phase varying within the given limits is a consequence of the fact that poles and zeros alternate for collocated systems; Preumont (2002) has listed feedback collocated configurations that are inherently stable for ideal systems without other delays. However, it has to be noted that practical systems always have some phase-lag due to sampling, restricted actuator or sensor bandwidth, their saturation, *etc.* The phase lag has to be taken into account when designing the control system.

Consider the equation of motion in Equation (18). Ideal collocated velocity feedback can be seen as a partial state feedback method

$$\begin{aligned} \dot{x}(t) &= \begin{bmatrix} 0 & I \\ -M^{-1}K & -M^{-1}(C+L_v) \end{bmatrix} x(t) + \begin{bmatrix} 0 \\ -M^{-1} \end{bmatrix} u_{ff}(t) \\ y(t) &= \begin{bmatrix} I & 0 \end{bmatrix} x(t) \end{aligned} \tag{31}$$

where L_v is the feedback matrix. When collocated velocity feedback is being used, L_v has positive terms in the diagonal corresponding to the controlled degrees-of-freedom. One element in the matrix corresponds to one sensor-actuator pair. The positive diagonal terms work in a stabilising manner, as if the system damping were increased.

Remark 3

Rotating machinery experts know that increasing the damping may lead to instabilities in rotor systems. The damping increase presented above has a stabilising effect on rotor systems, because it is "non-rotating" damping as the damping forces are exerted by the actuator. An example of rotating damping is the hysteretic damping in the rotor shaft. Increasing this kind of damping that rotates together with the rotor may lead to rotordynamic instability (Genta 2005).

The feedback control method described above is very simple and classical. However, as will be shown later this was found to be a sufficient solution, since the unbalance compensation methods were responsible for a reduction in vibration levels. Moreover in this work, the feedback system is used for tailoring the plant characteristics. An additional aim is to avoid the generation of a DC component in control, since the active vibration control concept proposed is intended as a supplementary system for a rotor on conventional bearings. This is another reason why velocity feedback control methods are well suited for the problem.

The importance of dedicated mass unbalance compensation was stated similarly by Qui *et al.* (2001) who explored active tilting pad bearings for the active control of synchronous force (*i.e.* the mass unbalance effects) compensation. They compared a PID controller with a controller designed with μ synthesis tools. With μ-controller, the performance of the controller was slightly improved in comparison with the classical one.

3.3.1 Sensor & actuator placement

Actuator and sensor placement is often left without discussion in practical research papers on active vibration control, because several restrictions exist in practice. An active control system is often not the primary function in a machine. For this reason, sensor and actuator locations are ruled by space requirements of several other functions. This can lead to non-optimal sensor and actuator positions in terms of active control.

As it will be reported later, the experimental work is carried out by using two layouts: 1) the Jeffcott rotor layout where the actuator and sensors locate at the rotor midpoint, and 2) the non-collocated layout where the actuator is located at the rotor endpoint and sensors at the endpoint and at the midpoint. For the Jeffcott rotor layout, the optimal location for the actuator and the sensor is in the vicinity of the disk, because the mass unbalance is located there, and because the vibration amplitude is largest at the midpoint. This can be understood by considering the observability and the controllability of the system.

As explained, the actuator and sensor locations cannot be chosen freely in practice. This is because many rotating machines carry out other function (*e.g.* a

work process) inside the bearing span and there is no place for vibration control equipment. Hence, moving the actuator location to the end of the rotor and changing to a non-collocated layout is relevant to the purpose of this study.

Utku (1998) suggested actuators to be placed in such a way that the energy absorbed by the actuators is maximised. This means placing the actuator at the spots where the motion-induced forces are largest in magnitude. These spots can be found by response analysis methods, provided that the excitation is well defined. Utku (1998) also states that this does not mean maximising the controllability of the system displacement. The statement can be understood if the criterion is the absorption of energy from the structure; the maximum displacement and the maximum energy over a frequency band do not necessarily occur in the same location.

Active vibration control systems are subjected to the *spill-over* phenomenon, *i.e.* the excitation of the un-observed high-frequency modes while achieving damping of the low-frequency modes. (Preumont 2002, Utku 1998). Spill-over can cause amplification of high-frequency components and also lead to instability, if non-modelled modes exist outside the control system bandwidth. Clark (1999) presented an overview of the methods to avoid such instability by sensor placement. The design methods presented are aimed at finding sensor placements that decouple the modes beyond the bandwidth of interest.

In this author's experience, the evaluation of modal amplitudes can help in the determination of actuator placement. A qualitative way is to survey the modes of interest and sum up their displacements. Suitable actuator or sensor placements occur in locations where the summed displacement is high and none of the components is zero.

3.4 Feedforward control

Feedforward control methods have been widely used in rotating machinery, because they provide an effective means of mass unbalance compensation. The common idea in the algorithms is to filter a sinusoidal reference signal $r(t)$ in such a way that it acts against the disturbances $d(t)$ to be compensated (Figure 6). The filter parameters are adapted using the control error $e(t)$ in the plant

output. Two different algorithms used in this work are presented in the forthcoming sections. The rotor system and the feedback control system form together the plant from the feedforward compensation point-of-view.

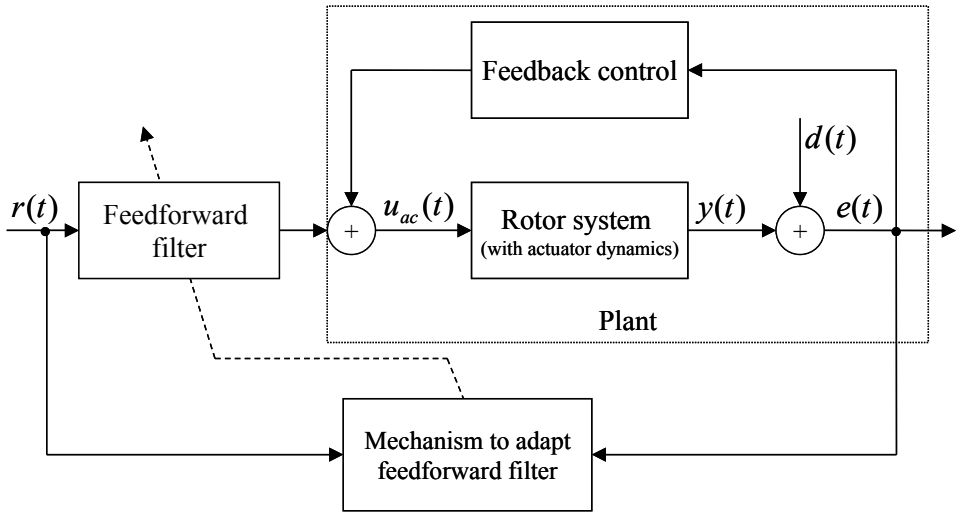

Figure 6. The general working principle of feedforward systems.

3.4.1 Adaptive FIR filter algorithm

Feedforward systems are based on the use of a reference signal to compensate a disturbance. The reference signal is fed through a FIR[8] (discrete-time) filter that is adapted on-line in such a way that the disturbance is compensated. The reference signal may be a measured disturbance or a signal that is known to correlate with the disturbance (Fuller *et al.* 1996, Elliot 2001). This approach has been used, for example, in the active sound control of vehicles and ducts (Couche & Fuller 1999, Kataja 1999). For the rotor systems, mass unbalance, bearings, and interactions with a process cause disturbances at the frequency of rotation and its multiples. For the Jeffcott rotor, its mass unbalance is the only source of excitation. For real rotors, mass unbalance is one of the largest sources of excitation. Hence, a significant part of the excitation can be compensated by tackling the disturbance caused by the mass unbalance. An estimate of rotation

[8] Finite Impulse Response

speed provides a possibility of generating a reference signal that has the same base frequency as the disturbances.

Consider the system shown in Figure 6; the objective is to minimise the absolute value of the output error signal where the plant is subjected to the disturbance. This is done by filtering the reference signal through a FIR filter; the control sequence is calculated according to

$$u(n) = \sum_{i=0}^{I} h_i r(n-i) \tag{32}$$

where h_i are the filter coefficients, and I is the order of the filter. The objective is to find such coefficients h_i that the reference signal $r(n)$ compensates the disturbance $d(n)$ and thus drives $e(n)$ to zero. The outline of the derivation of the adaptive law for a SISO system is shown below according to Fuller *et al.* (1996).

Figure 7 shows the basic adaptation problem without a dynamic system between the filter and the error. The FIR coefficients h_i must filter the reference signal $r(n)$ in such a way that $u(n) = -d(n)$.

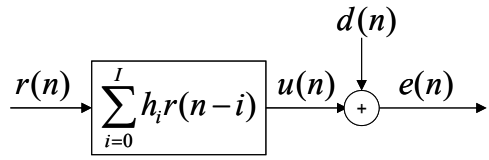

Figure 7. A simple adaptation problem to minimise the output error.

To minimise the square of the error, a quadratic cost function is defined as

$$J = \left(e(n)\right)^2 \tag{33}$$

Minimisation of the cost function J leads to an optimal set of filter coefficients (Fuller *et al.* 1996). This minimum is unique if the reference signal consists of at least half as many frequencies as the filter has real-valued coefficients; the reference signal is then said to be *persistently exciting* (Fuller *et al.* 1996, Elliot 2001). The optimal coefficients may be computed by using the autocorrelation properties of the reference signal and the cross-correlation between the reference

and desired signal. However, a considerable amount of data and computational effort are required to obtain a closed form solution for the optimal set of coefficients. (Widrow & Stearns 1987, Fuller *et al.* 1996, Elliot 2001).

An alternative solution to finding the optimal coefficients is to develop an adaptive filter. In the adaptive filter, the coefficients are adjusted sequentially in such a way that the mean square error converges towards to the minimum. Each new set of data is used to re-adjust the coefficients towards the optimal coefficients. One suggestion for updating the coefficients is the *steepest-descent algorithm*. The coefficients are updated in the negative direction of the local gradient of the cost function

$$h_i(n+1) = h_i(n) - \mu \frac{\partial J}{\partial h_i}(n) \tag{34}$$

where μ is the convergence coefficient. The convergence coefficient has to be a small positive number in order to ensure stability of the algorithm. According to Widrow & Stearns (1987), Widrow and Hoff proposed that the partial derivative of the cost function with respect the coefficients may be computed as the derivative of the instantaneous error with respect to the filter coefficients

$$\frac{\partial J}{\partial h_i} = \frac{\partial e^2(n)}{\partial h_i} = 2r(n-i)e(n) \tag{35}$$

By combining Equations (34) and (35) the weighting coefficients are updated according to

$$h_i(n+1) = h_i(n) - \alpha r(n-i)e(n) \tag{36}$$

where $\alpha = 2\mu$ is another convergence coefficient. This update law is known as the *LMS algorithm*[9]. (Widrow & Stearns 1987, Elliot 2001).

[9] Least Mean Squares algorithm.

In the basic configuration, no dynamic system occurred between the input and the output. This is rarely the case in practice. The dynamics of the plant to be damped are taken into account by the *filtered x-LMS algorithm.* The update law is then

$$h_i(n+1) = h_i(n) - \alpha r_f(n-i)e(n) \tag{37}$$

where $r_f(n)$ is generated from the reference signal by filtering it through a model of the plant (Fuller *et al.* 1996, Elliot 2001). The model is a time-domain model, a FIR or IIR model, for instance. In this work, IIR models are used to describe the pulse transfer function of the plant.

A known approximation for the upper limit of the convergence coefficient for the *filtered x-LMS algorithm* is

$$\alpha < \frac{1}{\bar{r}^2 I} \tag{38}$$

where I is the order of the FIR filter and $\bar{r}^2$ is the mean square value of the reference signal (Fuller *et al.* 1996, Elliot 2001). The given limit is an approximation and also other approximation exists in the literature (according to practical experiences, the limit is very approximate.

Remark 4

The LMS adaptation algorithm does not limit the number of frequencies to be compensated. Several spectral components may be fed through the same algorithm, if the order is sufficient. This may be considered an elegant feature compared with the other feedforward algorithms dealt with in this thesis.

Several modifications of the LMS algorithm exist. In order to adjust the stability and convergence characteristics, the leaky algorithm has been developed. Its update law is

$$h_i(n+1) = \gamma h_i(n) - \alpha r_f(n-i)e(n) \tag{39}$$

where γ is the leakage coefficient, a positive constant less than unity. By selecting $0 < \gamma < 1$, the integrating action of the update scheme is weakened. The weighting coefficients never achieve the optimal value since they "leak away" in every update.

The algorithm in Equation (39) is manipulated further to show the behaviour of the coefficients as a function of the disturbance signal and to introduce one more update law. The coefficients and the reference signal are defined as vectors

$$\begin{aligned} H^T(n) &= \begin{bmatrix} h_0(n) & \cdots & h_I(n) \end{bmatrix} \\ R_f^T(n) &= \begin{bmatrix} r_f(n) & \cdots & r_f(n-I) \end{bmatrix} \\ R_p^T(n) &= \begin{bmatrix} r_p(n) & \cdots & r_p(n-I) \end{bmatrix} \end{aligned} \tag{40}$$

where the length of the vectors is equal to I+1 (I is the filter order). Vectors $H(n)$ and $R_f(n)$ are formed from the filter coefficients and the reference signal presented above. Vector $R_p(n)$ represents a reference signal filtered trough the actual plant. The output error may approximated as

$$e(n) \approx d(n) + H^T(n) R_p(n) \tag{41}$$

Note that the manipulation means the change in the order of the plant and the FIR filter. It has been assumed that the FIR coefficients change slowly. Otherwise, the system is time-variant and the plant and the FIR filter are not commutative. With the chosen assumption and notation, the update law becomes a function of the disturbance

$$H(n+1) \approx \left(\gamma I - \alpha R_f(n) R_p^T(n)\right) H(n) - \alpha R_f(n) d(n) \tag{42}$$

The convergence rate of the FIR coefficients can be strongly dependent on the operation point, if the plant and the plant model have high magnitude changes in their frequency responses. The maximum stable convergence coefficient must be determined at the point of the highest magnitude. The normalised LMS algorithm is developed in order to provide roughly constant convergence rate regardless the operation point. The update law is

$$H(n+1) = \gamma H(n) - \frac{\alpha R_f(n) e(n)}{\delta + R_f{}^T(n) R_f(n)} \tag{43}$$

where δ is a small number to prevent division by zero. (Treichler *et al*. 2001, Elliot 2001).

Under certain assumptions, the feedforward compensation system may be interpreted as a feedback system consisting of a resonator at the frequency of the signal to be compensated (Figure 8). Elliot *et al.* (1987) showed that the adaptive FIR filter is equivalent to a feedback system with the pulse transfer function

$$H_{FIR}(q) = \frac{u(q)}{e(q)} = \frac{\alpha I r_a}{2} \frac{\left(q\cos(\omega_0 T_S - \phi) - \gamma\cos(\phi)\right)}{q^2 - 2q\gamma\cos(\omega_0 T_S) + \gamma^2} \tag{44}$$

where the filtered reference signal is defined as $R = r_a\, e^{i\phi}$, and ω_0 is the angular frequency of the disturbance signal to be compensated, and T_S is the sample interval. In the derivation, Elliot *et al.* (1987) have assumed a synchronously sampled reference signal and the number of FIR filter coefficients equal to an integer multiplied by half the number of samples per cycle. In addition, Elliot *et al.* (1987) have assumed the change of FIR coefficients to be slow with respect to other dynamics of the system.

In the same figure the transfer function from the reference signal to the FIR output is defined as

$$H(q) = \sum_{i=0}^{I} h_i q^{-i} \tag{45}$$

If $\gamma = 1$, the transfer function $H_{FIR}(q)$ represents a non-damped resonator that produces high (infinite) gain at frequency ω_0. This leads to a good disturbance rejection at that frequency, since the closed loop system from disturbance to the output error equals to

$$\frac{e(q)}{d(q)} = \frac{1}{1 + H_{FIR}(q) G(q)} \tag{46}$$

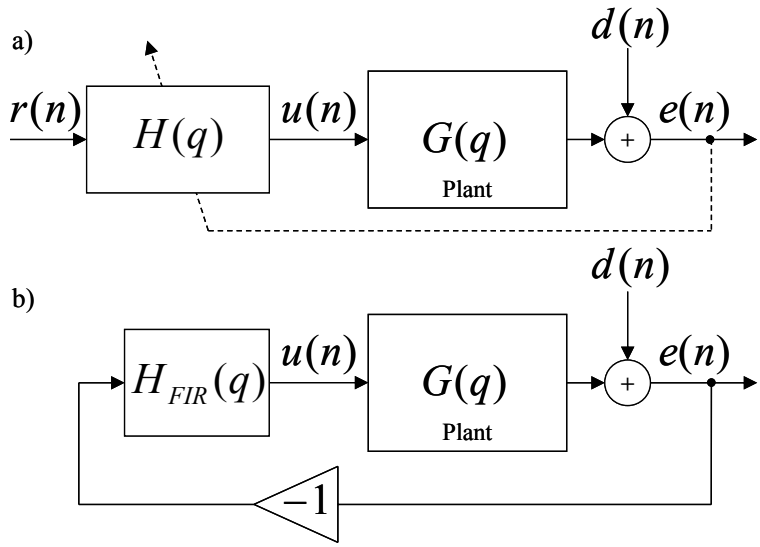

Figure 8. An adaptive feedforward controller (a) and the equivalent feedback system (b) (adopted from Fuller et al. (1996)).

Remark 5

The assumptions for the derivation of the feedback counterpart for an adaptive FIR filter are somewhat stringent compared to the adaptive FIR filter parameters used in this study. The requirements on synchronous sampling and on the number of filter coefficients are not satisfied in this study. Hence, the counterpart derived may exist approximately.

3.4.2 Convergent Control algorithm

The *Convergent Control* algorithm represents another group of feedforward compensation methods that are somewhat similar to the adaptive FIR system with the LMS algorithm. However, some differences exist between the algorithms and the purpose of this work was study those differences and compare them with respect each other.

The principle of the *Convergent Control* algorithm was presented by Burrows & Sahinkaya (1983) and Knospe *et al.* (1996, 1997). They showed how to compensate several (harmonic) frequencies in a rotor system. They also

discussed the robustness and the optimality of the control method for MIMO[10] systems. A very similar method, called *Higher Harmonic Control,* was developed by Sievers & von Flotow (1988) and Hall & Wereley (1989) for helicopter blade control. These works showed the relationship with the feedback equivalent system and the practical implementation, including the means for computing the *Fourier coefficients* approximately, as shown below. All these works dealt with compensating harmonic responses of rotating objects.

The feedforward method discussed in this section is based on adapting the feedforward filter coefficients in the frequency domain. The transformation to the frequency domain (the computation of *Fourier coefficients*) and the transformation back to the time domain are shown below after the introduction of the control law.

Consider a dynamic system whose response is expressed by the *Fourier coefficients* at discrete frequencies (N_f pieces). The responses are measured at sensors (N_s pieces) and the controls are exerted on actuators (N_a pieces). In terms of the Fourier coefficients, the system output error may be expressed as

$$E_F(n) = G_F U_F(n) + D_F(n) \tag{47}$$

where G_F is the complex frequency response matrix ($N_s N_f \times N_a N_f$) of the system, $U_F(n)$ is the system input (control), and $D_F(n)$ is the synchronous excitation due to rotation. $E_F(n)$ and $D_F(n)$ are vectors with the length equal $N_s N_f$. $U_F(n)$ is a vector with length equal to the $N_a N_f$. Note again that the equation describes the system dynamics at discrete frequencies, corresponding to the number of the complex Fourier coefficients. For instance, the responses of N_f pieces of harmonic frequency components from one input to one output can be expressed

$$\begin{bmatrix} E_F^{\omega_0} \\ \vdots \\ E_F^{\omega_{N_f-1}} \end{bmatrix} = \begin{bmatrix} G_F^{\omega_0} & \cdots & 0 \\ \vdots & \ddots & \vdots \\ 0 & \cdots & G_F^{\omega_{N_f-1}} \end{bmatrix} \begin{bmatrix} U_F^{\omega_0} \\ \vdots \\ U_F^{\omega_{N_f-1}} \end{bmatrix} + \begin{bmatrix} D_F^{\omega_0} \\ \vdots \\ D_F^{\omega_{N_f-1}} \end{bmatrix} \tag{48}$$

[10] Multiple Input Multiple Output

where $E_F^{\omega_k}, G_F^{\omega_k}, U_F^{\omega_k}, D_F^{\omega_k}$ are the Fourier coefficients of the output error, the frequency response, the control force, and the disturbance. The index $k = \{0, 1, \ldots, N_f - 1\}$ refers to the frequency concerned.

Using the notation in Equations (47) and (48), the control law is obtained by minimising the quadratic cost function

$$J = E_F^H E_F = \left(G_F U_F + D_F\right)^H \left(G_F U_F + D_F\right) \tag{49}$$

The minimum of the quadratic control error function is found at

$$U_F = -\left(\hat{G}_F^H \hat{G}_F\right)^{-1} \hat{G}_F^H D_F = -A_F D_F \tag{50}$$

where $\hat{G}_F$ is the estimated complex frequency response of the system (Knospe *et al.* 1996, Knospe *et al.* 1997, Åström & Wittenmark 1995). Matrix $\hat{G}_F$ may be inverted directly if the number of sensors is equal to the number of actuators and the matrix is well conditioned. To approach the optimum gradually during control, the Convergent Control method uses an integrative adaptation law

$$U_F(n+1) = U_F(n) - A_F E_F(n) \tag{51}$$

The present work used these results to compensate the disturbance at the frequency of rotation in the rotor test environment. In order to adjust the convergence and the stability properties, the adaptation law used was armed with two coefficients

$$U_F(n+1) = \gamma U_F(n) - \alpha A_F E_F(n) \tag{52}$$

where α is again the convergence coefficient (a positive number). The coefficient γ is again the leak coefficient, a positive number less than unity. The control commands $U_F(n)$ are realised in the time domain as will be shown in Equation (56). Finally, consider the adaptation law in the following form as a function of disturbance

$$U_F(n+1) = \left[\gamma I - \alpha A_F G_F\right] U_F(n) - \alpha A_F D_F(n) \tag{53}$$

3.4.3 Computation of Fourier coefficients

The control law of the Convergent Control method is presented in terms of *Fourier coefficients*, *i.e.* in the frequency domain. The definition of the discrete-time Fourier series of a periodic signal is

$$E_F^{\omega_k} = \frac{1}{N}\sum_{n=0}^{N-1} e(n)e^{-\mathrm{i}2\pi kn/N} \tag{54}$$

where $E_F^{\omega_k}$ are the Fourier coefficients of signal $e(n)$, and $n = 0, 1,..., N\text{-}1$; N being the number of samples matched with the period of the signal (Proakis & Manolakis 1996). The index k corresponds to the number of the spectral line proportional to the corresponding frequency (from 0 to N_f–1). The transformation to the time domain can be performed by

$$e(n) = \sum_{k=0}^{N-1} E_F^{\omega_k} e^{\mathrm{i}2\pi kn/N} \tag{55}$$

According to the author's knowledge, the common practice is to compute and update the Fourier coefficients at each time instant, or over a short time interval, without averaging over the full signal period. This approach leads to a simpler implementation and was also used in this work. The same approach has been used in the works of Sievers & von Flotow (1988), Hall & Wereley (1989). The approximate Fourier coefficients of the error signal are then

$$E_F^{\omega_k}(n) \approx e(n)e^{-\mathrm{i}\omega_k t} \tag{56}$$

Where $e(n)$ is the output error signal. Note that the complex reference signal may be continuous, but it is sampled at time instants $t = nT_s$. When averaged over an interval, the set of approximate Fourier coefficient becomes

$$E_F(n) = \begin{bmatrix} \frac{1}{N}\sum_{n'=0}^{N-1} E_F^{\omega_1}(n-n') \\ \vdots \\ \frac{1}{N}\sum_{n'=0}^{N-1} E_F^{\omega_{N_f}}(n-n') \end{bmatrix} \tag{57}$$

where N is number of averages not necessarily matched with the period of the error signal. The length of complex-valued vector $E_F(n)$ corresponds to the number of frequencies to be compensated (N_f).

The number of samples averaged was varied in the works of Tammi (2003a, 2005); no advantages were found to arise from using long averaging times or matching the number of averages exactly to the period of the error signal. This behaviour can be understood by noting that the update law itself already contains an integrator. For this reason, relatively short averaging times with respect to the period of the error signal, or instantaneous computation, were used in the experimental work.

Returning to the time domain is achieved by multiplying the Fourier coefficients with the complex conjugate of the reference signal at frequencies ω_k, taking the real part of the signal and adjusting the gain. The control signal was

$$u(n) = \sum_{k=0}^{N_f-1} 2\,\mathrm{Re}\left(e^{\mathrm{i}\omega_k n T_S} U_F^{\omega_k}(n)\right) \tag{58}$$

where $U_F^{\omega_k}(n)$ are the Fourier coefficients of controls (Sievers & von Flotow 1988, Lantto 1999). Lantto (1999) also explains the reason for real part operator in Equation (56): only the real part of a signal may be realised in a practical system. The gain (2) comes from the amplitude adjustment, because only the real part was taken into account.

Figure 9 shows the scheme of computing the approximate Fourier coefficients and synthesising the time signal that correlates with the error signal component at the frequency of the reference signal. The scheme is valid for a SISO[11] system operating at frequency ω_0.

[11] Single Input Single Output

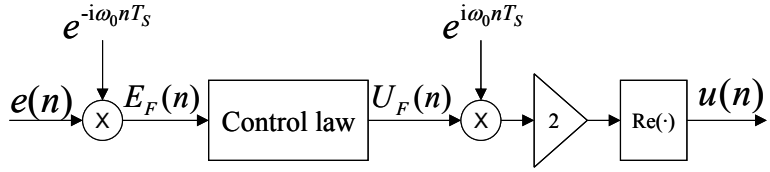

Figure 9. Extraction of the Fourier coefficients at the frequency of rotation and return to the time domain.

3.4.4 Instantaneous coefficient update

Although the coefficient update of the Convergent Control method was presented above as averaging the Fourier coefficients over a time interval, the update is made at each time instant in practical algorithms. Hätönen *et al.* (2006) and Daley *et al.* (2006) have shown that the Convergent Control algorithm with instantaneous coefficient update has a similar feedback counterpart as the adaptive FIR filter.

Let $U_F(n)$, $E_F(n)$, $D_F(n)$ and A_F be complex numbers representing the Fourier coefficients at one frequency only (ω_0), as in Figure 9. Taking the real part in Equation (58) is equivalent to

$$u(n) = 2\,\mathrm{Re}\left(e^{i\omega_0 nT_S} U_F(n)\right) = U_F(n)e^{i\omega_0 nT_S} + \overline{U}_F(n)e^{-i\omega_0 nT_S} \tag{59}$$

Let us describe the output $u(n)$ by means of two variables

$$\begin{aligned} U_F(n)e^{i\omega_0 nT_S} &= u_1(n) \\ \overline{U}_F(n)e^{-i\omega_0 nT_S} &= u_2(n) \end{aligned} \tag{60}$$

and then analyse $u_1(n)$ and $u_2(n)$ separately. Using the update law in Equation (52) and the approximation for $E_F(n)$ in Equation (56), the first one can be formulated

$$
\begin{aligned}
u_1(n+1) &= e^{\mathrm{i}\omega_0(n+1)T_S} U_F(n+1) \\
&= e^{\mathrm{i}\omega_0(n+1)T_S} \left(\gamma U_F(n) - \alpha A_F E_F(n)\right) \\
&= e^{\mathrm{i}\omega_0(n+1)T_S} \left(\gamma u_1(n) e^{-\mathrm{i}\omega_0 n T_S} - \alpha A_F e(n) e^{-\mathrm{i}\omega_0 n T_S}\right) \\
&= e^{\mathrm{i}\omega_0 T_S} \left(\gamma u_1(n) - \alpha A_F e(n)\right)
\end{aligned}
\tag{61}
$$

The latter one can be formulated similarly

$$
\begin{aligned}
u_2(n+1) &= e^{-\mathrm{i}\omega_0(n+1)T_S} \left(\gamma \overline{U}_F(n) - \alpha \overline{A}_F \overline{E}_F(n)\right) \\
&= e^{-\mathrm{i}\omega_0 T_S} \left(\gamma u_2(n) - \alpha \overline{A}_F e(n)\right)
\end{aligned}
\tag{62}
$$

In terms of pulse transfer functions, the systems (61) and (62) can be expressed as

$$
\begin{aligned}
u_1(n) &= \frac{-e^{\mathrm{i}\omega_0 T_S} \alpha A}{q - \gamma e^{\mathrm{i}\omega_0 T_S}} e(n) \\
u_2(n) &= \frac{-e^{-\mathrm{i}\omega_0 T_S} \alpha \overline{A}}{q - \gamma e^{-\mathrm{i}\omega_0 T_S}} e(n)
\end{aligned}
\tag{63}
$$

Bearing in mind that $u(n) = u_1(n) + u_2(n)$, the systems may be combined to one pulse transfer function from $e(n)$ to $u(n)$. Hence, the equivalent feedback compensator for the controller with instantaneous coefficient update is

$$
H_{CC}(q) = \frac{2\alpha\left(q\,\mathrm{Re}(A_F e^{\mathrm{i}\omega_0 T_S}) - \gamma\,\mathrm{Re}(A_F)\right)}{q^2 - 2q\gamma\cos(\omega_0 T_S) + \gamma^2}
\tag{64}
$$

This result is similar to that presented by Elliot *et al.* (1987) for an adaptive FIR filter with the LMS algorithm (Figure 8, Equation (42)), if the assumptions required in Section 3.4.1 are met. Herzog *et al.* (1996) have formulated the equivalent feedback compensators as continuous-time generalised notch filters in multivariable cases. The result in (61) – (62) holds for a MIMO system.

Both feedback equivalent systems have identical denominators representing a resonator at frequency ω_0, as explained before. By defining the system model as in the analysis regarding to the FIR system

$$A = \left(\hat{G}(e^{i\omega_0 T_S})\right)^{-1} = \left(r_a e^{i\phi}\right)^{-1} \tag{65}$$

a comparable feedback equivalent system can be obtained

$$H_{CC}(q) = \frac{2\alpha}{r_a} \frac{\left(q\cos(\omega_0 T_S - \phi) - \gamma\cos(\phi)\right)}{q^2 - 2q\gamma\cos(\omega_0 T_S) + \gamma^2} \tag{66}$$

Hence, only the gain factors are different between two feedback equivalent systems examined. Note that the gain is inversely proportional to r_a for Convergent Control whereas it is directly proportional for the FIR filter with the LMS algorithm. Thus, the algorithms have differences in effective feedback gain and their convergence properties. Those differences are presented in the next section. The convergence coefficients (α) are not equivalent for two different algorithms as there are differences in the gain factors.

3.5 Chapter summary

This chapter dealt with the identification and control methods to be validated and compared in the next chapter. The key idea of the identification method presented is to compensate the load disturbances due to rotation, before the actual identification. This feature is introduced to filter out forced vibrations from the responses for a more accurate identification result. The feedback control method shown is a relatively simple and robust way to add damping to a mechanical system. Two adaptive feedforward compensation methods have been introduced for rotor mass unbalance compensation: the adaptive FIR filter with the LMS algorithm and the Convergent Control method. The purpose of the algorithms is to create a compensation signal against the disturbances due to rotation. Both feedforward methods are based on the use of a reference signal correlating with the disturbance and an integrative update law to filter the reference signal in such a way that the disturbances are compensated. The reference signal can be generated when the rotation speed is known, since the excitation frequencies are correlated with the rotation frequency.

The derivation of the feedback equivalent systems showed that feedforward systems actually provide high feedback gain at the frequency to be compensated.

This leads to a good disturbance rejection at that particular frequency. Note that the FIR feedback equivalent system was derived for one synchronously sampled disturbance and with a FIR filter length equal to the half-cycle of the disturbance, or its multiple (see Section 3.4.1, and Elliot *et al.* 1987).

Examination of the stability of the algorithms shows that the feedforward systems require a model of the plant to be damped. The modelling accuracy has to be sufficient to describe the phase within ±90° (Ren & Kumar 1989, Elliot 2001). The convergence rate and the performance of the algorithms can be adjusted by the convergence coefficient (error feedback gain) and by the integrator leak.

4. Experimental validation in the rotor test environment

This chapter is concerned with validating the identification and controller synthesis methods presented. First, the desktop test environment where the experimental works were carried out is presented. A more detailed description with pictures of the test environment and its components can be found in Tammi (2003b). The test environment was studied in two different layouts. The first layout was a Jeffcott-rotor-like layout (Tammi 2003a, Tammi 2003b, and Tammi 2003c). In the second layout, the actuation point was located outside the bearing span, but the objective was to damp vibrations within the bearing span (Tammi 2005, Tammi *et al.* 2006a).

Parameter values used during each experiment are listed and explained in the corresponding sections. See Appendix C for exact coefficients of the system models and other filters used.

The coordinate directions used in the experimental setup are defined in Figure 1 consistently with the Jeffcott rotor model. The Z direction runs along the rotor shaft, X represents the direction in the horizontal plane, and Y in the vertical plane, respectively.

4.1 Main components

The rotor kit, modified from commercial demonstration equipment by Bently Nevada RK4, consisted of a 10-mm-diameter and 560-mm-long rotor supported by journal bearings. The mass of the rotor shaft alone was 350 g. The rotor was driven by an electrical motor with a separate control box. The desired rotational speed could be selected between 270 rpm and 10 000 rpm. The torque was transferred from the electrical motor to the rotor by means of a flexible coupling. Figure 10 shows a view of the test environment.

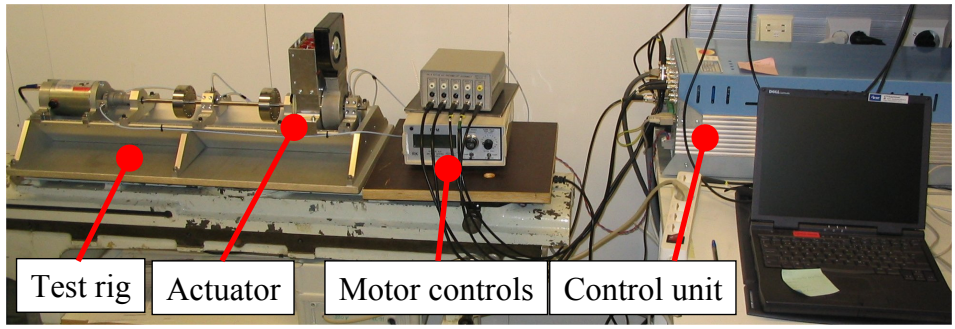

Figure 10. A general view of the test environment.

The body of the actuator was composed of stamped electrical steel sheets joined together by several longitudinal welds on the outer surface. A laminated structure of this kind was used to minimise iron losses in the body as is usual in magnetic circuits. The actuator body (*i.e.* the actuator stator part) had eight teeth forming the iron core for the radially located horseshoe electromagnets. The teeth, pointing to the centre of the actuator, were wound and the windings connected together, forming a hetero-polar actuator, *i.e.* the polarities of the magnets alternated along the circumference. The outside diameter of the body was 100 mm and the inside diameter was 50 mm. The actuator was fixed to the rotor kit body (Figure 11).

An armature (*i.e.* the actuator rotor part), also a laminated disk pack, was constructed and fixed to the rotor shaft. The actuating forces were induced through the air gap to the armature and the rotor. The outer diameter of the cylindrical armature was 47.5 mm and its length was 65 mm. The part had a conical locking mechanism for low-eccentricity fixing to the rotor. The weight of the armature and the locking mechanism together was 760 g.

Hall effect transducers were glued onto each tooth in order to measure the magnetic flux density in the air gap. This feature was incorporated in order to estimate the force exerted on the rotor. The force can be estimated without information on the flux density if the distance and the coil currents are known. However, the accuracy of the force measurement can be improved with the Hall transducers (Knopf & Nordmann 1998). The vibration amplitude of the rotor was mechanically restricted using a backup bearing to prevent the rotor from hitting the Hall transducers, the maximum allowable radial displacement being 0.3 mm.

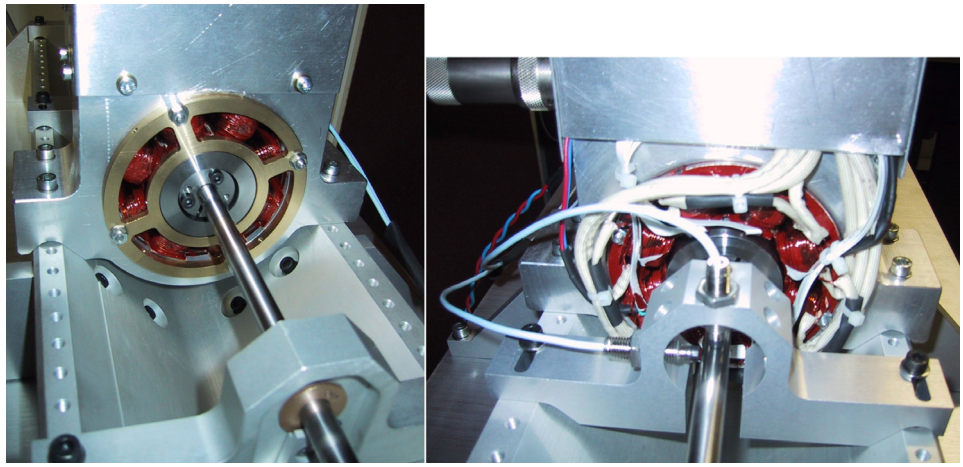

Figure 11. Left: the actuator seen from the drive end (in the collocated layout). The backup bearing is mounted in front of the coils. Right: the actuator seen from the non-drive end; the eddy current displacement transducers are located at the front.

The control hardware (called "the control unit" below) was modified from a commercial active magnetic bearing control system (type MBC-11 provided by High Speed Tech, Ltd). It is an extensive system for controlling a magnetically levitated rotor comprising one axial and four radial degrees of freedom. Amplifiers for controlling the output currents, programmable signal processing hardware, inputs, and outputs are integrated into the control unit. The whole system including inputs, outputs, signal conditioning systems and amplifiers is run by a digital signal processor.

Each magnet in the actuator is driven by one half-bridge amplifier that can generate a current from zero to a maximum value. In other words, the direction of the coil current does not change; each pair of coils is able to exert an attraction force on the rotor. The control unit feeds a constant bias flux density into each magnet; the resulting net force exerted on the rotor is zero. In order to exert a radial force on the rotor, the currents are increased on one side of the actuator and reduced on the other side. (Lantto 1999).

In the modifications, the functions for levitating the rotor were removed from the code because the system was only used to attenuate vibrations in this research design. In the control unit, the outputs for driving the actuator currents,

communications with a personal computer, and revolution pulse input provided were used as such. The rest of the communication signals were modified for the purpose. Inputs for magnetic field measurement, seven analogue inputs for arbitrary use, and force output signals were added.

The procedures for producing the control forces were available in the control unit. The control system designed (in the control unit) determines the force required and applies the force commands to the force control system (Figure 12). The force control system is run using either flux feedback or current feedback. The flux signals are provided by the Hall transducers; the current signals are measured in the amplifiers.

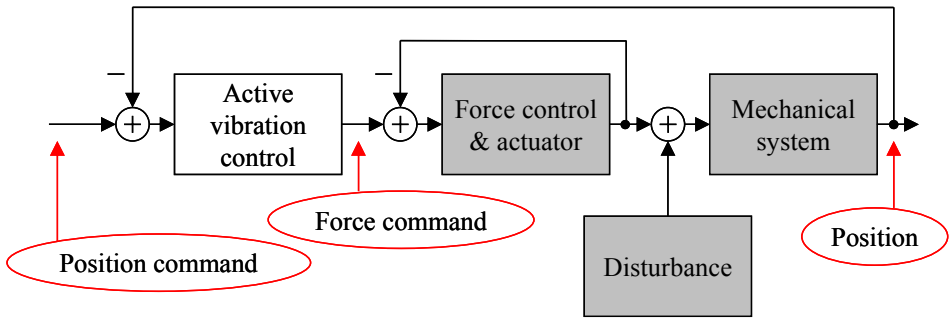

Figure 12. The control unit incorporates the current control, driven in either flux or current feedback mode. The control system applies the force commands to the force control loop.

4.2 Collocated Jeffcott rotor layout

The journal bearings, the actuator and the driving motor were all mounted on a stiff foundation, considered ideally rigid in this study. The actuator was over-sized for this particular purpose due to technical limitations. However, the forces used during active control were low, being less than the weight of the rotor.

The goal was to minimise the radial response in the middle of the rotor. The system was damped using a velocity-feedback controller. The control force was derived from the displacement measurements, provided by two transducers approximately collocated with the actuator. The results are originally presented

in Tammi (2003a) for the Convergent Control algorithm, and in Tammi (2003b, 2003c) for the adaptive FIR algorithm.

4.2.1 Layout and dynamics

The first experimental set-up was tailored to resemble the Jeffcott rotor. It was used for studying collocated control; collocation meaning that the actuator and sensor are located at the same spot. The actuator and the armature were located at the midpoint of the bearing span. The armature served as the disk of the Jeffcott rotor. The actuation point is marked by *A* in Figure 13; and the displacement measurement point by *S*. Note that the actuator and the sensor were not exactly collocated but located near each others. Hence, the experimental setup was only approximately collocated. The rotor was tailored to have the lowest bending mode with a sharp resonance at about 40 Hz (Figure 13 and Figure 14). The tailoring of the resonance frequency was made by adjusting the bearing span of the rotor.

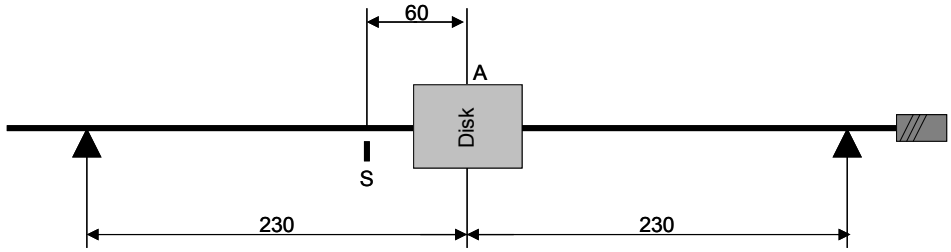

Figure 13. The rotor was driven at the right end. The armature was located at the centre; the radial displacements were measured at the black mark (S). (Dimensions in millimetres).

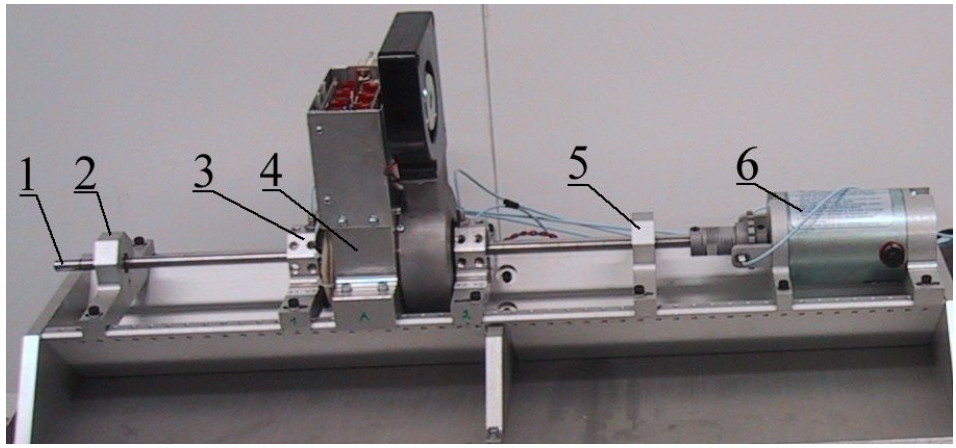

Figure 14. The test environment in the Jeffcott rotor layout: 1) rotor, 2) and 5) bearings, 3) displacement transducers, 4) actuator, and 6) driving electrical motor. (Tammi 2003d).

A modal analysis was carried out in order to estimate the modal parameters (*i.e.* the modal deflection shapes, the natural frequencies, and the equivalent viscous damping values) of the mechanical system and to validate the assumption that the system behaves like a Jeffcott rotor (*i.e.* Equation (5) is valid). See Section 2.2 for the definition of natural modes and frequencies. The measurements were carried out on a stationary rotating rotor in the vertical and horizontal planes. The rotor was excited with an impact hammer at the non-drive end. The frequency responses were measured at six points along the rotor with eddy current transducers. The data was analysed on modal analysis software using the SDOF[12] method. Altogether four natural modes were found in the modal analysis: the two lowest natural modes in both vertical and horizontal planes, Table 1. Figure 15 shows the corresponding deflection shapes of the rotor centre line. The results correspond to expectations; the lowest modes have a relatively low frequency while the second modes occur at distinctly higher frequencies. The results validated the Jeffcott rotor assumption. Naturally, modes at higher frequencies existed. However, the response of the second modes is weak, if excited at the centre of the rotor. This is because the excitation takes place close

[12] Single Degree of Freedom method, a standard curve fitting method in modal parameter estimation

to the nodal point[13]. The third natural modes do not have a nodal point at the centre of the shaft, but they occur at frequencies higher than those of interest for this work. The natural modes indicate rotor movement at bearings. This is due to relatively low stiffness of the bearings.

Table 1. The results of the modal analysis for the Jeffcott rotor layout (Tammi 2003b).

Mode	Frequency [Hz]		Damping [%]	
	horizontal (X)	vertical (Y)	horizontal (X)	vertical (Y)
1st	43	43	3	2
2nd	296	297	2	2

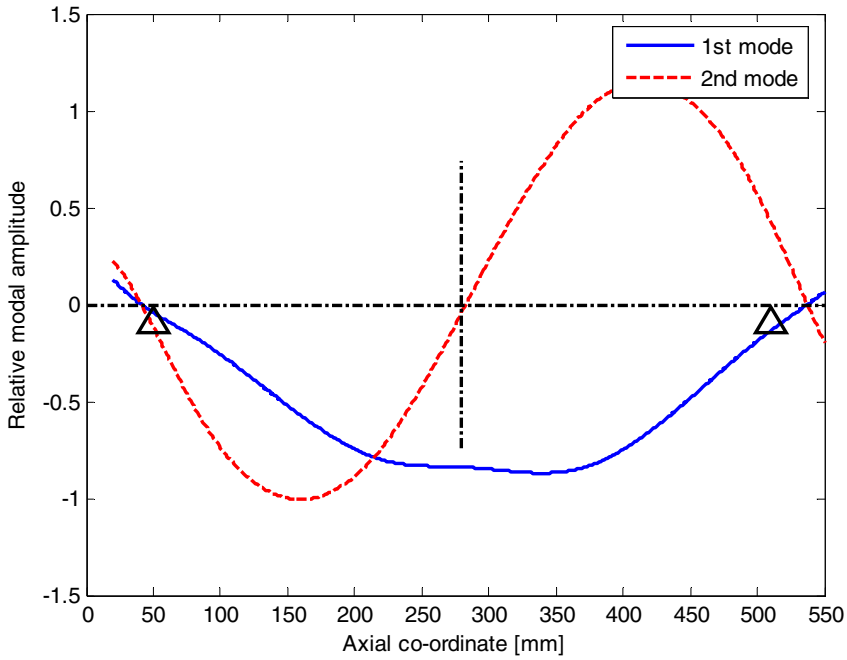

Figure 15. The two lowest mode shapes of the rotor. The non-deformed shape and the disk centre line are shown by the straight black lines. The triangles indicate the bearing positions.

[13] A Nodal point of a natural mode has zero displacement amplitude in that particular mode

The open-loop frequency responses were measured in order to identify the mechanical system, the actuator, and the control system together. This was to define the system parameters and again to validate the assumption concerning the Jeffcott rotor. The measurements were carried out by exciting the rotor with the actuator and measuring the frequency responses from force commands to the rotor displacement. Sinusoidal sweeps were used as the excitation. The measurements showed that the first natural modes were dominant, as expected. Figure 16 shows the second order oscillator response fitted to the measured responses.

The measurements of the open-loop system indicated a slightly lower first natural frequency than was predicted by the modal analysis. This was due to an interaction between the actuator and the mechanical system. It was mainly compensated by the flux-control loop in the control unit but a small effect remained (this negative spring effect is commonly known in electrical machines). The linearity was tested by varying the level of excitation; the system was found to be approximately linear.

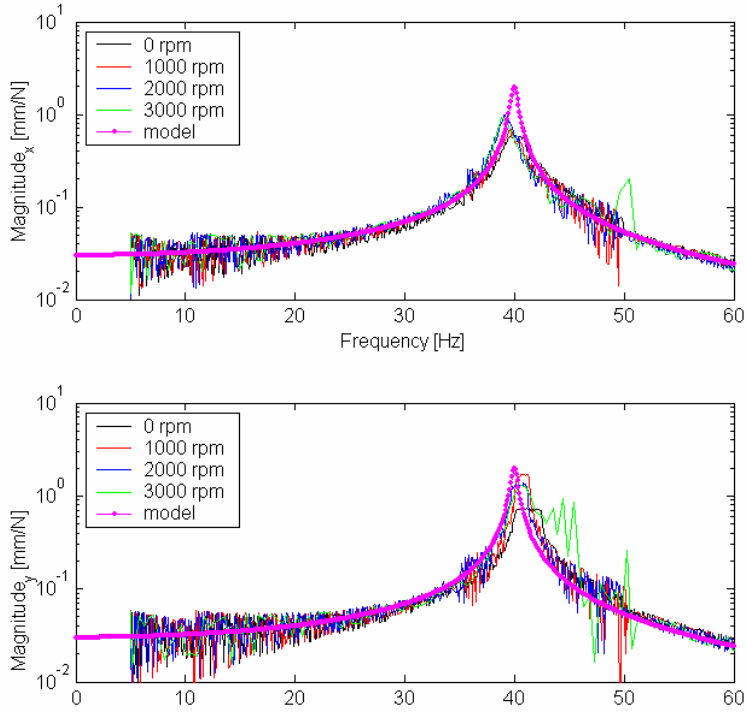

Figure 16. The responses measured at different rotational speeds, compared to the response of a one-degree-of-freedom oscillator (Tammi 2003b).

The test environment was assumed to represent a Jeffcott rotor. To make this assumption valid, the cylindrical armature was located at the midpoint of the slim shaft. Of course, there were some discrepancies: the bearings had finite stiffness, the shaft had a mass, and the shaft was not perfectly balanced. However, the shaft stiffness was assumed dominant compared to the stiffness of the other flexible parts (the bearing stiffness, the actuator mounting stiffness, *etc.*). Similarly, the mass concentrated at the centre of the shaft was assumed dominant. The flexible coupling between the electrical motor and rotor was assumed to have a negligible effect. The Jeffcott rotor assumption was found to be a good first approximation. It appeared substantially simple, since it contained one natural mode with no gyroscopic effects. The actuating point of the force and the placement of the displacement transducers were approximately co-located. In practice, the displacements were measured close to the end of the armature fixed to the rotor. This approximation was justified by the fact that most of the deformation occurred in the slim shaft and not in the stiff armature.

Note that the approximation of collocated system was not particularly accurate for the second natural mode. The actuator was located at the nodal point of the second mode and the sensor was clearly off from the nodal point. However, the second mode was weakly excited because the actuator located at the nodal point and unbalance concentrated in the rotor armature.

The cross-coupling between the orthogonal degrees-of-freedom was assumed to be sufficiently low to be neglected. The magnitude of the transfer function from an excitation force to the displacement in the orthogonal direction was less than one third of the transfer function in the parallel direction (Tammi 2003b).

4.2.2 Control systems used

The Jeffcott rotor was considered as two one-degree-of-freedom oscillators. A simple derivative controller was applied as a feedback controller to increase the damping of the system. The closed-loop transfer function of the oscillator with derivative control becomes

$$H_{cl}(s) = \frac{1}{ms^2 + (c + K_D)s + k} \tag{67}$$

where K_D is the derivative gain (m = 0.528 kg, c = 2 Ns/m, k = 33333 N/m). The gain was selected such that the poles of the closed-loop system exhibited a damping ratio of 0.707, resulting the following closed-loop poles

$$p = -\lambda \pm \mathrm{i}\lambda \tag{68}$$

where λ is a positive constant. The pole placement led to a derivative gain of 186 Ns/m, the poles of the closed-loop system being at (–178 ± i 177) rad/s. An averaging low-pass filter was connected in series with the derivative controller. The pulse transfer function of the discretised feedback compensator is

$$H_{FB}(q) = \left(\frac{K_D}{T_S} \left(1 - q^{-1}\right) \right) \frac{1}{2} \left(q^{-1} + 1\right) \tag{69}$$

where T_S is the sample time, equal to 0.0001 s in the control unit. (Tammi 2003b).

The adaptive FIR filter of order 2 would be *persistently excited* by one frequency (Elliot 2001). However, simulations indicated that the use of an order higher than 2 might lead to a smoother behaviour. For this reason, an order I = 12 was used in the experiments. The weighting coefficients and the filter output were updated with a frequency of 500 Hz. The closed-loop system in Equation (67) was discretised by the zero-order-hold method and used as the system model for the coefficient update in Equation (39). The convergence coefficient was taken as α = 0.01. The sinusoidal reference signal $r(n)$, at an amplitude of unity, was filtered through the closed-loop system model defined in the identification. The sinusoidal reference signal was generated by using revolution pulse sensor. (Tammi 2003b).

For the Convergent Control implementation, the update law in Equation (52) was used. In order to compute the Fourier coefficients, they were first averaged over a time period in order to improve their accuracy. Different integration times were used, from 0.01 s to 1 s. However, no advantages due to this integration were observed and the integration feature was removed for the experiments with the non-collocated layout. Note that this discussion only concerns the computation of the Fourier coefficients; the adaptation law remained the same during the tests. The convergence coefficient used in the tests was equal to 0.1. No leaky feature was introduced (*i.e.* γ = 1). The output of the Convergent Control was updated every 100th control period (about every 0.01 seconds).

The convergence coefficients were different in the case of adaptive FIR and Convergent Control, because the stability limits were different. This, unfortunately, lead to different convergence properties of the algorithms.

4.2.3 Experimental results

Figure 17 shows the displacement signals measured in a run-up test. The run-up was performed from 4.2 Hz to 65 Hz at a rate of 16.7 Hz/min. Feedback control was switched on at 38 Hz, just before crossing the critical speed. The control was switched off at 52 Hz. Active control reduced the response from about 200 microns to about 20 microns. Switching the active control off caused first a transient in the response and then increased the response permanently. Another run-up was performed, from 4.2 Hz to 83.3 Hz, with active control constantly on. The behaviour was smooth; the amplitude of the response did not exceed 22 microns (peak) at any speed (Figure 18).

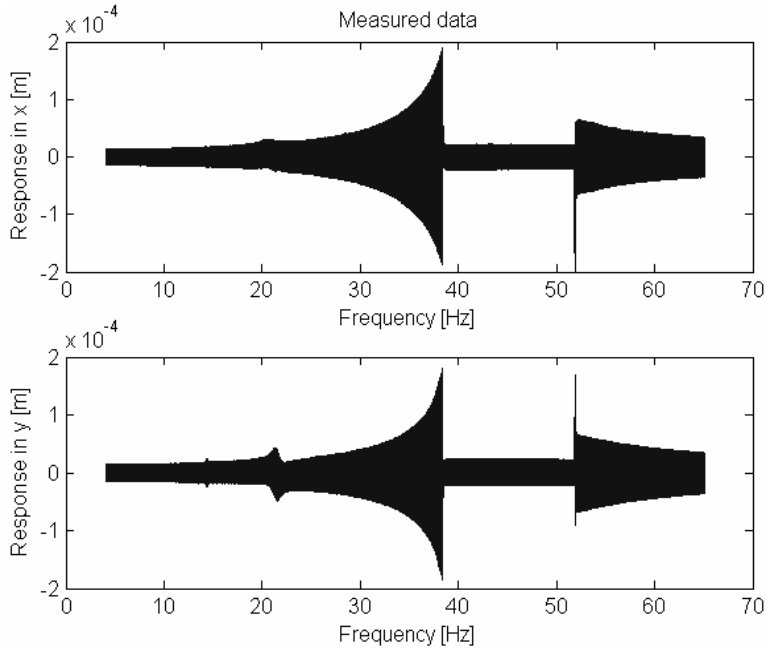

Figure 17. The measured response shown as a function of the rotational frequency (horizontal response at the top, vertical response at the bottom). The feedback control system was switched on at 38 Hz and switched off 52 Hz to demonstrate its effect on the responses.

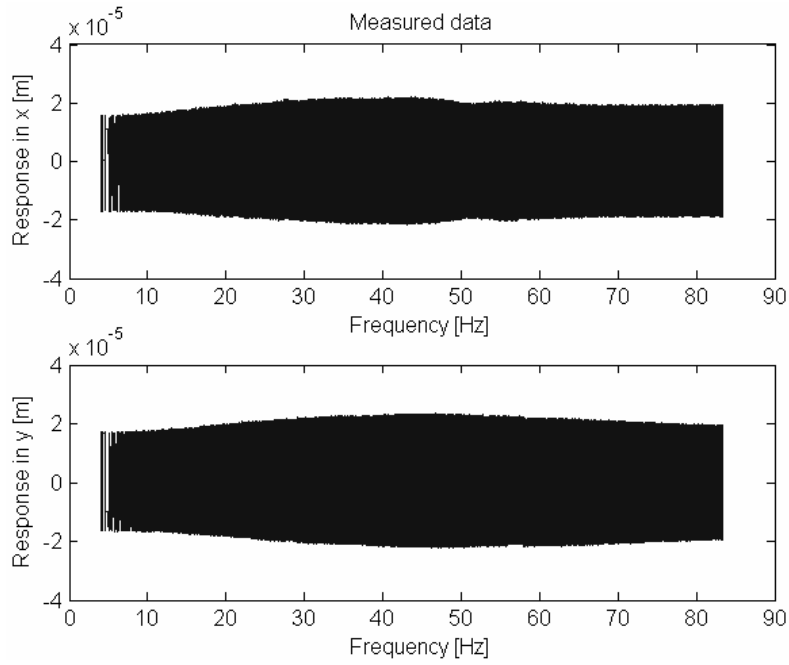

Figure 18. Run-up with active control on from 4.2 Hz (250 rpm) to 83.3 Hz (5000 rpm).

The tests were also carried out with the adaptive x-LMS algorithm running together with feedback control. Figure 19 shows the response during a switch-on period when running at the critical speed. The feedback control system was working alone at the beginning of the time record. The adaptive FIR filter was switched on at about 0.2 s. The response was reduced again: from about 30 microns to about 2 microns. The effect of disregarding the system model was tested briefly. The algorithm with $G_m = 1$ (basic LMS algorithm) worked in sub-critical conditions, but it diverged when the critical speed was approached. The responses increased until the rotor hit the backup bearing. This behaviour was considered consistent with theory, because the phase error between the plant and its model exceeds 90^o at resonance.

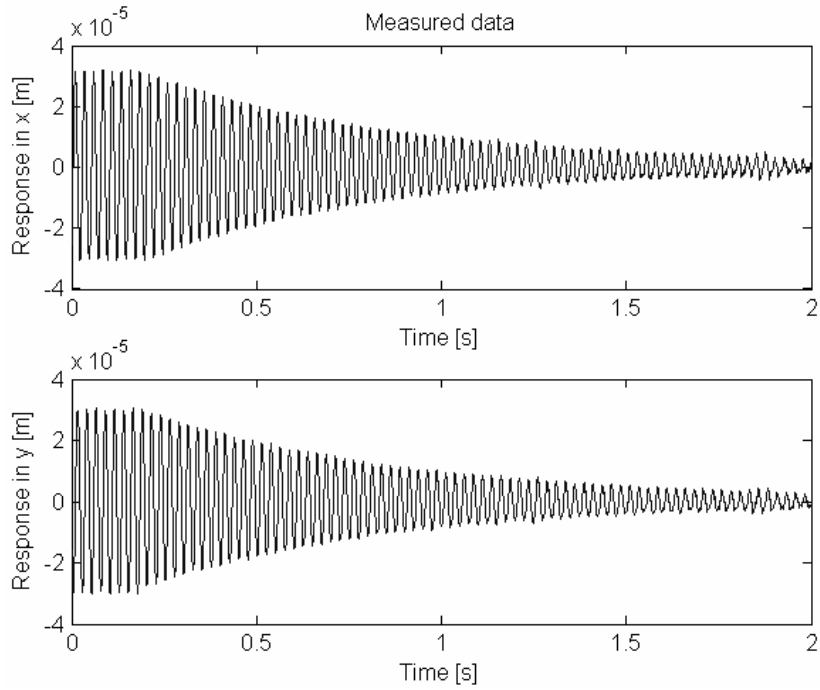

Figure 19. The adaptive FIR filter with system model was switched on when running at 40 Hz. The system converged, reaching the steady-state condition in about 1.5 s.

Figure 20 shows the responses in the horizontal and vertical directions during a sweep from 11 rps to 65 rps. The frequency of the reference signal was changed on-line corresponding to the rotation speed. The response diminished from 5 microns to 2 microns as the rotational speed increased from 11 rps to 18 rps. From 18 rps to 45 rps, the response was approximately constant, being about 2 microns. Above 45 rps, higher peaks in the response occurred randomly. The highest peak observed was 42 microns in the vertical direction. Correlation with the quality of the reference signal was observed. The reference signal had a discontinuity at the instant when the peak occurred.

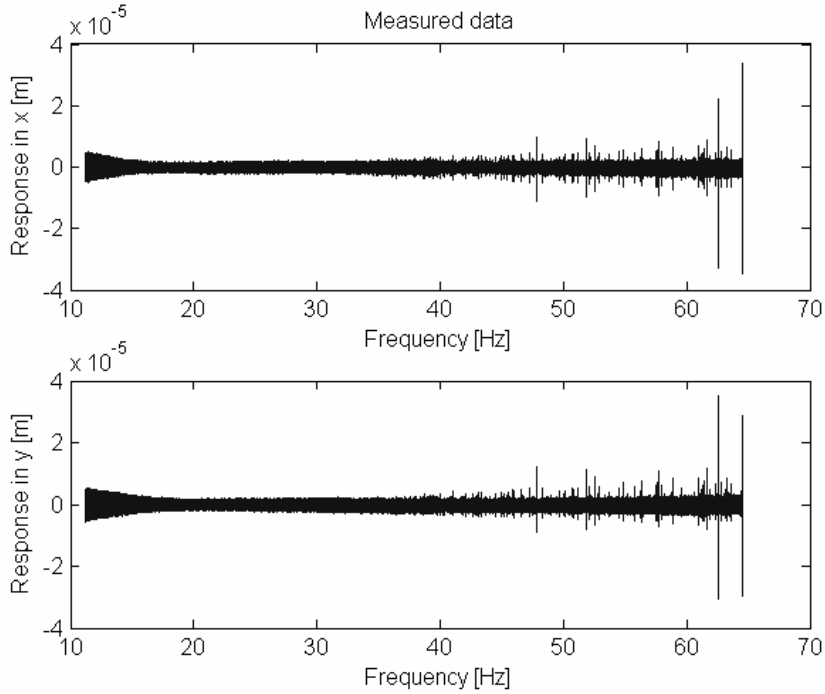

Figure 20. The radial responses with adaptive FIR switched on and the rotational speed swept from 11 rps to 65 rps. (Tammi 2003b)

When carrying out the experiments with Convergent Control, the feedback control path remained the same; only the adaptive feedforward path was changed. Figure 21 shows the displacement response at the rotor midpoint when the Convergent Control algorithm was switched on; the rotational speed was 40 rps (2400 rpm). At the beginning of the time record, feedback control was running alone, the displacement being about 30 microns (peak). The Convergent Control algorithm was switched on and the response decreased to approximately two microns. The convergence was relatively fast; the steady-state condition was achieved in about 0.25 seconds. It should be noted that the convergence rates between the adaptive FIR filter and Convergent Control are not comparable in these results. The over-estimated order of the FIR filter made it necessary to use a lower convergence coefficient, as the maximum stable convergence coefficient α is inversely proportional to the order. Furthermore, searching for the maximum convergence coefficient for the adaptive FIR filter was slightly more difficult than for Convergent Control. This was because the adaptive FIR algorithm used was not of a normalised type whereas the Convergent Control

algorithm was. This means that the feedback gain of the adaptive FIR is dependent on the operating point whereas the feedback gain of the Convergent Control is constant. For these reasons, the convergence coefficient for the adaptive FIR filter was not maximised and thus the convergence rates are not fully comparable. The convergence rate is further discussed in Chapter 6, where all the results achieved are compared.

The performance of the Convergent Control algorithm was also tested in a run-up from 11 rps to 65 rps. The ramp rate was 0.3 rps/s (1000 rpm/min). The displacement response was approximately constant (about 2 microns peak) over the operating range, excluding two separate instants of time (Figure 22). The reason for these peaks was a discontinuity in the reference signals caused by a missed revolution pulse.

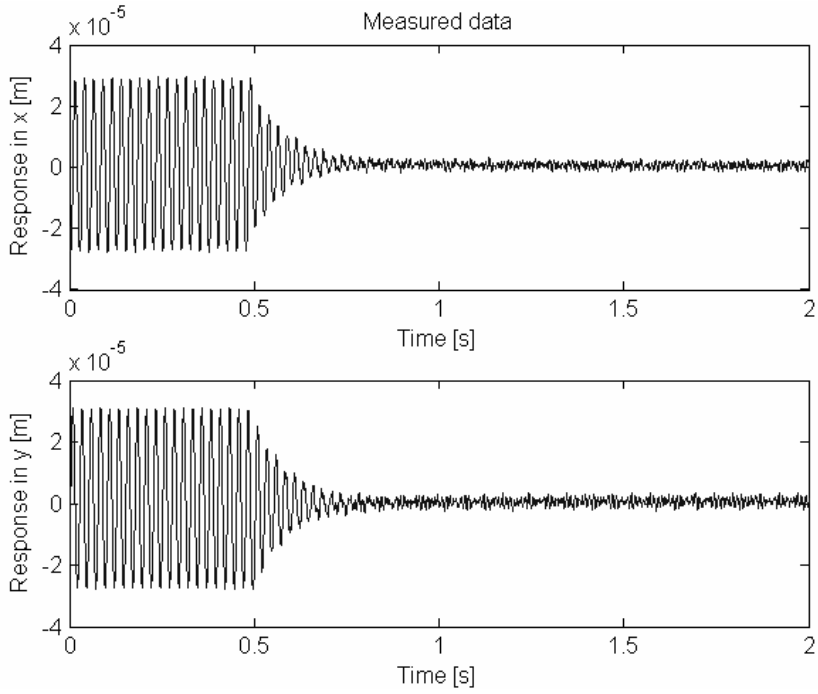

Figure 21. The radial responses measured at switch-on of Convergent Control when running at the critical speed of the rotor (40 rps) (Tammi 2003a).

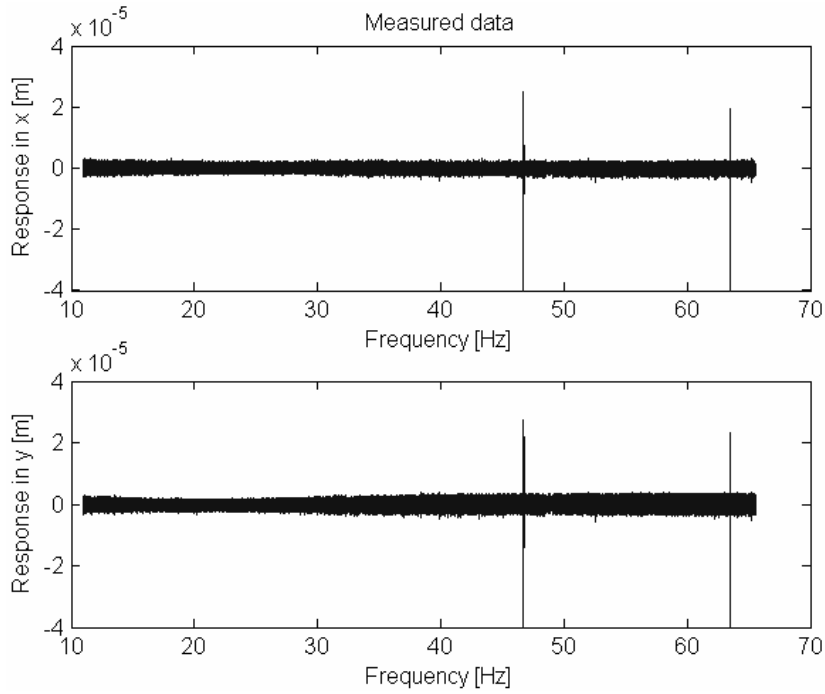

Figure 22. The radial responses with Convergent Control when sweeping the rotational speed from 11 rps to 65 rps at a rate of 1000 rpm/min. The two peaks in each signal were due to discontinuities in the reference signal. (Tammi 2003a).

Table 2 shows the *rms* values of the displacement and control force commands at three rotational speeds. The adaptive FIR and the Convergent Control algorithm reached approximately the same steady-state conditions in terms of the displacements and the forces. It is important to note that the total control force (*i.e.* the net force command) was not increased when using the feedforward compensation although the response was substantially reduced. Hence, the control force was used in a more effective way by the feedforward systems.

Table 2. The rms displacements and the control force commands without control, with the feedback control alone (FB), with the adaptive FIR, and with Convergent Control.

	No control	FB control only		FB + adaptive FIR		FB + Convergent C.	
Speed	Displ.	Displ.	Force	Displ.	Force	Displ.	Force
[rps]	[μm]	[μm]	[N]	[μm]	[N]	[μm]	[N]
25	34	26.2	0.9	1.2	1.1	2.3	1.1
40	220	27.6	1.4	1.1	1.4	1.6	1.4
65	40	24.1	2.1	1.5	2.5	1.6	2.2

4.2.4 Conclusions

Vibrations around the critical speed were efficiently damped by velocity feedback control. It provided a possibility to run the rotor at critical speed by virtue of increased damping. The velocity feedback is a textbook example of active vibration control in general. One reason for this is the characteristically low damping of mechanical systems; a significant reduction in responses can be achieved by a simple controller acting against vibration velocity. Another reason is that the stability of the collocated system can be guaranteed for an ideal control system (Preumont 2002). As in this study, a derivative-type controller was used with a magnetic actuator for controlling rotor vibrations (Cheung *et al.* 1994). The present study supports the use of velocity feedback for active vibration control of rotors.

The results achieved suggested slightly better performance in a steady-state condition for the adaptive FIR than for Convergent Control. On the other hand, the convergence rate of the adaptive FIR remained low compared with Convergent Control.

4.3 Non-collocated layout

The rotor test environment was changed into a more challenging set-up for further studies. Again, the goal was to minimise the radial response at the middle of the rotor, but the actuator was moved outside the bearing span. The position

of the actuator is not optimal for attenuating vibrations at the rotor midpoint. However, in real-life applications, access to the end of the rotor may be much more realistic than to the middle of the rotor. The approach remained similar: the system was first damped using a collocated derivative-type controller. Then, the periodic disturbances were compensated with a feedforward controller. Portions of these results were originally presented in Tammi (2005) and Daley *et al.* (2006).

4.3.1 Layout and dynamics

For the second layout, the dynamics and control objective were more complicated. The vibrations were to be attenuated inside the bearing span of the rotor while the actuator was located outside the bearing span. The test environment had the same 560-mm long slim shaft, but with three disks attached (Figure 23, Figure 24). The disks were fixed to the shaft to make it resemble a machine and to tailor the dynamics of the shaft. The disk locations were chosen in such a way that the rotor exhibits a speed-dependent behaviour, although the speed-dependence was later found weak. The disks' masses determine the dynamic behaviour of the rotor, together with the stiffness of the rotor and the bearings, since the mass of the shaft is considered negligible. The total weight of the rotor including the shaft and three disks was 2.7 kg. The rotor was supported by two journal bearings, 360 mm apart. Radial displacements sensors were situated at two locations along the shaft: at the midpoint and at the end of the rotor (*S1* and *S2* in Figure 23). The electromagnetic actuator was located at the non-drive end of the rotor; the armature corresponds to *Disk 3* in Figure 23.

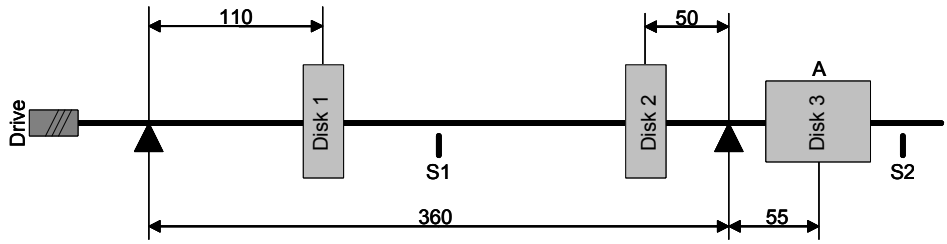

Figure 23. The rotor layout: the displacement sensors at "S1" and "S2" the actuator at "A". The dimensions are in millimetres. (Tammi 2005).

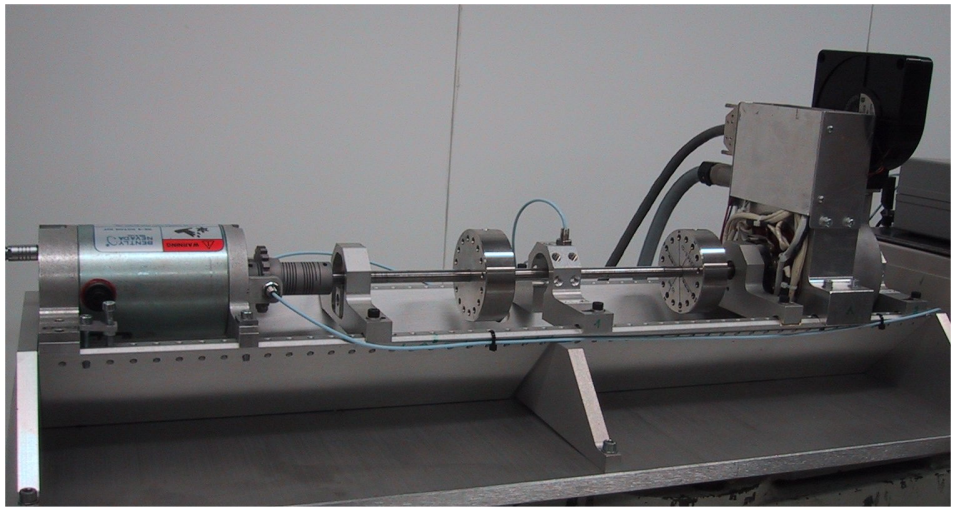

Figure 24. The driving motor (left), the rotor with the disks, and the actuator (right).

Similarly to the Jeffcott rotor layout, the non-collocated layout was subjected to experimental modal analysis. Three modes were detected in both planes (Table 3). The natural frequencies corresponded to the expected values computed using FEM. The equivalent viscous damping values were larger than expected. This was explained by rotor displacement at the bearings whose contribution to the damping was somewhat difficult to estimate. The mode shapes are shown in Figure 25.

Table 3. The results of the modal analysis of the non-collocated layout.

Mode	Frequency [Hz]		Damping [%]	
	horizontal (X)	vertical (Y)	horizontal (X)	vertical (Y)
1st	46	46	2	2
2nd	71	78	12	10
3rd	123	137	12	2

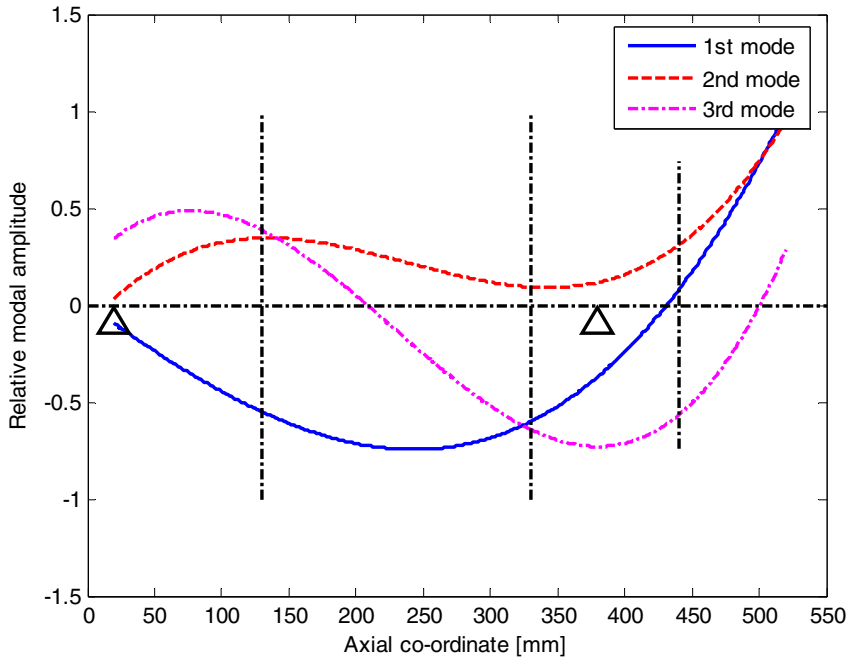

Figure 25. The three lowest mode shapes of the rotor (achieved by the experiments). The non-deformed shape and the disk centre line are shown by the straight black lines. The triangles indicate the bearing positions.

The identification method presented was applied to the rotor desktop test environment in the second layout where the actuator was located outside the bearing span. The modal analysis results were shown above in connection with the description of the layout. This section focuses on the estimation of the transfer functions from the actuator to the rotor midpoint response. These transfer functions will be utilised by the active control algorithms dealt with in the thesis.

The rotor was excited with band-limited white noise by the actuator and responses were recorded at the sensor locations at different speeds of rotation. The band of the noise was from 0 Hz to 400 Hz. The reference signal was generated from the revolution pulse signal (the rotation speed estimate). The reference signal was a sinusoidal signal at a single frequency. Thus, only the disturbances, or forced vibrations, at the frequency of rotation were compensated in the identification. The identification was then performed off-line, using the least squares fit according to Equation (29).

Exciting the rotor properly was found difficult, because of a sharp resonance and the relatively small air gap between the actuator and the rotor armature. A low excitation level was required in order to avoid contact between the rotor and the actuator. On the other hand, the excitation level was not sufficiently high to excite higher frequencies above the first resonance of the rotor. For these reasons, the identification was carried out with the active control system on. The use of the feedback controller prevented the rotor from hitting the actuator. A collocated proportional-derivative control with a low-pass filter was used, as will be defined in Equation (70). During the identification, the proportional control produced an equivalent stiffness of 7 N/mm. The derivative part produced an equivalent damping of 43 Ns/m.

In identification, the order of the dynamic model to be fitted was chosen as $m = 5$ (numerator) and $n = 6$ (denominator). The orders were selected corresponding to the estimated number of significant natural modes of the system. The disturbance model was a two-tap FIR filter as a minimal filter for a sinusoid at one frequency. The two-tap filter was chosen to have a persistently excited filter with a sufficient number of parameters. The identification was carried out at different speeds of rotation. Figure 26 and Figure 27 show the least squares fits with the disturbance compensation method presented, in comparison with the direct frequency response function measurement (FRF) without any disturbance compensation. The frequency responses are shown from the force commands to the rotor displacement. The disturbance compensation was able to remove the peak due to forced vibration at the frequency of rotation. The identification results showed that the first critical speed dominated at about 50 Hz. The next two modes at about 70–80 Hz and 120–140 Hz were weakly observable at the midpoint. This was due to the high damping and low displacement at the midpoint of those modes. The phase curves, however, indicate the existence of the modes. Note that the rotor damping was increased in comparison with the modal analysis results, because the controllers were working during the measurements. Note that the shown phase curves start at 180° because a static force outside the bearing span causes a displacement in the opposite direction at the rotor midpoint.

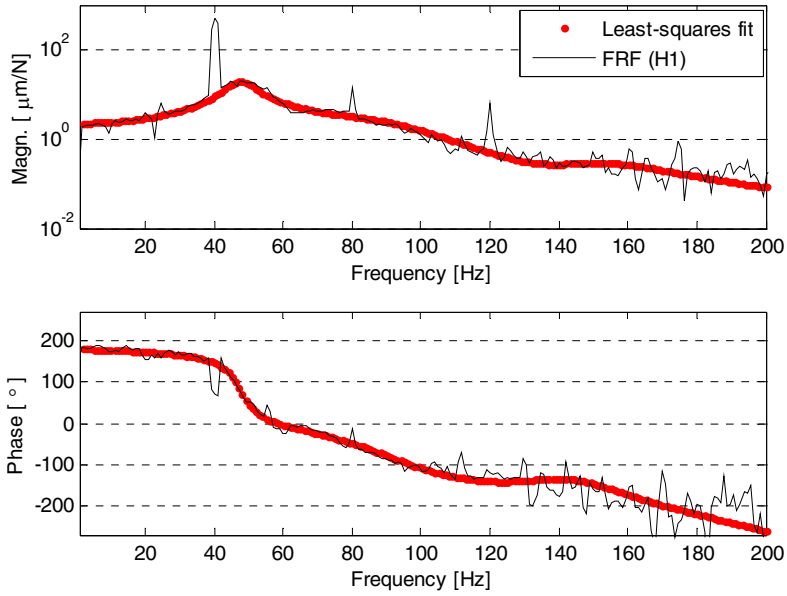

Figure 26. The frequency response function from the actuation point to the rotor midpoint when running at 40 rps. The identification method developed distinguished the rotor resonance from the forced vibration.

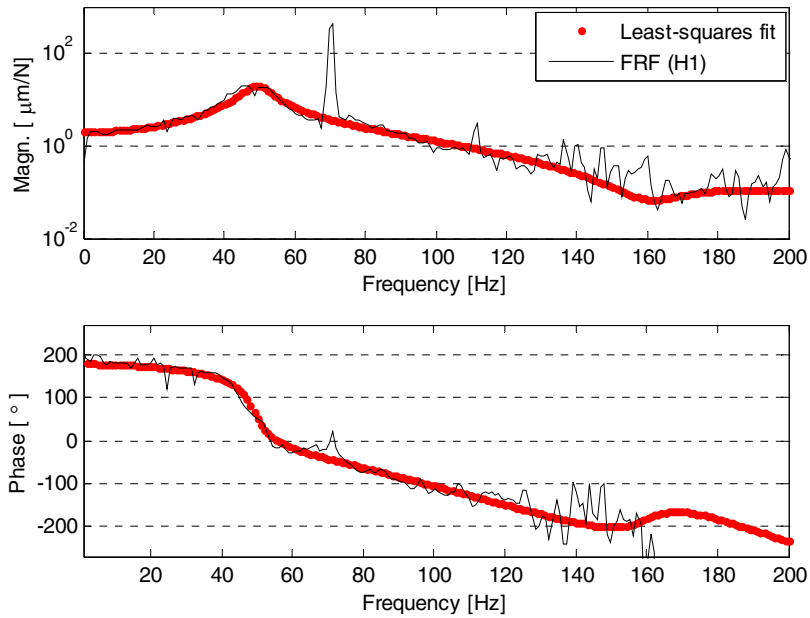

Figure 27. The frequency response function from the actuation point to the rotor midpoint when running at 70 rps.

4.3.2 Control systems used

Two proportional-derivative (PD) controllers together with an averaging low-pass filter were used in the feedback system. The transfer function from the displacement at the rotor endpoint to the force at the actuator was

$$H_{FB}(q) = \left(\frac{K_D}{T_S}\left(1 - q^{-1}\right) + K_P \right) \frac{1}{2}\left(q^{-1} + 1\right) \tag{70}$$

where again K_D is the derivative gain, K_P is the proportional gain, T_S is the sample time. The PD controller was mainly derivative in order to increase the damping of the system. The proportional term was minimal, because a load-carrying effect was to be avoided. The actuator was to have a minimal effect on the stiffness of the rotor. However, a light proportional control was utilised to generate a light centring force due to a relatively flexible overhanging rotor end.

For the feedforward controller, the Convergent Control algorithm in Equation (52) was used. The control systems are shown in Figure 28. The active force at the actuator is generated according to

$$f_{ac}(n) = H_{FB}(q)e_{ep}(n) + H_{CC1}(q)e_{mp}(n) + H_{CC2}(q)e_{mp}(n) \tag{71}$$

where $e_{ep}(n)$ and $e_{mp}(n)$ are the output errors at the rotor end and midpoint, respectively. The pulse transfer functions of the Convergent Control method $H_{CC1}(q)$ are $H_{CC2}(q)$ are defined by its feedback equivalent systems in Equation (66). $H_{CC1}(q)$ is tuned to compensate the first harmonic (the disturbance at the frequency of rotation) and $H_{CC2}(q)$ is tuned to compensate the second harmonic. The first loop ($H_{CC1}(q)$) uses the reference signals (sine and cosine) at the frequency of rotation. The second loop ($H_{CC2}(q)$) uses the reference signals at the two times the frequency of rotation.

Two first harmonics are now compensated in order to compare the algorithms in a multi-harmonic case. However in the current test rig, the excitation levels of higher harmonics are relatively low compared with the first harmonic excitation.

The Fourier coefficients were computed again in each time instant and the results were not averaged (see Section 3.4.3 for the definition of the coefficients). Four feedforward compensation systems were implemented in total, two in each orthogonal radial direction. For both of the control topologies concerned, similar controllers with the same parameters were used in both orthogonal radial directions, except that the model inverses in the feedforward controllers were slightly different, as the identification result suggested.

The model inverses for the feedforward compensation were represented as linear polynomial functions of the rotation speed. The real and imaginary parts of both transfer function inverses were described separately, using fourth order polynomial functions of the rotation speed. This was considered a practical approach; the functions were convenient to fit beforehand and the use of the polynomials reduced the computational effort in the control unit. Another practical choice would have been a look-up table with complex system models as functions of rotation speed.

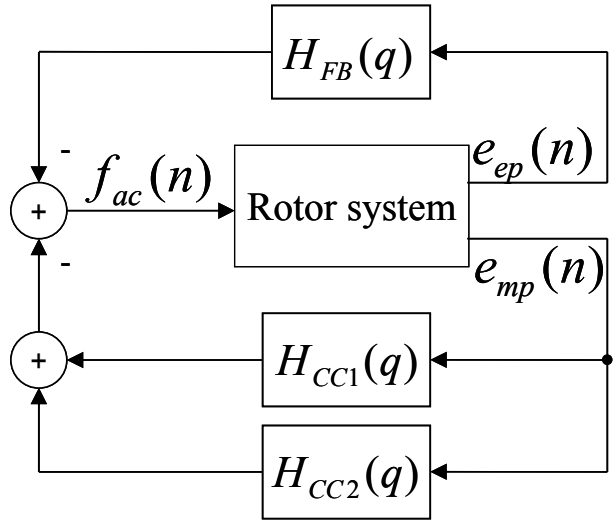

Figure 28. The control systems: feedback above, Convergent Control below.

For the adaptive FIR with the LMS algorithm, a similar control topology was used. The feedback system used was similar; the Convergent Control algorithm was replaced by the adaptive FIR. For the coefficient update, the normalised update scheme in Equation (43) was used. The FIR order was over-estimated to

eight ($I = 8$), as previous findings suggested that over-estimation has positive effects on performance. Similarly to Convergent Control, two reference signals were applied to damp the first two harmonic frequencies. The active force at the actuator was generated according to

$$f_{ac}(n) \approx H_{FB}(q)e_{ep}(n) + H_{FIR1}(q)e_{mp}(n) + H_{FIR2}(q)e_{mp}(n) \qquad (72)$$

where $H_{FIR1}(q)$ are $H_{FIR2}(q)$ are defined by the feedback equivalent systems in Equation (42). $H_{FIR1}(q)$ is tuned to compensate the first harmonic and $H_{FIR2}(q)$ to compensate the second harmonic. Note that the exact feedback equivalent system is valid for compensation of one synchronously sampled disturbance with a FIR filter length equal to the half-cycle of the disturbance, or its multiple. Hence, $H_{FIR1}(q)$ are $H_{FIR2}(q)$ can only considered as approximations (see Section 3.4.1, and Elliot *et al.* (1987)).

The difference from the Convergent Control system is that the FIR system is realised with one filter with a higher order, not with cascaded filters as in Convergent Control. This means that the reference signal is a sum of two sinusoids.

4.3.3 Experimental results with Convergent Control

For the feedback control part, the following parameter values were used in the experiments: $K_D = 86$ Ns/m (derivative gain), $K_P = 7$ N/mm (proportional gain), $T_s = 0.0001$ s (sample time). The same parameters were used throughout the study for the feedback controller. The parameters remained constant also for the experiments with the adaptive FIR and with repetitive control.

The Convergent Control system was designed to damp the first two harmonic frequencies at the rotor midpoint. The convergence coefficient was adjusted such that the convergence was as fast as possible without a risk of instability or fluctuations during the convergence. The leak coefficient was less than unity at the speed of 70 rps and higher (see Table 4 for the exact figures). Because of the dynamic characteristics of the system, to achieve vibration attenuation at the rotor midpoint it was required to amplify vibrations at the endpoint at super-critical speeds. For this reason, the control actions caused the rotor armature to

hit the actuator at high speeds. The leak coefficient γ was then used to reduce the control force at higher speeds in order to prevent the rotor armature from hitting the actuator. Unfortunately, this reduced the effectiveness of the control at higher speeds.

Note that the use of the leak coefficient was caused by the test rig geometry and dimensions, not by bad characteristics of a control algorithm. The frequency response from the actuator to the rotor endpoint had higher gain than the response to the midpoint (Figure 29). In terms of the phase curves, the responses were approximately opposite for sub-critical speeds. When the resonance was approached and exceeded, the phase difference decreased. Due to the geometry, simultaneous attenuation at the midpoint and at the endpoint was possible only for the frequencies where the responses were in roughly opposite phase.

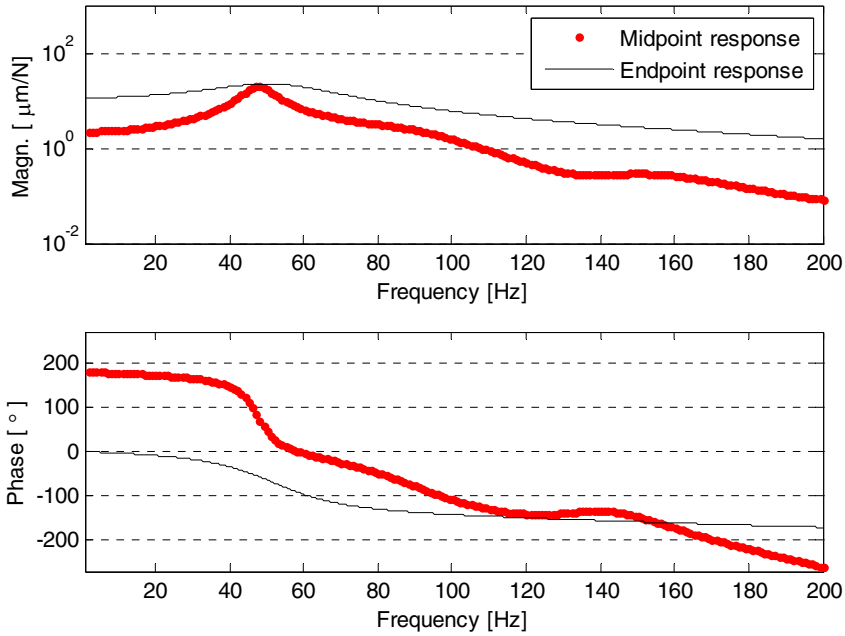

Figure 29. Comparison of the frequency responses at from the force commands to the rotor midpoint and to the endpoint.

The results are shown as radial displacements of the rotor shaft as a function of time or frequency. Those functions are defined

$$|r(n)| = \sqrt{(e_X(n))^2 + (e_Y(n))^2}$$
$$|S_r(f)| = \sqrt{(S_X(f))^2 + (S_Y(f))^2} \quad (73)$$

where $r(n)$, $e_X(n)$, and $e_Y(n)$ are the displacements in the radial direction, in the X plane, and in the Y plane, respectively. $S_r(f)$, $S_X(f)$, $S_Y(f)$ are the spectra in the corresponding directions. The Autopower method (see *e.g.* Proakis & Manolakis (1996)) to compute the spectra $(S_X(f))^2$ and $(S_Y(f))^2$ have been used in this work. The spectrum graphs show the peak values of the signals analysed. A standard format to show the steady state results is adopted in this work: The autopower spectra are compared in the upper panel of the figure, and the relative attenuation in dB is shown in the lower panel. Attenuations are plotted against the relative frequency scaled with respect to the critical speed of the rotor

$$f_r = \frac{f}{f_{cr}} = \frac{\omega}{\omega_{cr}} \quad (74)$$

where f is frequency and f_{cr} is the critical speed of the rotor. Those plots also contain green lines to indicate the level of 1 μm in responses (upper panel) and 0 dB level in attenuation (lower panel).

Figure 30 shows the radial response spectra at 25 rps without control, with the feedback controller, and with the Convergent Controller working on the first two harmonic frequencies. At the first harmonic (25 Hz), the attenuation achieved was nearly 30 dB (referring to the difference between the non-controlled and the feedforward controlled responses). At the second harmonic, the attenuation was less than 10 dB, but also the peak to be attenuated was also significantly lower. Note also that the absolute vibration levels were relatively low; the green line is drawn in Figure 30 to indicate 1 μm displacement level. The vibration levels measured were close to the estimated noise floor of the sensors.

The *rms* responses were measured at different rotation speeds; they are shown in the next section together with the responses achieved with the adaptive FIR filter (Table 4 and Table 5).

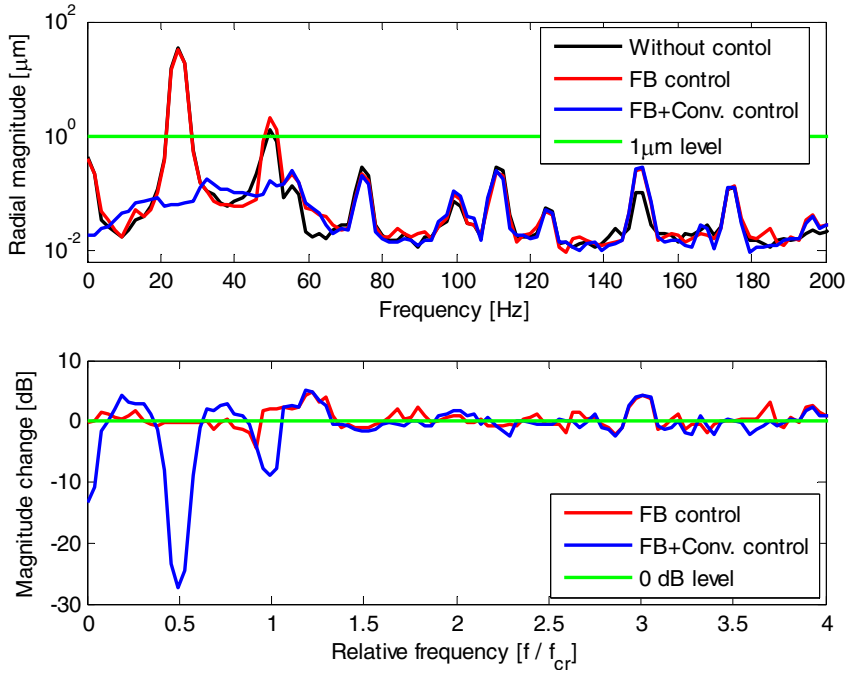

Figure 30. The rotor midpoint radial response when running at a constant speed of 25 rps. (Daley et al. 2006).

Figure 31 shows the ramp responses with the feedback control and Convergent Control, measured during a constant ramp down at a rate of 4000 rpm/min (1.1 rps/s). The radial response with Convergent Control remained below one micrometer over the rotation speed span from 10 rps to 65 rps (a figure with a better scaling is provided together with the responses of the adaptive FIR).

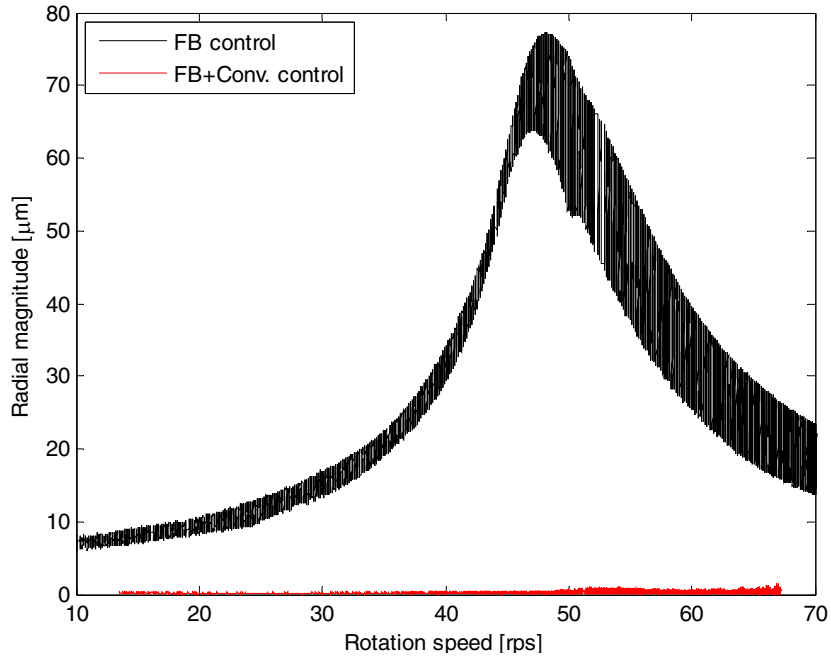

Figure 31. The radial responses during a ramp down at the rotor midpoint with the feedback controller working alone, and together with Convergent Control.

4.3.4 Comparative results with adaptive FIR

In comparison with the Convergent Control arrangement, the adaptive FIR system contained the same feedback control system and it was also designed to attenuate the first two harmonic frequencies. The convergence coefficient was adjusted is such a way that the convergence was as fast as possible without risk of instability or fluctuations during the convergence. The leak coefficient was less than unity at the speed of 90 rps and higher (see Table 4 for the exact figures). Again, the integrator's leak coefficient γ was used to reduce the control force at higher speeds of rotation in order to prevent the rotor armature from hitting the actuator. This was again due to fact that vibration attenuation at the midpoint required vibration amplification at the endpoint.

Figure 32 shows the responses without control, with feedback control, and with the adaptive FIR. The attenuation of the first harmonic exceeded 20 dB, but it remained somewhat smaller than with Convergent Control.

A significant difference was that the second harmonic was not attenuated at all, although the corresponding frequency component was included in the reference signal. This was suspected to be due to a large difference between the disturbance amplitudes of the first and the second harmonic. Dominating first harmonic was suspected to prevent the compensation of the second harmonic.

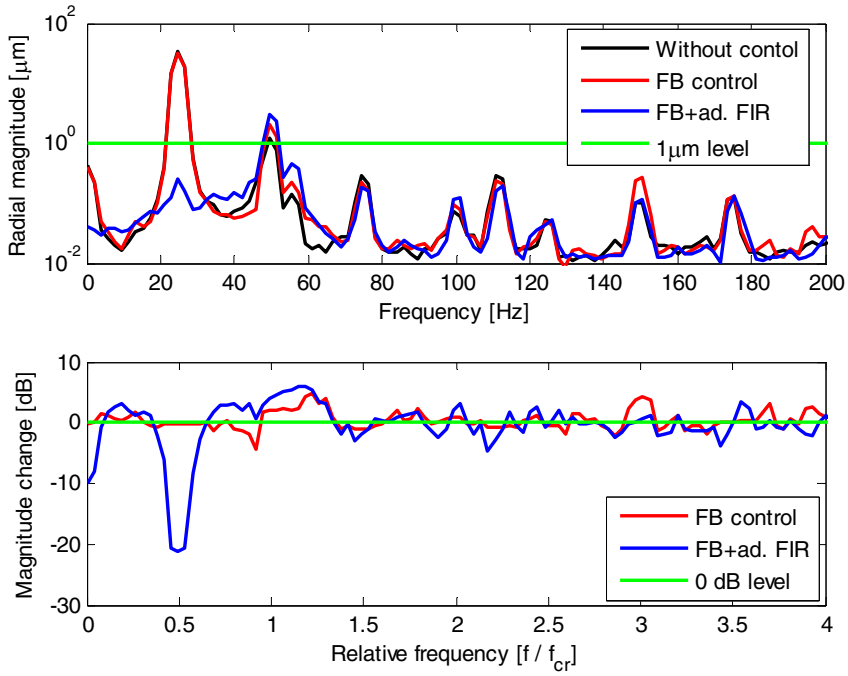

Figure 32. The rotor midpoint responses at 25 rps.

Table 4 shows the responses at the rotor midpoint at different rotation speeds in three operating modes: without active control, with feedback control working alone, and with feedback and feedforward control working together. The responses presented are the *rms* values of the radial displacements, computed in the frequency band from 0 Hz to 1 kHz. Table 4 shows the displacement at the midpoint and at the end together with the control force commands. The responses at the speeds of 90 and 110 rps with the adaptive FIR are shown in parentheses, because the FIR behaviour was restless at those speeds. The system converged, but the convergence was uneven and interrupted by fluctuations. The algorithm was not considered usable in the region, because of fluctuations and sudden peaks. The exact reason for the behaviour was not found, but the quality of the reference signal was suspected to be one reason. As in the previous

experiments, the adaptive FIR was found sensitive even for small discontinuations in the reference signal.

The response magnitude at 50 Hz without any active control on was estimated because it was not possible to run at that speed without the rotor hitting the actuator. Table 5 shows the corresponding response values at the rotor end. The responses show that attenuation of vibrations at the midpoint required amplification at the endpoint for super-critical speeds.

Table 4. The rms displacements and control force commands at the rotor midpoint with different speeds.

	No control	FB control only		FB + adaptive FIR		Leak	FB + Convergent C.		Leak
Speed	Displ.	Displ.	Force	Displ.	Force	Coeff.	Displ.	Force	Coeff.
[rps]	[μm]	[μm]	[N]	[μm]	[N]	γ	[μm]	[N]	γ
10	15	11.0	0.8	1.6	2.8	1	0.5	2.3	1
30	33	17.3	1.7	1.3	2.8	1	0.9	2.5	1
50	111	61.2	2.9	1.2	3.0	1	1.3	2.6	1
70	21	17.9	1.8	2.5	8.1	1	11.8	4.8	0.99995
90	13	16.2	1.5	(18)	(7)	0.999	10.7	7.7	0.9999
110	15	16.3	2.3	(20)	(2)	0.995	13.2	4.6	0.9995

Table 5. The rms displacements at the rotor end.

	No control	FB control only		FB + adaptive FIR		Leak	FB + Convergent C.		Leak
Speed	Displ.	Displ.	Force	Displ.	Force	Coeff.	Displ.	Force	Coeff.
[rps]	[μm]	[μm]	[N]	[μm]	[N]	γ	[μm]	[N]	γ
10	107	91.2	0.8	57.3	2.8	1	52.2	2.3	1
30	137	94.7	1.7	70.2	2.8	1	62.9	2.5	1
50	194	101.4	2.9	116.9	3.0	1	125.8	2.6	1
70	83	45.9	1.8	200.4	8.1	1	141.1	4.8	0.99995
90	39	28.6	1.5	(115)	(7)	0.999	121.2	7.7	0.9999
110	45	36.6	2.3	(40)	(2)	0.995	65.2	4.6	0.9995

Again, a test ramp, at a rate of 4000 rpm/min downwards, was run with the adaptive FIR (Figure 33). The midpoint response with the adaptive FIR was in the order of two micrometers, whereas the response with Convergent Control remained below one micrometer.

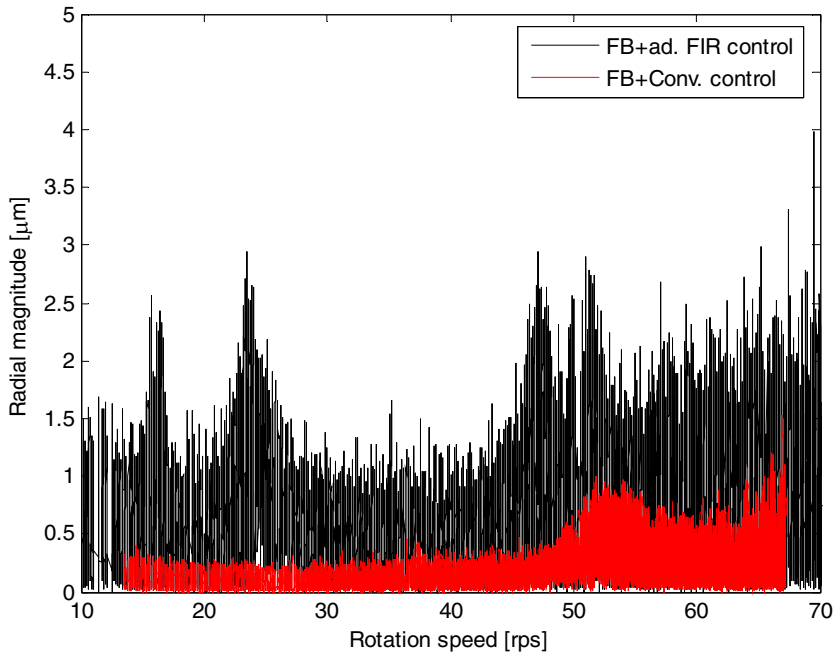

Figure 33. Comparison of radial responses at the rotor midpoint with Convergent Control and with the adaptive FIR working.

4.3.5 Conclusions

The identification method presented was shown to work with the rotor kit and it is considered to be one potential way of compensating the disturbance in the output when identifying a rotor system during operation. Other solutions exist, but they are only mentioned briefly in this section, because identification was not in the main focus of this work. The following approaches are left for further consideration:

- The use of a pseudo random excitation and time domain averaging in such a way that the disturbances are averaged out. The length of the pseudo random sequence should be relatively long with respect to the disturbance period.
- The use of windowing functions in data acquisition in such a way that the forced vibrations are filtered out. The length and the shape of the window should be set according to the speed of rotation.

- Filtering the effects of excitation out with a notch filter before identification. The approach is very close to the present approach where the disturbance is fitted to a model and compensated by a reference signal.
- Carrying out the identification procedure as such and then removing the forced vibration peaks in the frequency plane. This procedure is traditionally used in manual identification.
- Using the orthogonal direction displacement and assuming negligible cross-coupling in the system. The disturbance acts in a similar manner in both directions, but the excitation acts mainly in the excitation direction. The effect of the response can then be computed by applying the superposition principle.

In the case of the Convergent Control method, the vibration attenuation at the midpoint of the rotor with an actuator located outside the bearing span was found effective. At sub-critical speeds the remaining controlled response was from 1 % to 3 % of the uncontrolled response at the midpoint. For super-critical speeds, the remaining responses were larger, from 60 % to 90 %, because of restrictions of the allowable control force at super-critical speeds. Firstly, attenuation at the midpoint was realised at the expense of amplification at the actuator (or at the rotor end). This behaviour was considered understandable, because of the phase change over the critical speed. Secondly, a more practical restriction was the limited control authority at the actuator. The control authority was limited by the leaky coefficient, less than unity, in order to prevent the rotor armature from hitting the actuator. Limited amplitude at the actuator caused limited achievable damping at the midpoint when running above the critical speed.

The performance of the adaptive FIR filter was poorer than the performance of the Convergent Control method in steady-state and in transient conditions. In steady-state conditions, the differences were not that large as in ramp-down conditions. Also, the adaptive FIR gave a less robust impression in the tests than the Convergent Control. The adaptive FIR exhibited uneven convergence in different planes (X and Y directions), fluctuation in responses and a higher sensitivity to disturbances in reference signal or to external excitations. This behaviour was particularly evident at speeds higher than 70 rps. No specific reason was found for uneven convergence rates. Also, an unexpected result was that the FIR system was incapable of attenuating the second harmonic.

Theoretically, the system should work at all frequency components present in the reference signal (Elliot 2001). The author suspects that the behaviour was due to low vibration levels at the second harmonic compared with the dominating first harmonic. The behaviour can also be linked to the length of the adaptive FIR filter with respect to the disturbance period. By the filter length, the author means the filter order multiplied by the sample time. This argument comes from successful applications that use a relatively long adaptive FIR and the LMS algorithm for wideband damping, see *e.g.* Kuo & Morgan (1996), Van Der Poel *et al.* (2006), or Kataja (1999).

The results show clearly how controlling one point amplifies another in the shaft. Having a smaller number of actuators than natural modes to be controlled is a compromise with regard to the overall damping (Gawronski 1996, Utku 1998). The results indicated that the derivative control was able to provide some attenuation at the midpoint in the super-critical region. This was due to the dissipative nature of the controller. The damping increase at the end of the rotor was able to contribute to the damping of the first natural mode. The increase, however, was not very effective, owing to the location of the actuator and the geometry of the rotor. The feedforward algorithms were effective also in the super-critical region. However, the displacement at the end increased rapidly with increasing speed.

4.4 Roles of controllers

Earlier in this work it was mentioned that dissipative feedback control was implemented in order to increase the damping of the system. In the experimental results, the contribution of the feedback system may be modest under certain operating conditions. This raises the question: why use the dissipative feedback control? One reason is to design a system that is capable of damping wideband excitation. Such excitations did not occur in the test, but they do occur in practical environments in the form of different noises and impacts in the machine surroundings. Another reason for feedback control is to tailor plant characteristics or to condition the plant for feedforward control. This section presents a justification of the use of feedback control for plant conditioning from the feedforward control point-of-view.

For adaptive feedforward compensation systems, the model used by an adaptation algorithm has to describe the phase of the plant to within ±90° (Ren & Kumar 1989, Elliot 2001) (note that the derivation of the requirement contained assumptions of small gains and slowly-changing dynamics of the plant). Moreover, analysis gave the requirements for the modelling accuracy of the system gain. These requirements are, however, less stringent if the α convergence coefficient is chosen conservatively. The requirement is often considered loose and easy to meet. However, in the author's experience, the requirement can be difficult to meet in the vicinity of lightly damped poles or zeros where phase varies rapidly. Especially, for lightly damped mechanical systems, the limit could be exceeded if the system parameters were estimated incorrectly or parameters vary over time. A cause for a change may be variation of the machine temperature, or wear, for instance.

Consider the complex response of a single resonance of the plant to be compensated.

$$G(\mathrm{i}\omega) = \frac{\omega_p^2}{\omega_p^2 - \omega^2 + \mathrm{i}2\xi_p\omega_p\omega} \tag{75}$$

where ω is the angular frequency variable, ω_p is the natural angular frequency, and ξ_p is the damping of the plant. Assume that this resonance dominates the phase characteristics in a certain frequency band of interest, say from ω_1 to ω_2. Also, assume the order of the system in Equation (75) has been estimated correctly. Thus, the model of the plant can be expressed as

$$G_m(\mathrm{i}\omega) = \frac{\omega_m^2}{\omega_m^2 - \omega^2 + \mathrm{i}2\xi_m\omega_m\omega} \tag{76}$$

where ω_m and ξ_m are the estimated natural frequency and the damping of the model used by the feedforward compensation system. Consider then the phase errors caused by an incorrect estimate of the natural frequency or the relative damping.

$$E_{phase} = \max\left(\left|\angle G_m(\mathrm{i}\omega) - \angle G(\mathrm{i}\omega)\right|\right), \quad \omega \in [\omega_1 \quad \omega_2] \tag{77}$$

Figure 34 shows the phase error contours between the model and the plant as a function of the modelling error and of the relative damping. The contour plot shows the phase error curves of 60° and 90°; the former representing a limit for an appropriate performance and the latter the absolute stability limit. In particular, relatively small modelling errors in natural frequency can cause large phase errors for a lightly damped system, because of the rapid changes in phase in the resonance region. For instance, if the natural frequency estimate had an error of 5 %, and the damping were less than 3 %, it could lead to an unstable feedforward system. In this example, the damping was assumed to be estimated correctly. Figure 35 shows the error contours as functions of the errors in the natural frequency and the damping; 10 % of nominal damping was assumed. The plot indicates that the phase errors are not as sensitive to errors in the estimated damping as they are to errors in the natural frequency. Again, this is due to the rapid phase change in the resonance region.

The discussion above provides a new viewpoint for engineering design. The design charts presented here (Figure 34 and Figure 35) are helpful in estimating the conditions from the feedforward control point of view. If the damping of the plant is low and the estimated natural frequency values are uncertain, it is advantageous to make the phase behaviour smooth with a feedback controller. The discussion also indicates that it may be safe to exaggerate the damping in the plant model. A smoother phase curve would cause smaller maximum errors than an absolutely correct phase curve, if there is a modelling error in the natural frequency.

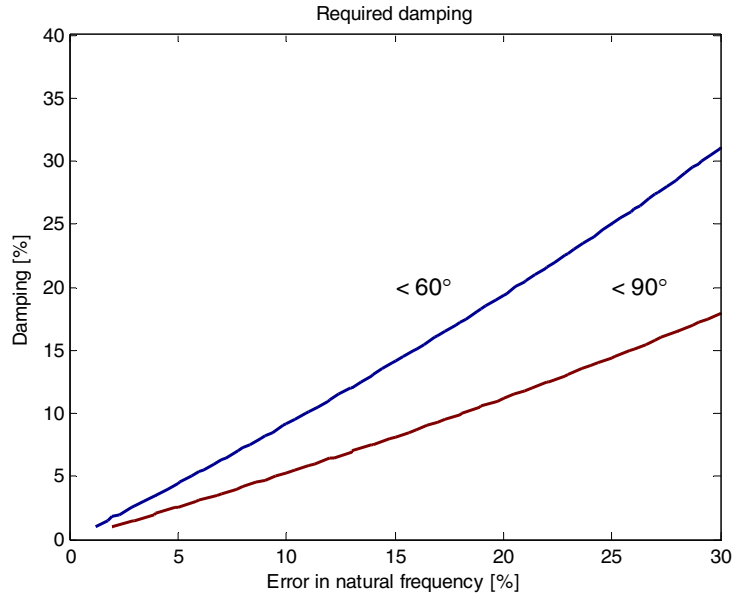

Figure 34. The phase error contour curves as a function of the modelling error in the natural frequency and in the relative damping. The largest stability margins are close to the Y-axis. (Tammi 2005).

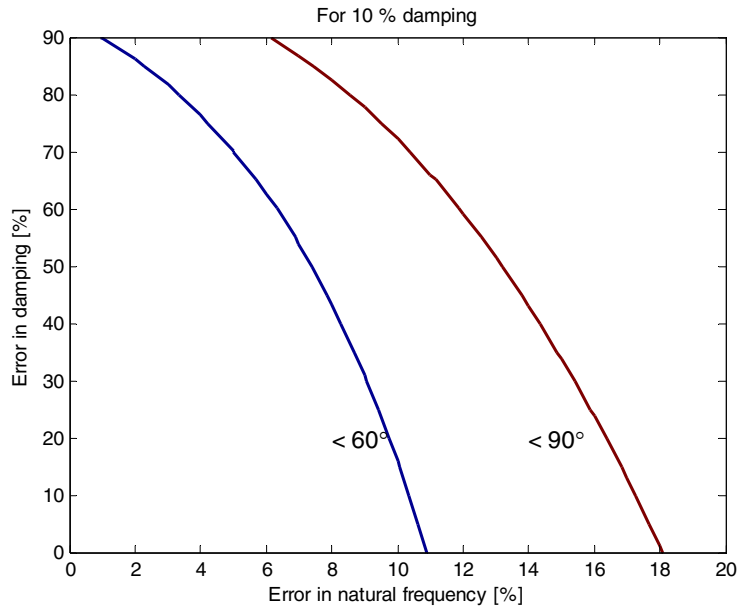

Figure 35. The phase error contour curves as a function of modelling error in the natural frequency and in the relative damping (Tammi 2005).

In practice, usually only the model of the system is available. To evaluate the robustness of the adaptive feedforward system, the author suggests successive frequency responses to be used as an error indicator

$$E_{ind} = \left|G_m(\mathrm{i}\omega)\right|^{-2} G_m(\mathrm{i}\omega)\overline{G}_m(\mathrm{i}(\omega+\Delta\omega)), \quad \omega \in \left[\omega_1, \quad \omega_2\right] \tag{78}$$

where $\overline{G}_m(\mathrm{i}\omega+\Delta\omega)$ is the adjacent of the complex response computed at a slightly different frequency, $\omega + \Delta\omega$, than the base frequency ω. For small $\Delta\omega$, the indicator should be approximately unity (matrix). A suitable magnitude for $\Delta\omega$ should be considered according to the application. Figure 36 shows an example of the error indicator phase for a transfer function of a non-collocated layout ($\Delta\omega$ = 31.4 rad/s).

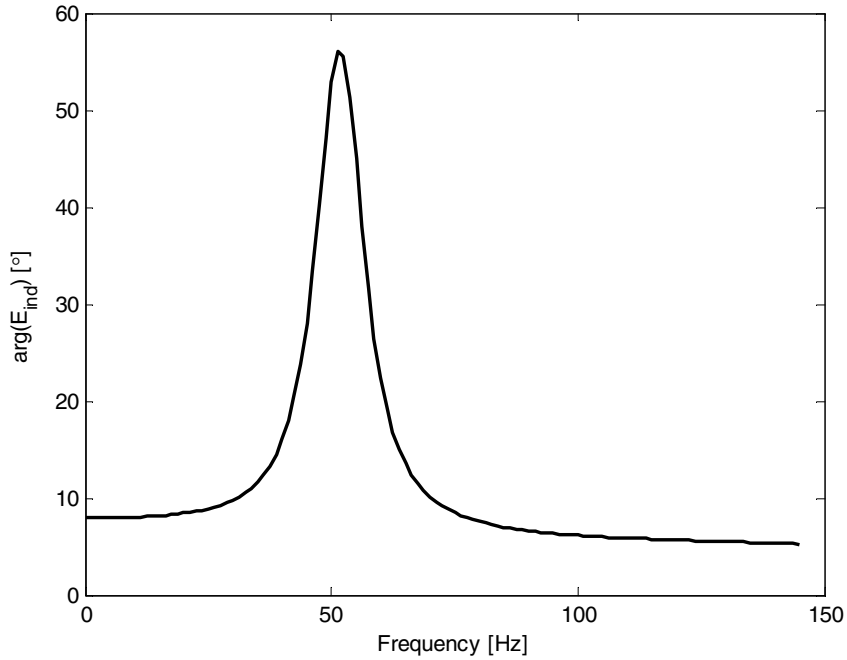

Figure 36. The phase of error indicator for evaluation of the phase curve smoothness in Equation (78) ($\Delta\omega$ *= 31.4 rad/s).*

4.5 Chapter summary

This chapter dealt with the experimental validation of the identification method and feedforward algorithms. The identification method consists of compensating load disturbances due to rotation, ahead of the actual identification procedure. The adaptive FIR with the LMS algorithm and the Convergent Control algorithm were tested on the Jeffcott rotor and on non-collocated layouts. Briefly, the Convergent Control method was found a more suitable algorithm for rotor vibration control than the adaptive FIR. The statement is due to the smooth behaviour of Convergent Control over the operating range, its ability to damp both harmonics concerned, and better performance during a speed ramp. The results achieved will be compared with a repetitive control implementation presented in the next chapter.

The required modelling accuracy of a feedforward system imposes requirements on the plant to be damped and on the plant model to be used, in terms of sufficiently smooth phase characteristics. The discussion showed that lightly damped systems require additional damping provided by another controller besides a feedforward controller. Also, the discussion presented tools (the design charts and the error indicator) for evaluating the robustness and stability properties of an active feedforward system.

5. Repetitive control

The internal model principle states that a system has to contain a model of a signal in order to track or compensate the signal perfectly (Francis & Wonham 1975). This idea has been utilised in the compensation of rotation harmonics in rotor vibration control. The three methods studied in this thesis make use of the internal model principle. In the feedforward systems, the model of the signal is in the form of a reference signal. In the repetitive control systems, the signal is learnt by means of a delay line with positive feedback.

The original idea of repetitive control was presented by Inoue *et al.* (1981) for high accuracy control of a magnet power supply. The aim was to develop a controller that tracks a periodic control signal. The use of positive feedback and a delay line made it possible to track the control signal perfectly. This property made repetitive control an attractive solution for compensation of periodic disturbance signals. Figure 37 shows a basic disturbance compensation scheme with a repetitive controller. The magnitude of the output error, $e(s)$, to be minimised, is fed back. Also, the old control outputs are fed back, with a positive loop gain. This leads to a control law where controller outputs are updated (taught) by the realised output errors.

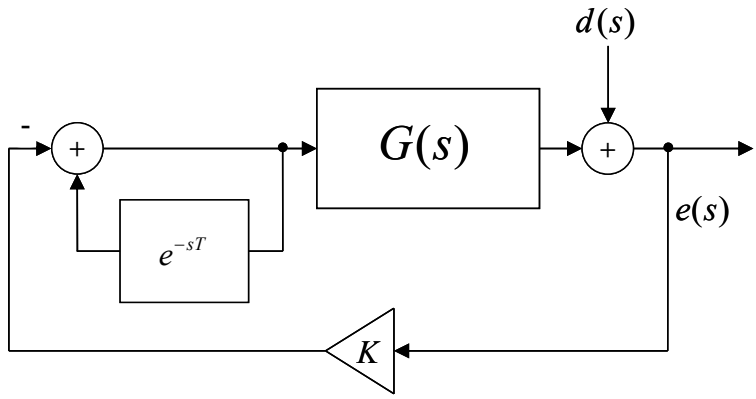

Figure 37. The basic scheme of the repetitive control.

Figure 38 shows a simulation example carried out on the system in Figure 37 with $G(s) = 1$. The delay T is set such that it matches the frequency components

in the disturbance signal ($1/T$ and $2/T$). The control signal is learnt during about eight periods in such away that the output error $e(t)$ is driven to zero.

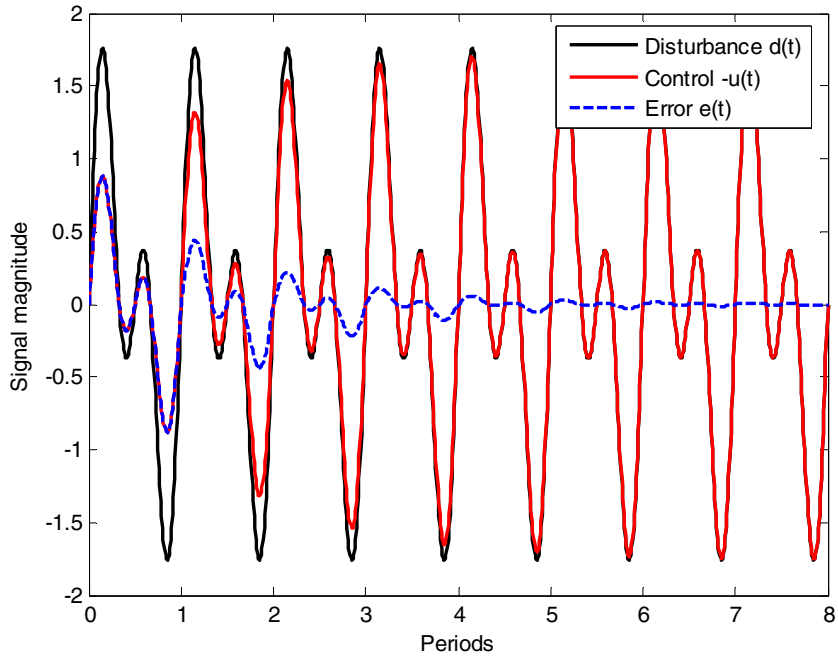

*Figure 38. Simulation example of the basic repetitive controller. The signals are plotted against the fundamental period of the disturbance (1/*T*).*

Potential solutions for repetitive control have been found in tracking or compensation problems generally (Medvedev & Hillerström 1993, Hillerström & Sternby 1994), in robotics (Fung *et al.* 2000), in computer disk drives (Tomizuka *et al.* 1989, Kempf *et al.* 1993, Smith *et al.* 1999), in peristaltic pumps (Hillerström 1996), *etc.* A periodic disturbance, often due to rotary movement, can be found as the common denominator behind the applications.

5.1 Introduction to repetitive control

As explained above, repetitive controllers were developed to track or to compensate periodic signals. The idea behind the repetitive control method is to continuously refine the control output by using old control outputs and error data. The control law in continuous time, as its simplest, is

$$u(t) = u(t-T) - Ke(t) \tag{79}$$

where $u(t)$ are the control outputs, $e(t)$ is the error quantity and T is the delay time, and K is the feedback gain. The delay time is to be set equal to the period of the signal to be tracked or compensated. Positive feedback of the delayed signal leads to high, ideally infinite, feedback gain at frequencies matching the inverse of the delay time

$$f = \frac{n}{T} \tag{80}$$

where n is a non-negative integer corresponding to the harmonic number. A sufficient condition for stability of the repetitive controller is that the system loop gain must be positive real, because of the high feedback loop gain. In Figure 39, the loop gain is plotted against the harmonic number (n). The requirement of positive realness can be understood by considering the denominator of the closed-loop system with repetitive controller

$$H_{rep}(s) = \frac{u(s)}{d(s)} = \frac{-K}{1 - e^{-sT} + KG(s)} \tag{81}$$

where $KG(s)$ represents the loop gain transfer function of the system. The real part of the $KG(s)$ must be positive in order to maintain the stability (to prevent the denominator from being zero). In the other words, the phase of $KG(s)$ must be within $\pm 90^{o}$. These requirements guarantee stability, because positive real systems can tolerate infinite feedback gain. The result can be understood by considering the classical Nyquist stability criterion that states that the loop gain must not encircle the point (–1, i 0) in the complex plane. If $KG(\mathrm{i}\omega)$ has a positive real part, it cannot encircle the point, regardless of the feedback gain. Note again that the requirement stated is a sufficient condition for stability and less conservative requirements exist.

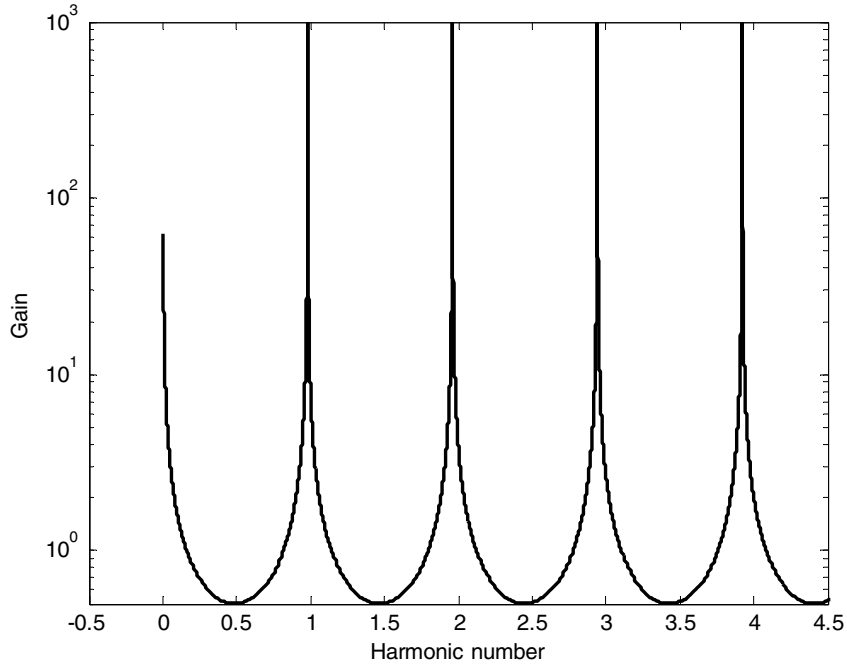

Figure 39. The loop gain of a repetitive controller.

Remark 6

The requirement of positive realness is the same as the model accuracy requirement for the feedforward compensators, which states that the plant model must represent the plant within a phase range of ±90^o over the bandwidth of the controller.

Remark 7

The requirement of positive realness is relatively stringent for mechanical systems, which often have resonances and anti-resonances, where phase changes often exceed 90^o.

The basic repetitive controller was presented above using the continuous time formulation. Moving to the discrete time domain may ruin the stability, since sampled systems are rarely positive real. It has been shown that a discrete system can be a positive real system only if the system's output is directly influenced by the inputs, *i.e.* the direct term in the state-space representation is

not equal to zero (Hätönen 2004). As known, the direct term is frequently equal to zero in practical systems with finite sampling frequency. This can be understood by considering the signal delay due to sampling. The phase lag of a sampled and reconstructed signal with respect to the actual continuous-time signal grows as the Nyquist frequency is approached.

Because practical control systems are usually implemented digitally and operate in discrete time, the repetitive control theory has been developed in the discrete time domain, respectively. In order to tune stability and convergence characteristics, the basic repetitive control law in Equation (79) has been modified to contain pre-filters for the old-control (learning) component and for the control error component

$$u(n) = Q(q)q^{-N}u(n) + K(q)e(n) \tag{82}$$

where $Q(q)$ is a filter or a constant number and $K(q)$ is the feedback gain, also a filter or a constant number, and q is the forward shift operator with q^{-N} representing a backward shift of N samples. Filter $Q(q)$, which has a gain of less or equal to unity, has been used for restricting the control actions to a desired frequency band. It will later be referred to as the *Q filter*. The filter $K(q)$ has been used to appropriately modify the loop gain $K(q)G(q)$ (Tomizuka *et al.* 1989). At least, it means having the loop gain positive real at the frequencies where $|Q| \approx 1$. As will be shown, the delay line gives more freedom in the design of $K(q)$; it actually provides an opportunity for a non-causal implementation that makes a zero-phase-lag filter possible.

Remark 8

Similarly to the integrator gain in a feedforward controller, the Q filter is chosen to tune stability and performance characteristics of the algorithm.

5.2 Gradient-based repetitive controller

The starting point for the development of a repetitive controller with adaptive delay time was the gradient-based method whose feedback path consisted of a truncated FIR filter that has inverse phase behaviour with respect to the actual

plant. The behaviour is obtained by using the time-inversed impulse response of the plant as the FIR filter (Hätönen *et al.* 2004). This particular approach was selected because it was considered a computationally inexpensive method, possible to implement in the control unit. Also, its stability was guaranteed by sufficient model accuracy; sufficient modelling accuracy again meaning a phase error of ±90° (Hätönen *et al.* 2004). Another way to examine the stability is to study destabilising effects due to the FIR truncation, similar to the leakage phenomena in data acquisition. Chen & Longman (2002) showed the existence of these effects and applied certain windowing techniques for repetitive control to avoid them. Both approaches lead to a somewhat similar result requiring the modelling accuracy to be sufficient.

The idea is to use a pre-filter $K(q)$ that makes the loop gain positive real. In the current work, this is realised with a non-causal filter derived from the plant model.

$$K(q) = \alpha G_m(q) \tag{83}$$

where α is again a real-valued convergence coefficient and $G_m(q)$ is the non-causal FIR model of the plant $G(q)$ where variable q is substituted by q^{-1}. The plant is approximated by a time-reversed truncated FIR model

$$G_m(q) = a_M q^M + a_{M-1} q^{M-1} + \ldots + a_1 q + a_0, M \leq N \tag{84}$$

where $[a_M \ldots a_0]$ are the FIR coefficients and M is the order of the FIR filter. The causality of the control law is guaranteed by truncating the FIR filter (restricting the order M) and by implementing it together with the delay line.

Hence, the FIR length must be lower or equal to the delay filter length in order to ensure the causality of the algorithm. As many FIR coefficients are chosen for the approximation as the delay filter length allows. Then, the FIR approximation is formed by flipping the truncated impulse response in the inverse order. The resulting filter has amplitude characteristics similar to the original plant (of course, within the accuracy of the approximation). The phase characteristics of the FIR are inversed with respect to the plant. A phase lag in the plant corresponds to a phase lead in the FIR filter, and vice versa.

With the truncated FIR, the control law becomes

$$u(n) = q^{-N}\left(Q(q)u(n) + \alpha G_m(q)e(n)\right) \tag{85}$$

(Hätönen *et al.* 2004). Similarly to the FIR approximation, the *Q filter* can be non-causal alone without the time delay. A symmetric filter can be applied

$$Q(q) = c_P q^{-P} + c_{P-1} q^{-P+1} + \ldots + c_0 + \ldots + c_{P-1} q^{P-1} + c_P q^P, P \le N \tag{86}$$

where $[c_P \ldots c_0]$ are the FIR coefficients and P is the order of the filter. The filter works usually as a low-pass or as a band-pass filter, but with zero phase lag.

Remark 9

Although the pre-filters Q(q) and K(q) (or $G_m(q)$) may contain non-causal components, the control law itself remains causal if the orders of the filters are lower than the order of the time delay.

The shown realisation of the *Q filter* makes it a filter without phase lag. In other words, the frequency response of the filter is always real-valued

$$\begin{aligned} &\mathrm{Re}\left(Q(e^{\mathrm{i}\omega'})\right) = Q(e^{\mathrm{i}\omega'}), \\ &\mathrm{Im}\left(Q(e^{\mathrm{i}\omega'})\right) = 0, \forall \omega' \in \left[0 \quad 2\pi\right] \end{aligned} \tag{87}$$

where ω' is a normalised angular frequency between [0 2π].

5.2.1 Convergence to zero error

Algebraic examination shows how the repetitive control algorithm rejects a periodic disturbance. The result can be expected intuitively because the high (infinite) gain at the frequencies determined by the time delay provides a good disturbance rejection at those frequencies. However, the analysis below provides an algebraic insight in repetitive control.

Consider a polynomial $D(q)$ that works as an annihilator (or an internal model by Francis & Wonham 1975) for a periodic disturbance signal $d(n)$

$$\begin{aligned} D(q)d(n) &= \left(1 - Q(q)q^{-N}\right)d(n) = d(n) - Q(q)d(n-N) = 0 \\ d(n) &= d(n-N) \end{aligned} \tag{88}$$

if $|Q| = 1$ and the period of the disturbance is N samples. The output of the plant $y(n)$ and the output of the repetitive controller $u(n)$ can be expressed as

$$\begin{aligned} y(n) &= G(q)u(n) \\ u(n) &= q^{-N}\left(Q(q)u(n) - \alpha G_m(q)e(n)\right) \end{aligned} \tag{89}$$

Hence, the plant output can be expressed by

$$y(n) = G(q)\frac{-q^{-N}\alpha G_m(q)}{D(q)}e(n) \tag{90}$$

Consider then the control error. Also, note that the error is defined in a slightly unusual manner (the definition is the same throughout the thesis)

$$e(n) = y(n) + d(n) = d(n) - \frac{q^{-N}\alpha G_m(q)G(q)}{D(q)}e(n) \tag{91}$$

Multiplication by the stable polynomial $D(q)$ gives

$$D(q)e(n) = D(q)d(n) - q^{-N}\alpha G_m(q)G(q)e(n) \tag{92}$$

As noted above, the term $D(q)d(n) = 0$ if $|Q| = 1$.

$$\begin{aligned} &\left(D(q) + q^{-N}\alpha G_m(q)G(q)\right)e(n) = 0 \\ &\left(1 - q^{-N}Q(q) + q^{-N}\alpha G_m(q)G(q)\right)e(n) = 0 \end{aligned} \tag{93}$$

This shows that the disturbance signal is annihilated and the control error converges to zero with given assumptions.

5.2.2 Stability

The pulse transfer function from the disturbance to the control signal of the gradient-based repetitive controller presented above becomes

$$H_r(q) = \frac{u(q)}{d(q)} = \frac{-q^{-N}\alpha G_m(q)}{1 - q^{-N}\left((Q(q)) - \alpha G_m(q)G(q)\right)} \tag{94}$$

By using the *small gain theorem* (see *e.g.* Glad & Ljung 2000), the stability boundary for the system is

$$\begin{aligned} &\left|e^{iN\omega'}\left(Q(e^{i\omega'}) - \alpha\overline{G}_m(e^{i\omega'})G(e^{i\omega'})\right)\right| < 1 \\ &\left|Q(e^{i\omega'}) - \alpha\overline{G}_m(e^{i\omega'})G(e^{i\omega'})\right| < 1, \forall\,\omega' \in \begin{bmatrix}0 & 2\pi\end{bmatrix} \end{aligned} \tag{95}$$

If we assume a non-leaking integrator for all the frequencies ($Q(q) \equiv 1$), and if the plant model perfectly describes the system ($G_m(q) = G(q)$), we have the stability condition for the convergence coefficient, or the learning gain

$$0 < \alpha < \sup\left(\frac{2}{\left|G(e^{\mathrm{i}\omega'})\right|^2}\right), \forall\,\omega' \in [0, 2\pi] \tag{96}$$

This result was derived in Hätönen *et al*. (2004). The result can be considered conservative, since the requirement in Equation (96) concerns all frequencies.

The truncation of the filter raises questions about the accuracy of the approximation and possible leakage effects due to the truncation. In practice, $G_m(q) \neq G(q)$, because of the truncated FIR approximation. According to the example by Chen & Longman (2002), the plant may be presented by two components, the actual model part and the residual part. Let the plant frequency response be

$$G(e^{\mathrm{i}\omega T_S}) = G_m(e^{\mathrm{i}\omega T_S}) + G_r(e^{\mathrm{i}\omega T_S}) = \sum_{i=0}^{M-1} h_i e^{-\mathrm{i}\omega T_S i} + \sum_{i=M}^{\infty} h_i e^{-\mathrm{i}\omega T_S i} \tag{97}$$

where $G_r(e^{i\omega T_S})$ is the residual part not included in the plant model, of order M. The FIR coefficients of the frequency response are represented by h_i. The model and the residual parts describe the system perfectly. In other words

$$G(e^{i\omega'})\left(\overline{G}_m(e^{i\omega'}) + \overline{G}_r(e^{i\omega'})\right) = \left|G(e^{i\omega'})\right|^2, \forall\,\omega' \in [0 \quad 2\pi] \tag{98}$$

$\overline{G}_m(e^{i\omega'})$ and $\overline{G}_r(e^{i\omega'})$ are the complex conjugates of the plant model and the residual term. Stability analysis by Chen & Longman (2002) is based on the small gain theorem to limit the loop gain below unity and to obtain a sufficient condition for stability by this way. The terms of Equation (98) may be examined graphically on the complex plane where $-\alpha|G|^2$ represents the desired coefficient update and $-\alpha\overline{G}_m G$ represents the realised coefficient update. If the realised coefficient update does not stay within the unit circle, the algorithm is under a risk of instability. Figure 40 shows two imaginary scenarios for the significance of the residual term: a) the residual term does not have an effect and the system is stable, and b) the closed-loop system can be unstable without the residual term.

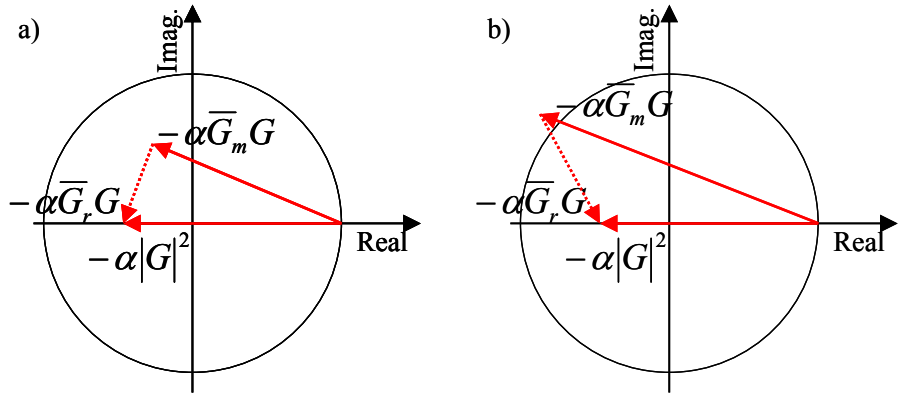

Figure 40. The illustration of the ideal, the plant model, and the residual gain vectors within the stability limits represented by the unit circle. Situation a) is acceptable. Situation b) where the residual vector contains stabilising components should be avoided.

If we use the plant and the residual to describe the model, we can estimate their contribution to the stability. The substitution

$$G_m(e^{i\omega'}) = G(e^{i\omega'}) - G_r(e^{i\omega'}) \tag{99}$$

modifies the stability condition into

$$\left|Q(e^{i\omega'}) - \alpha\left(\overline{G}(e^{i\omega'}) - \overline{G}_r(e^{i\omega'})\right)G(e^{i\omega'})\right| < 1, \forall\,\omega' \in \left[0 \quad 2\pi\right] \tag{100}$$

Examination of the complex vectors shows that the plant contains all the frequency components whereas the residual vector contains only the high frequency components (the minimum frequency being determined by $\omega T_S M$). The residual vector spins rapidly with respect to the plant vector in the complex plane, because it contains those high frequency components. To keep on the safe side, we may require that the plant vector is never closer to the unit circle than the maximum length of the residual vector. Requiring

$$\left|Q(e^{i\omega'}) - \alpha\left|G(e^{i\omega'})\right|^2\right| < 1 - \alpha\left\|\overline{G}_r(e^{i\omega'})G(e^{i\omega'})\right\|, \forall\,\omega' \in \left[0 \quad 2\pi\right] \tag{101}$$

makes the stability limits conservative. Chen & Longman (2002) used norm $\left\|\overline{G}_r(e^{i\omega'})G(e^{i\omega'})\right\|$ in the equation above. This action was done in order to keep safe side in the stability analysis. As explained before, the residual term with high-frequency components spins rapidly in the complex plane.

The practical difficulty is that the true transfer function of the plant is usually unknown. Thus, the exact residual term is also unknown. The situation is shown graphically in Figure 41. The condition indicates a fundamental problem: if $\left|Q(e^{i\omega'})\right| = 1$ and $\left|G_r(e^{i\omega'})\right| > \left|G(e^{i\omega'})\right|$, a small positive stabilising α does not exist. On the other hand, this means that the loop gain is not positive real.

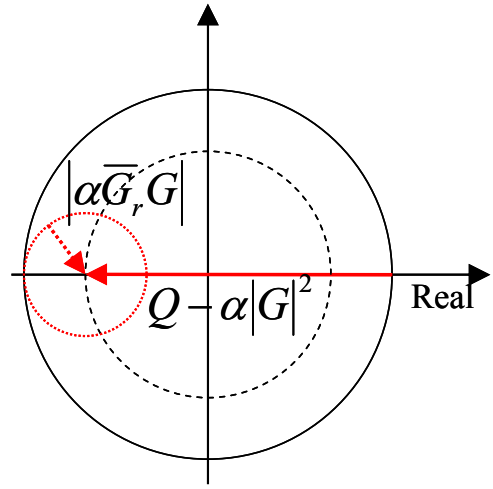

Figure 41. The graphical interpretation of the criteria in Equation (101).

Chen & Longman (2002) compared different windowing techniques to be used together with truncation. They ended up proposing exponential, and accelerated exponential, windows. Effectively this means using a frequency-dependent complex convergence coefficient that corrects the loop gain in such a way that its positive realness is maintained. The criterion for evaluating the windows was the stability of the algorithm. Again, the conclusion was that stability is maintained if the truncated FIR model is capable of describing the phase within ±90° corresponding to the result derived in Hätönen *et al.* (2004)

As the discussion shows, stability problems may occur at high frequencies if the residual term dominates. Besides windowing, another option is to use the *Q filter* to restrict the control action at high frequencies.

Remark 10

Several windowing techniques have been proposed for FRF estimation in dynamic systems. Those techniques are aimed at preventing the leakage, that is the generation of high-frequency components, from corrupting the result. Similar problems can occur with a truncated FIR repetitive controller.

5.2.3 Novel repetitive controller with adaptive delay time

The update scheme for the truncated-FIR repetitive controller is

$$u(n) = q^{-N}(\gamma Q(q)u(n) - \alpha G_m(q)e(n)) \tag{102}$$

where $G_m(q)$ is the model of the system represented as a truncated FIR approximation of the system $G(q)$. Again, γ is a scalar leakage coefficient, less or equal to unity. The system model alone is a non-causal filter. However, the algorithm is causal, because the order of the FIR model does not exceed the delay length N.

The capability of tracking any periodic signal makes repetitive control an attractive solution for rotating machines. The delay time, however, has to be adjusted according to the speed of rotation. For variable-speed machines, the delay time must thus be adjustable. Another option is to use the rotation phase-based delay, as was done by Fung *et al.* (2000) who applied repetitive control on control of robot arms. The solution makes it possible to use a constant delay, typically one revolution, *i.e.* 2 π rad. The author's experimental work exploited time-based repetitive algorithms. The choice was justified by two technical facts: 1) The measurement of the phase signals was not considered sufficiently reliable and accurate compared with the signal processor's capability of maintaining constant sampling intervals, 2) The technical restrictions made it difficult to trigger the signal processing based on the rotor revolution pulses.

In the algorithm presented, the filter length is selected on-line according to the rotation speed estimation. The fundamental period of the disturbance is then determined by the rotation speed. The integer number of samples required is always rounded downwards to the nearest integer below by the algorithm

$$N = \text{floor}\left(\frac{1}{f_{rot}T_S}\right) \tag{103}$$

where f_{rot} is the measured speed of rotation. The fact that the required delay does not exactly meet the integer number of samples was taken into account by

introducing a relative length error variable. The relative length error l_e between the realisable delay time and the required delay time is

$$l_e = \frac{1}{f_{rot} T_S} - N, \quad 0 \le l_e \le 1 \tag{104}$$

The length error is then used for the interpolation of the new control output by using two successive old outputs $u(n–N)$ and $u(n–N–1)$. The control law then becomes

$$u(n) = q^{-N}\left((1 - l_e + l_e q^{-1})u(n) - \alpha G_m(q) e(n)\right) \tag{105}$$

and the pulse transfer function from the disturbance to the control output equals

$$H_{ip}(q) = \frac{u(q)}{d(q)} = \frac{-q^{-N}\alpha G_m(q)}{1 - q^{-N}\left((1 - l_e + l_e q^{-1}) - \alpha G_m(q) G(q)\right)} \tag{106}$$

The interpolation is implemented in order have a more accurate frequency adjustment for the repetitive controller. Figure 42 shows the gain of the repetitive controller with the interpolation feature in the vicinity of the first harmonic frequency. With the chosen parameters (T_S = 0.0001 s, N = [20, 21], l_e = [0, 0.25, 0.5, 0.75]), the peak in the gain may be adjusted from 48.8 Hz to 51.1 Hz.

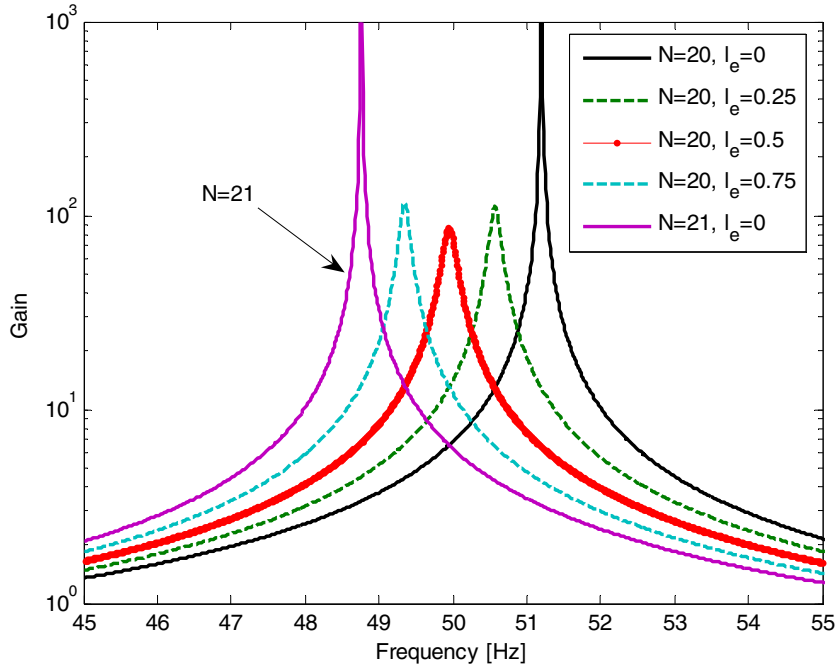

Figure 42. The gain of repetitive control loop as a function of frequency for different delay times (the filter order and the length error).

The interpolation, however, modifies the phase of the system and has a certain destabilising effect. This feature diverges from the original idea of having a zero-phase system to ensure stability with high feedback gain (Tomizuka *et al.* 1989, Hätönen 2004). The issue is discussed below, after the completion of the algorithm used in the experimental work.

As explained above, the *Q filter* is used for limiting the frequency band of control actions. The type of *Q filter* used is a low-pass filter. A band-pass filter would have been required in order to avoid developing a DC component in control. The repetitive control method, being integrative, provides high feedback gain at zero frequency. It was, however, impossible to realise a sufficiently long and accurate band-pass filter due to technical restrictions of the control unit. Making an FIR-based band-pass-type *Q filter* that accurately has unity amplitude in the frequency band of interest requires a relatively high order filter. On the other hand, the maximum order of the filter is limited due to computational restrictions. Note that the *Q filter* alone was not requiring excessive computational power, but the overall algorithm (using FIR representations for

systems models, feedback control, and the DC removal feature presented below). The computational cost of the algorithm increased rather rapidly.

This problem is avoided by implementing a separate DC removal system. The DC removal function is realised with a feedback of the integrated control signal. The transfer function of the feedback integrator alone equals

$$H_{in}(q) = \frac{1 - q^{-1}}{1 - q^{-1} - \omega_{LP} T_S} \tag{107}$$

where ω_{LP} is the integrator gain, used for the adjustment of the high-pass corner frequency. Finally, the control law, shown in Figure 43, with adaptive delay time, interpolation, and the DC-removal function is expressed as

$$\begin{aligned} u(n) = \gamma q^{-N} Q(q)\left((1 - l_e) + l_e q^{-1}\right) u(n) + \\ - \alpha q^{-N} G_m(q) e(n) - \alpha \left(\frac{\omega_{LP} T_S}{1 - q^{-1}} \right) u(n) \end{aligned} \tag{108}$$

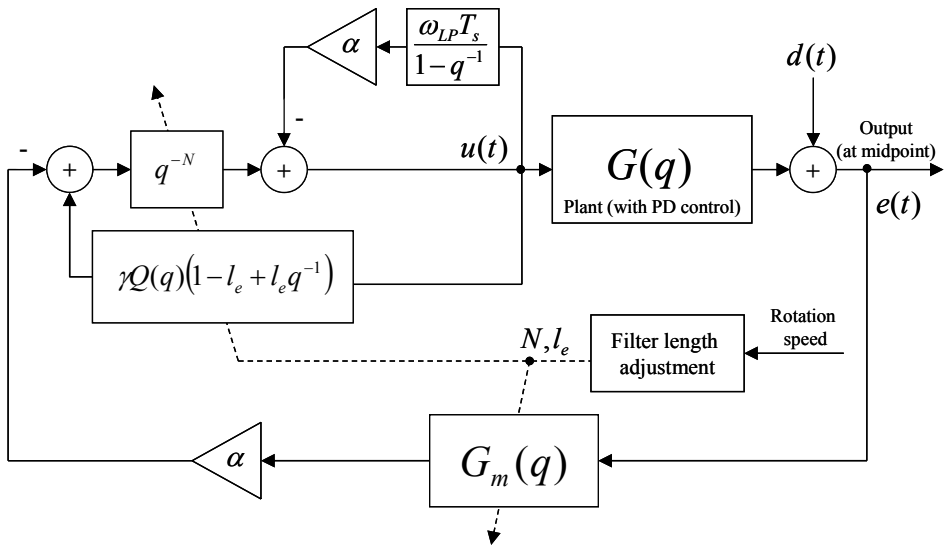

Figure 43. The repetitive control system applied to the test environment.

Similarly to the interpolation function, the DC removal function modifies the phase of the system and needs attention in terms of stability. As in the case of feedforward controllers, the parameters γ and α determine the convergence and the stability properties of the algorithm. The pulse transfer function from the error signal to control output is

$$H_r(q) = \frac{-\alpha q^{-N} G_m(q)}{1 + q^{-N}\left(\alpha G_m(q)G(q) - \gamma Q(q)\left((1-l_e) + l_e q^{-1}\right)\right) + \alpha \dfrac{\omega_{LP} T_S}{1-q^{-1}}} \tag{109}$$

The system is time invariant for a constant rotation frequency, but N and l_e are updated according to the speed of rotation. Without the DC-removal integrator, $\gamma Q \equiv 1, l_e \equiv 0$, the transfer function becomes

$$\frac{u(q)}{d(q)} = \frac{-\alpha q^{-N} G_m(q)}{1 + q^{-N}\left(\alpha G_m(q)G(q) - 1\right)} \tag{110}$$

Furthermore, if we assume that the model perfectly describes the system, we arrive at the stability condition stated in Equation (96). If there are modelling errors $\alpha G_m(q)G(q)$, becomes complex valued.

The next effort is to study the stability of the algorithm presented in Equation (109) and shown in Figure 43. Multiplication by $(1–q^{-1})$ gives for the characteristic polynomial

$$\begin{aligned} P(q) &= 1 - q^{-1} + \\ &+ (1-q^{-1}) q^{-N}\left(\alpha G_m(q)G(q) - \gamma Q(q)\left((1-l_e) + l_e q^{-1}\right)\right) + \alpha \omega_{LP} T_S \end{aligned} \tag{111}$$

The polynomial does not have a closed form solution for the roots. The interpolation feature induces a destabilising component in the algorithms regardless the modelling error. A numerical examination shows that increasing the length error l_e pushes the high-frequency poles of Equation (111) outside the unit circle (Figure 44). Achieving stability requires the use of the *Q filter* for relative frequencies $\omega' > \pi/2$. The frequency limit is approximate and comes from a heuristic examination of the algorithm. The real part of term

$\gamma Q(e^{i\omega'})\left((1-l_e)+l_e e^{-i\omega'}\right)$ changes its sign $\omega' = \pi/2$ for $l_e = 1$. With the use of a low-pass type Q filter the poles remain inside the unit circle.

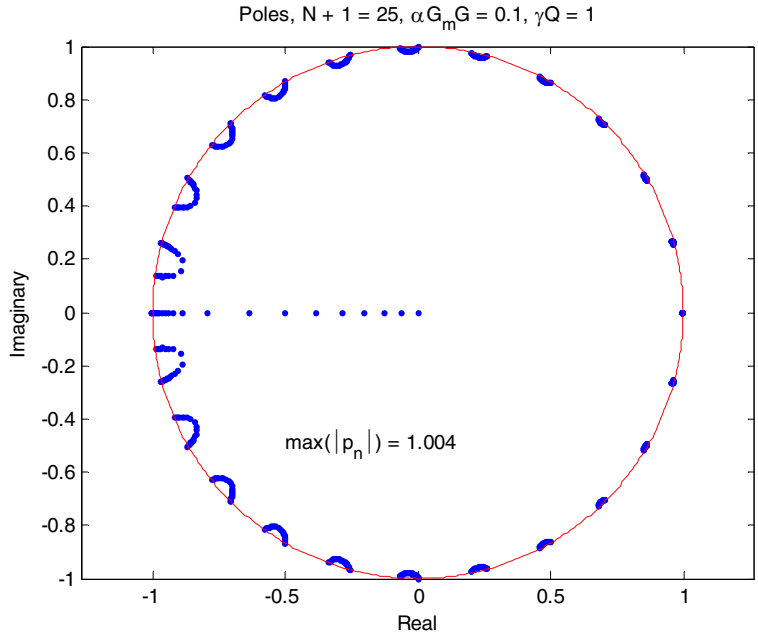

Figure 44. An example of the pole map of Equation (111).

5.2.4 Experimental results

The control algorithm presented was implemented on the rotor kit in the non-collocated layout (Figure 23). As described above, the length of the delay time and the length of the FIR plant-model filters were adjusted according to the rotation speed estimation. The computational requirements of the algorithm and the performance of hardware caused restrictions on the operating range. A certain number of operations were available per control cycle. The algorithm parameters were chosen such that the algorithm was operable at least in the vicinity of the critical speed.

The maximum repetitive length selected was 35 (*i.e.* the FIR model order $N = 34$), and the minimum length was 15 ($N = 14$). These figures correspond to rotation speeds from 27 rps to 61 rps, for the implementation chosen. The FIR

model filters were defined by impulse responses of the identified transfer functions in both planes separately. The FIR filters did not describe the system accurately, because relatively short filters were used. Figure 45 and Figure 46 show comparisons of the longest and shortest FIR filters with the plant models. The implemented *Q filter* was a symmetric low-pass filter of length 15 (the current sample, 7 samples forwards and 7 samples backwards). Its –3 dB point lay at 240 Hz to limit high-frequency control actions. Standard filter design tools were utilised to compute the filter coefficients. An important aspect was to design a filter without overshoot in its frequency response. *Q filter*s with the same characteristics were implemented in both orthogonal planes (*X* and *Y*), see Appendix C for the filter coefficients.

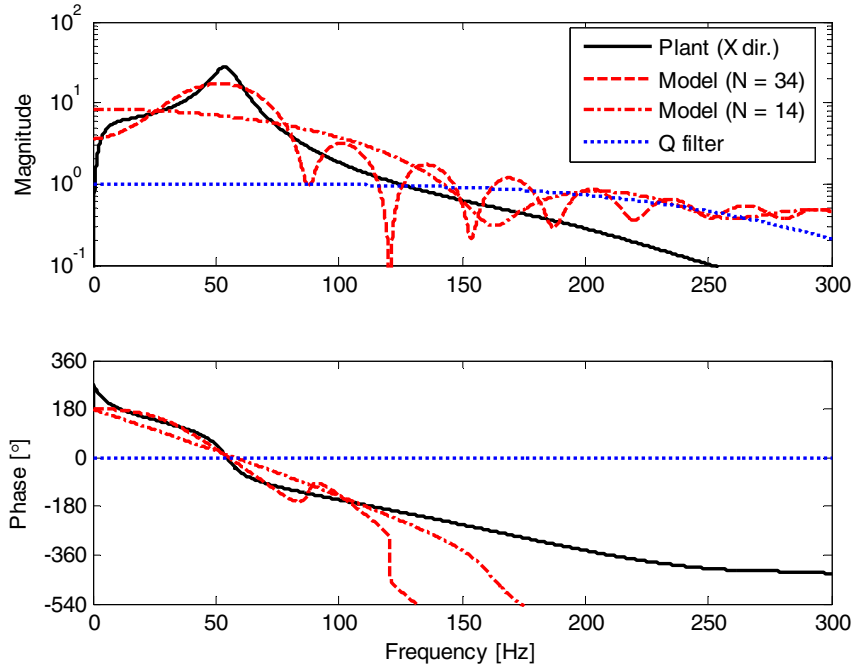

Figure 45. The implemented filters in the X plane.

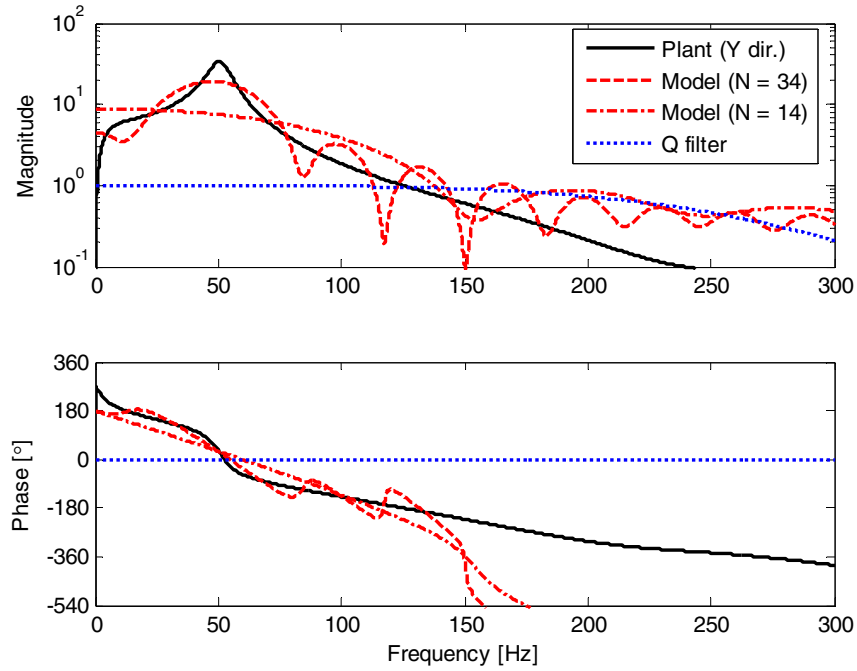

Figure 46. The implemented filters in the Y plane.

The feedback gain from the output error signal was influenced by the changing length of the plant-model filters. Figure 47 shows the effective repetitive feedback gains as a function of the repetitive filter length. The difference in the effective gains is caused by the different system models in the orthogonal directions. Figure 48 shows the open loop response for the complete repetitive control system from the control error $e(n)$ to the controller output $u(n)$.

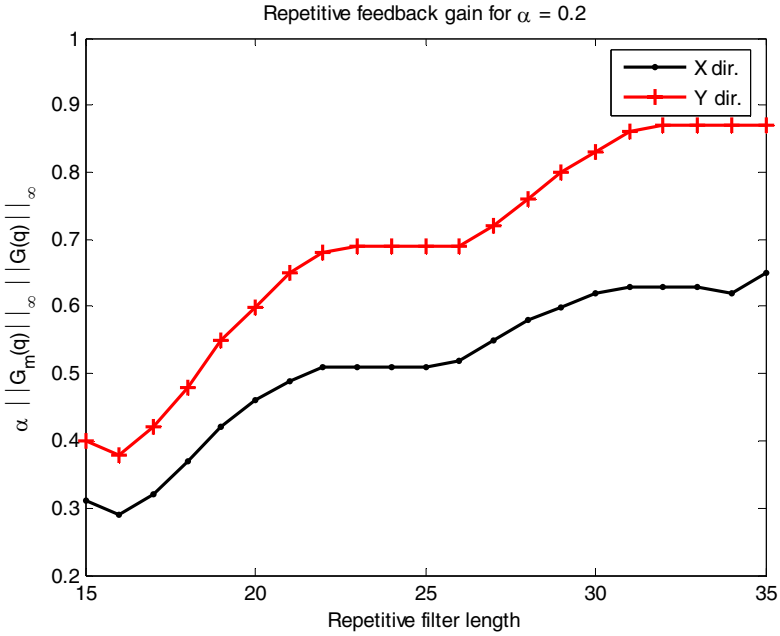

Figure 47. The feedback gain of repetitive control as a function of the filter length (delay time).

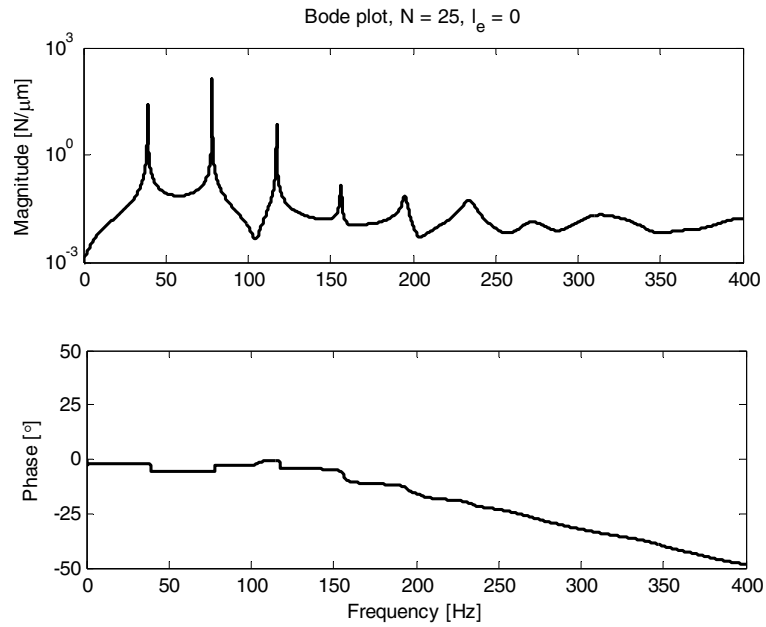

Figure 48. The open-loop response from the error to the repetitive controller output (computed for $\alpha = 0.1$, $N = 25$, and $l_e = 0$).

Figure 49 shows the rotor midpoint responses with the repetitive controller at a speed of 30 rps. The damping achieved was 12 dB at the first and second harmonics. The response of the repetitive controller was found to be strongly dependent on the rotation speed. The performance was at its best when the disturbance period allowed an integer ratio between the required delay length and the sampling interval. In other words, the required delay time, stated by the rotation speed, was then realisable with an integer number of unit delays and the length error variable was close to zero. Later in this thesis, the situation is called a match between the disturbance and the delay length. In this respect, the response plot shown did not present a good match between the disturbance and the delay length. Figure 50 shows the responses in case when the disturbance matched the delay length (40.7 rps).

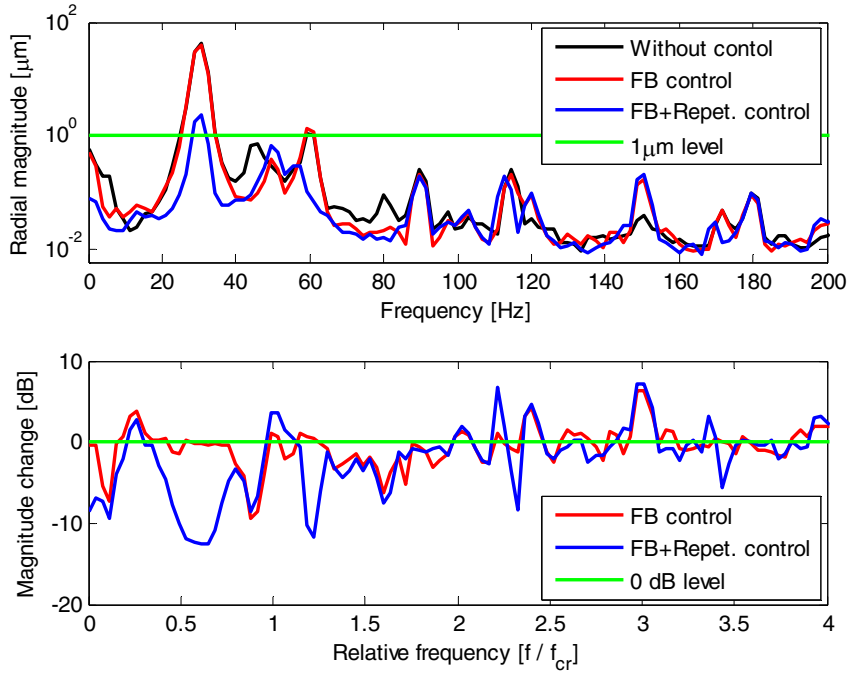

Figure 49. The rotor midpoint responses with repetitive control when running at 30 rps.

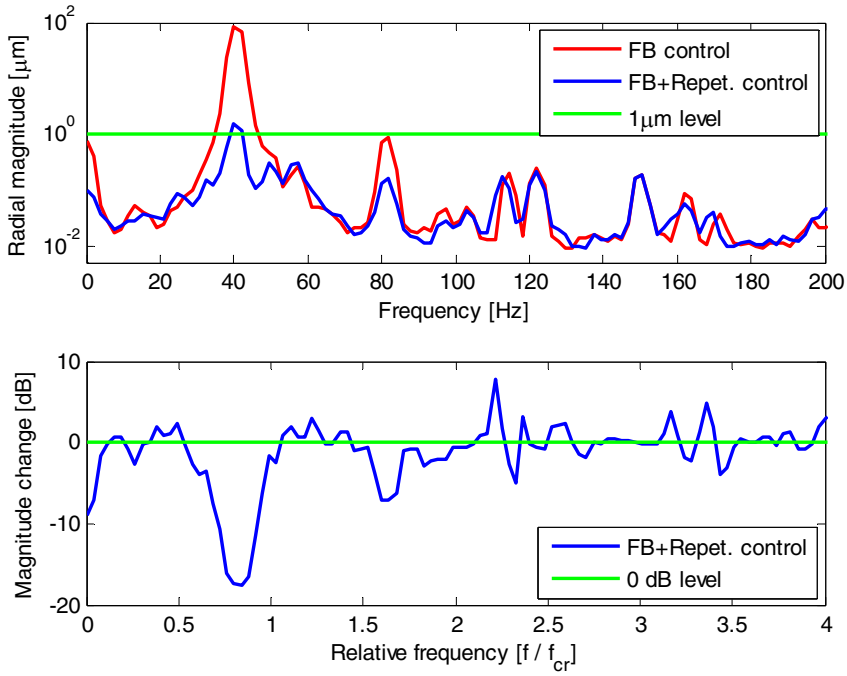

Figure 50. The rotor midpoint responses with feedback control, and with repetitive control when running at 40.7 rps. Speed matched with the filter length (24). $\alpha = 0.2$.

The *rms* values of the rotor midpoint and endpoint displacement with and without control are shown in Table 6. As in the case of Convergent Control, the leak coefficient was used to restrict the force at high speeds. This was again due to the restricted amplitude at the actuator.

Table 6. The rms displacements and control force commands with repetitive control with adaptive delay time.

Speed [rps]	Repetitive length *N*	Speed match with length? [Yes/No]	Midpoint Displ. [μm]	Force [N]	Endpoint Displ. [μm]	Aver. gain [-]	Leak Coeff. γ
27.2	35…36	Yes	3.9	2.8	54.0	0.4	1
30	32	No	1.9	2.8	64.1	0.8	1
40	24	No	3.5	2.9	76.2	0.3	1
40	24	No	2.1	2.9	79.5	0.6	1
40.7	23...24	Yes	1.4	2.9	84.7	0.3	1
40.7	23...24	Yes	1.4	2.9	85.3	0.6	1
50	19	No	4.2	2.9	108.7	0.5	1
51.1	18...19	Yes	2.2	3.0	109.2	0.2	1
60	16	No	8.7	3.3	130.4	0.4	0.9999
61	15...16	Yes	3.5	3.7	167.2	0.3	0.9999

The algorithm was also run without *Q filter* for experimental purposes. The use of the filter with low-pass characteristics made the behaviour of the algorithm substantially smoother.

For variable-speed experiments, the repetitive controller was tested in a rotor run-down condition (Figure 51). The run-down was performed from a rotation speed of 63 rps down to 32 rps with ramp rate of 4000 rpm/min (1.1 rps/s). The vertical dashed lines in the figure indicate the speed where the delay filter length matched the disturbance period. The local minima in the response did not occur exactly at the dashed lines, because of the transient (run down) operating condition. The figure shows that the performance was strongly frequency-dependent at high-speeds and the dependency weakened at lower speeds.

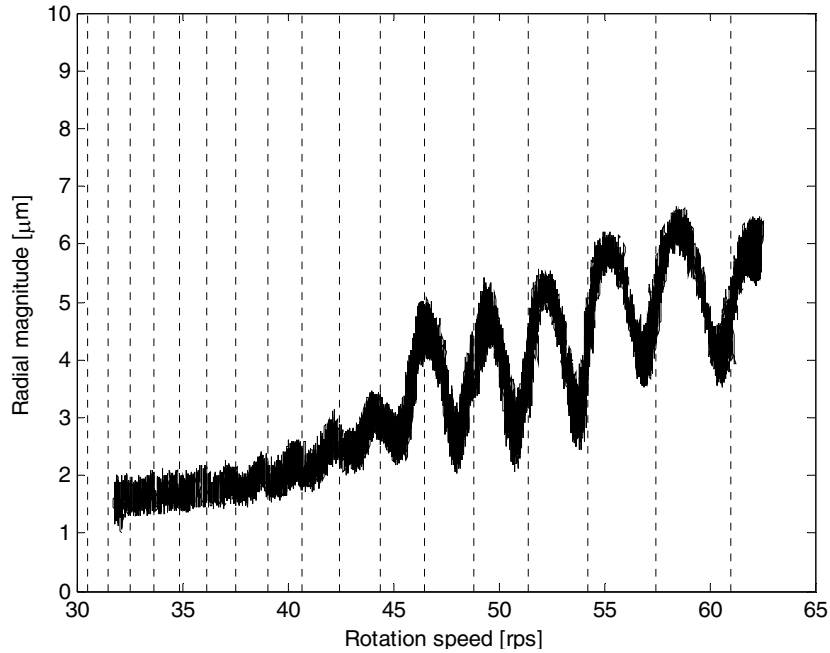

Figure 51. The radial displacement with repetitive control during a rotor run down (ramp rate equal to 4000 rpm/min).

5.3 Conclusions and chapter summary

The performance of the repetitive control method was close to that achieved with the feedforward control method when the delay time matched the disturbance period. At those speeds, the required repetitive length was realisable by an integer number of unit delays. Otherwise, the performance of repetitive control was poorer than that achieved with the feedforward methods. The worsening of the performance can be understood by considering the integrative update law. A non-match situation causes a withdrawal of the integrator poles inwards from the unit circle. The situation is equivalent to a leaking integrator in the update law (parameter γ in the update law).

The tests presented did not do full justice to the repetitive control method's ability to track any periodic disturbance matching the delay time (of course, limited by the *Q filter*). In certain rotating machines, the frequencies of the most significant excitations may not be predictable. For example, rolls working in a

nip contact may develop different barring vibration frequencies. This kind of applications are good candidates for repetitive control.

The performance of the repetitive controller was relatively good and comparable to the performance of the feedforward algorithms for higher delay filter lengths ($N > 22$). For lower lengths ($15 < N < 22$), the performance became more dependent on the match between the disturbance period and the delay filter length. This was suspected to be caused by worsened plant model accuracy. The plant model accuracy was a function of the disturbance period, because the delay filter determined the maximum time-reversed FIR filter length. Using higher-order filters would have given smaller unit delays in the algorithm implementation.

Remark 11

It has been mentioned that a repetitive controller can track a signal of any periodic waveform. The ability to compensate a signal is not restricted by the form of the reference signal as it is in the feedforward systems. However, the use of the Q filter restricts the frequency content of the control action. As the frequency content is limited, the number of possible waveforms is also limited.

Interpolation was used in the repetitive control law in order to provide a better match with the excitation frequency. On the other hand, the same feature introduced a destabilising term at high frequencies. The final form of a good way to formulate the interpolation may still need to be studied.

The repetitive control method presented is not normalised such as to provide constant convergence over the operating range. Furthermore, the effective feedback gain changed as a function of the FIR model length. These features make the adaptation of the repetitive controller heavily dependent on the operating point.

6. Comparison of mass unbalance compensation algorithms

This chapter aims to survey the attenuation results under steady-state conditions as shown in previous chapters and to show comparison results in transient conditions. The results are focused on the non-collocated layout, since it has been used to test all the algorithms examined. At the end of the chapter, the implementation of algorithms is discussed and major differences and advantages are pointed out.

6.1 Steady-state responses

The steady-state responses were presented thoroughly in the previous chapter. It can be concluded that the feedforward algorithms did not have significant differences in their steady-state behaviour and repetitive control exhibited slightly larger responses. Table 7 and Table 8 show the responses obtained with the feedforward algorithms. The responses of the repetitive control were dependent on the operating point (Table 9). The responses were smallest when the rotation speed resulted in an integer ratio between the sample time and the disturbance period. In other words, the required delay was realisable by an integer number of samples, the length error being close to zero. At those operating points the performance of the repetitive control method was comparable to the performance of the feedforward methods. For lower rotation speeds and thus higher delay filter lengths, the responses with repetitive control were nearly as good as with the feedforward methods.

Table 7. The midpoint responses obtained with the Jeffcott rotor layout.

	FB control only		FB + adaptive FIR		Leak	FB + Convergent C.		Leak
Speed	Displacement	Force	Displacement	Force	Coeff.	Displacement	Force	Coeff.
[rps]	[μm]	[N]	[μm]	[N]	γ	[μm]	[N]	γ
25	26.2	0.9	1.2	1.1	1	2.3	1.1	1
40	27.6	1.4	1.1	1.4	1	1.6	1.4	1
65	24.1	2.1	1.5	2.5	1	1.6	2.2	1

Table 8. The midpoint responses obtained with the non-collocated layout.

	FB control only		FB + adaptive FIR		Leak	FB + Convergent C.		Leak
Speed	Displacement	Force	Displacement	Force	Coeff.	Displacement	Force	Coeff.
[rps]	[μm]	[N]	[μm]	[N]	γ	[μm]	[N]	γ
10	11.0	0.8	1.6	2.8	1	0.5	2.3	1
30	17.3	1.7	1.3	2.8	1	0.9	2.5	1
50	61.2	2.9	1.2	3.0	1	1.3	2.6	1
70	17.9	1.8	2.5	8.1	1	11.8	4.8	0.99995

Table 9. The midpoint responses obtained with the non-collocated layout.

	FB control only		FB + repetitive		Leak
Speed	Displacement	Force	Displacement	Force	Coeff.
[rps]	[μm]	[N]	[μm]	[N]	γ
30	17.3	1.7	1.9	2.8	1
50	61.2	2.9	4.2	2.9	1
51.1	-	-	2.2	3.0	1

Figure 52 shows the spectra recorded during constant speed operation at 50 rps, the critical speed. The spectra show that Convergent Control had the best performance with regard to the damping of the first and second harmonic components. The adaptive FIR showed better performance with regard to the first harmonic component than the repetitive controller. At the second harmonic, the repetitive controller performed slightly better than the adaptive FIR.

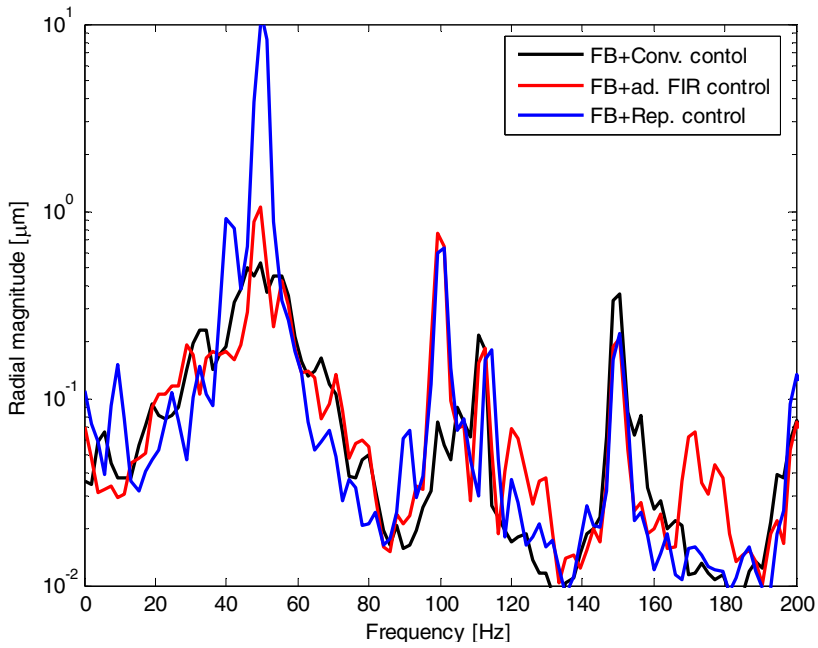

Figure 52. The midpoint responses with different algorithms when running at 50 rps (i.e. the critical speed).

6.2 Transient responses

Figure 53 shows the responses of three algorithms compared during a ramp down, at a rate of 4000 rpm/min. The performance of the Convergent Control method was the best, and the performance of the repetitive control method was the poorest. The performance of the repetitive control method was strongly dependent on the rotation speed, because the match between the disturbance period and the delay filter length varied as a function of speed. The performance of the adaptive FIR was between the other two methods. When tracking a rotor speed ramp, the fundamental difference between the feedforward algorithms and repetitive control worked in favour of the feedforward algorithms. For the feedforward algorithms, no re-adaptation is required if the plant dynamics, or the disturbance, does not change. In contrast, the repetitive control algorithm requires continuous adaptation as the filter length changes. For this reason, the feedforward algorithms tracked ramps well in comparison with the repetitive control algorithm. Note that the rotation phase based repetitive control algorithm proposed by Fung *et al.* (2000) would work as the feedforward systems in this respect.

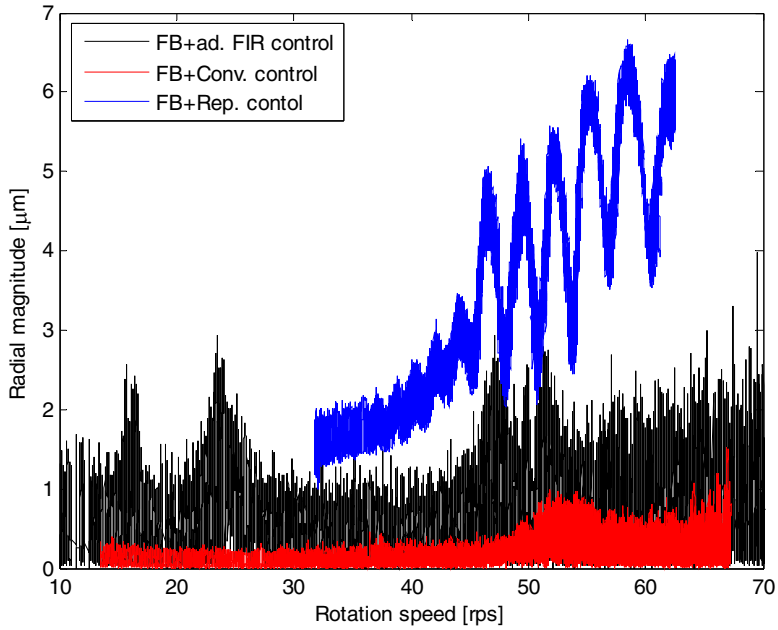

Figure 53. Comparison of responses with different algorithms during a rotation speed ramp.

As discussed before, the convergence rates of the adaptive FIR filter and Convergent Control are not fully comparable. The experiments, however, indicated that the Convergent Control algorithm had shorter convergence times than the adaptive FIR. Two reasons were found for this behaviour:

1. The over-estimated order of the FIR filter makes it necessary to use a lower convergence coefficient, as the approximation for the maximum stable convergence coefficient α is proportional to the order inverse. Furthermore, searching for the maximum convergence coefficient for a non-normalised adaptive FIR filter is slightly more difficult than for Convergent Control. This is caused by a variable feedback gain of the adaptive FIR that is dependent on the operating point, while the feedback gain of the Convergent Control is constant. Hence, the convergence coefficient for the adaptive FIR filter cannot be maximised for all the frequencies to be compensated.

2. The maximum stabilising convergence coefficient of an adaptive FIR is dependent on the statistical properties of the signals. In certain

experiments, the adaptive FIR algorithm exhibited different convergence rates in the X and Y direction, although these were roughly identical. The behaviour was observed for the normalised as well as the non-normalised algorithms. This is suspected to be caused by differences in error signal quality. For Convergent Control the situation is different, because the adaptation law is applied to the Fourier coefficients which correlate with the frequency to be compensated. Convergent Control always exhibited similar convergence rates in the X and Y directions.

For the repetitive control method, the convergence rate was dependent on the operating point, because the method was always non-normalised and the feedback gain varied. The convergence rate, similarly to the steady-state performance, was also dependent on the operating point.

6.3 Implementation issues of algorithms

6.3.1 Convergent Control vs. adaptive FIR

The Convergent Control method was found to be the simplest algorithm in terms of implementation and the amount of computer code required. The algorithm requires two reference signals per frequency to be compensated (cosine and sine for real and imaginary parts). Then, the algorithm requires the system model at the respective frequencies; one complex number per frequency to be compensated is required. The algorithm performs the following operations in a loop:

1. Extraction of the Fourier coefficients from the error signal by means of the reference signals correlating with the frequency to be compensated.
2. Adaptation in the frequency plane. New Fourier coefficients of the control outputs are computed by an integrative adaptation law using the old control outputs, the output error, and the system model. The system model inverse is utilised to adjust the adaptation direction.
3. Realisation of the control force using the Fourier coefficients of the control output and the reference signal. A time signal is synthesised.
4. Update of the old control outputs and continue to the next control loop.

The adaptive FIR filter performs an algorithm similar to that in Convergent Control. On the flow chart, the adaptive FIR is a compact algorithm. However, its use of a wideband system model makes it computationally more demanding than Convergent Control. The adaptive FIR uses one reference signal per frequency to be compensated. In contrast with Convergent Control, the algorithm is executed completely in the time domain. The algorithm carries out the following loop:

1. Computation of the filtered reference signal using the system model and the reference signal. The filtered reference signal must be available as a sequence with a length equal to the FIR order.
2. Adaptation of the FIR filter coefficients by applying an integrative adaptation law to the old FIR coefficients, the output error, and the filtered reference signal.
3. Realisation of the control force using the non-filtered reference signal and the FIR coefficient.
4. Update of the old FIR coefficients, the filtered reference signal, and continue to the next control loop.

The adaptive FIR filter demands a somewhat greater computational effort than Convergent Control because of the use of a time domain system model and the filtered reference signal that needs to be updated. Depending on the chosen FIR model order, the adaptive FIR filter requires two to three times more operations per control cycle than the Convergent Control method. The author is unwilling to state the difference as an exact number, because the suitable order of the FIR filter may be different from the theoretical. In the experiment, Convergent Control always worked with the order corresponding to the number of the frequencies to be compensated. However, this work showed indications that it may be advantageous to exaggerate the FIR order. This increases the computational effort required. The computational effort required should not be a significant issue in selection between the two algorithms, if there are other benefits available, considering that modern computer systems are becoming ever more powerful.

The simplicity of the implementation provides an argument for Convergent Control. This was found a positive feature when implementing and debugging

the algorithm in practice. The way the system model is implemented in Convergent Control, also makes it attractive in practice. The model (or the frequency response) is required in a compact form only at the frequencies to be compensated. Thus, it is sufficient to identify the model at discrete frequencies. On-line updating can also be carried out at other frequencies simultaneously, if required.

The advantage of the adaptive FIR filter lies in its theoretical flexibility. An algorithm with a sufficient FIR order is capable of compensating any given set of frequencies with a correlating reference signal. However, the experimental work indicated a poor performance in compensating several frequencies.

6.3.2 The repetitive control algorithm

The repetitive control method does not make use of reference signals, but a similar application of the internal model principle is realised by a feedback loop and a delay. Compared with the other two algorithms, the repetitive control solution requires a significant amount of computational effort and memory, because of the number of filters and signal sequences, equal to the order of the delay filter. The gradient based repetitive control method examined performs the following procedure:

1. Determining the order of the repetitive control delay filter and the length error between the actually required delay time and realised delay time.
2. Filtering the output error through the phase-mirroring system model (time-reversed impulse response model).
3. Filtering of the old control outputs through the *Q filter* limiting the control actions to the chosen frequency band of interest.
4. Computation of control outputs using the filtered error and the filtered old control output signals.
5. Update of the old control outputs and continue to the next control loop.

The algorithm implemented required about ten times more operations per control cycle than Convergent Control, and the results suggested that computationally

more expensive algorithm could improve the performance. Achievement of a more accurate time-reversed plant model and a smaller length error could motivate the use of a higher delay filter order. This would further increase the computational effort required.

The potential advantage of the repetitive control method is the ability to compensate any given signal without the requirement of a correlating reference signal. This feature is desirable in applications where the signal form or the frequency is not known beforehand. However, the need of the Q filter restricts the frequencies to be compensated.

7. Discussion

The work described the design path of the active control system from identification to controller implementation. Dealing with the periodic disturbance due to the rotation was the core of the work. The identification methods presented concentrated on ignoring this disturbance while the control methods presented concentrated on compensating it.

The identification method developed made it possible to discard the load disturbance automatically in rotor identification. The idea was to use the reference signal for ignoring the load disturbance, since it was also used for compensation by the feedforward methods. This enabled a simple automatic identification scheme that can be used, and is very likely needed, by an adaptive rotor vibration control system. Similar approaches have been developed for secondary path estimation in active noise control (Kuo & Morgan 1996, Hansen & Snyder 1997).

Traditional feedback control methods were implemented in order to provide a certain amount of wideband damping in the system. Vibrations around the critical speed were efficiently damped by velocity feedback control. This enabled rotor operation at critical speed, but the performance was modest compared with the feedforward and repetitive methods. However, the significance of feedback control lay in making the system phase-characteristics sufficiently smooth for the other control methods. Also, the implementation of a dissipative control algorithm carries little risk, because the stability of the collocated system can be guaranteed for an ideal control system (Preumont 2002). A similar control approach, a combination of feedback and feedforward controllers, was also promoted by Carme (1999). In this thesis, the connection between sufficient damping and the required modelling accuracy was shown in order to justify the use of feedback control. Engineering tools were developed for evaluating the possibilities of a feedforward system. These design charts and the phase error indicator were to be used during system design.

Several feedforward compensation algorithms have been studied for synchronous force cancellation in rotating machines, mainly with active magnetic bearings (Knospe *et al.* 1997, Lantto 1999). They are usually

variations of the Higher Harmonic Control or Convergent Control algorithms. On the other hand, adaptive FIR filters have been used in noise and vibration control (Fuller *et al.* 1996, Elliot 2001, Kuo & Morgan 1996, Kataja 1999). The adaptive FIR with the LMS algorithm has been also applied for unbalance control in AMB applications (Betschon & Schöb 1998, Zhao *et al.* 2000). However, according to the author's understanding the use of the adaptive FIR systems has not been common for rotor vibration control.

The present work compared three algorithms for mass unbalance compensation in a rotating machine. For the current purpose, the Convergent Control method was found the most suitable. The finding is supported by the use of the method in several rotating machine applications (Sievers & von Flotow 1988, Hall & Wereley 1989, Knospe *et al.* 1997, Lantto 1999).

The adaptive FIR with the LMS algorithm exhibited slightly inferior performance than Convergent Control. However, it also exhibited a restless, non-robust, behaviour at high speeds. This may be due to the quality of signals, because the algorithm used a wideband system model whereas the Convergent Control solution used the system model at the frequencies to be compensated. Nevertheless, the behaviour did not encourage the use of the FIR in practice. On the other hand, the adaptive FIR has been successfully used in several noise control applications (Fuller *et al.* 1996, Elliot 2001, Kataja 1999). Its theoretical advantage over Convergent Control is the capability to act on several frequency components within the same filter, if the filter order is sufficient. This advantage, however, was not confirmed in the current experimental work. The system was not capable of attenuating two frequency components simultaneously. One could implement several separate FIR systems, similarly to Convergent Control. In that case the FIR method is believed, but not validated with experiments, to perform in a manner similar to Convergent Control, because the FIR method was able to damp the frequencies concerned separately.

The repetitive controller had the worst performance in the tests. The performance was worst when the disturbance period did not match the repetitive length. The present tests did not do full justice to the repetitive control method's ability to track any periodic disturbance matching the delay time (of course, limited by the *Q filter*). In some rotating machine applications, the frequencies of the most significant excitations may not be predictable. For example, rolls

working in a nip contact may develop different barring vibration frequencies that cannot be estimated beforehand. Applications of this kind are potential candidates for repetitive control. In the current application, a rotation-phase based implementation such as proposed by Fung *et al.* (2000) would probably have provided a better performance, but was not realisable for technical reasons.

Sahinkaya *et al.* (2002) applied a similar control method to repetitive control in order to update Fourier coefficients in the control of harmonic vibrations in magnetic bearing systems. This kind of mixed approach was not considered in this thesis.

It is noteworthy that the repetitive controller worked at a relatively low system order and still provided a significant amount of attenuation. A straightforward way to improve the performance of the repetitive controller is to shorten the unit time delay used in the algorithm. In this way, the average mismatch between the disturbance period and the delay filter length is reduced. The plant model order, and thus the modelling accuracy, are also increased by the same modification. Hardware restrictions, however, did not allow testing the modification in the present test environment.

The results with the non-collocated layout showed how controlling one point amplifies another on the shaft. Having a smaller number of actuators than natural modes to be controlled is a compromise with regard to the overall damping. The results indicated that the derivative control was able to provide some attenuation at the midpoint in the super-critical region. This was due to the dissipative nature of the controller. The damping increase at the end of the rotor was able to contribute to the damping of the first natural mode. The increase, however, was not effective due to the location of the actuator and the geometry of the rotor. The feedforward algorithms and the repetitive control were effective also in the super-critical region. However, they increased the displacement at the end rapidly together with increasing speed.

In practical real-life implementations, the required damping level is often a compromise between different factors. The convergence of the algorithms must be monitored in order to avoid instability or excessive amplification of vibrations at other frequencies. The convergence and robustness properties may be adjusted as a function of the operating point, the required attenuation, the

reliability of the model at a particular frequency, *etc*. This adjustment can be done by tuning the convergence and the leaky coefficients. For instance, the convergence coefficient may be reset when a feasible attenuation level is achieved; or the leaky coefficient should be used, if the actuator capability is limited. In this respect, none of the algorithms examined should be considered "a bad algorithm". The practical choice involves other factors than performance alone.

In terms of hardware requirements, the magnitude of the *rms* damping force required was from 1 N to 2 N for the collocated layout, and from 1 N to 8 N for the non-collocated layout. Naturally, the magnitude of the forces required is dependent on the mass unbalance of the rotor. For the current case, the forces required represent 10 % to 30 % of the rotor weight. The results correspond with the author's experience of the force levels required. In a feasibility study on an electrical machine by Tammi *et al.* (2004), the forces were less than 5 % of the rotor weight. According to those simulations, the force magnitude was sufficient to obtain over 90 % reduction in the rotor responses.

The computational effort required by the different algorithms varied largely. Compared to the Convergent Control method, the adaptive FIR with the LMS algorithm required two to four times more operations per control cycle. The exact figure depends on the FIR order used, but the algorithm is always computationally more expensive than Convergent Control, owing to the differences in the system models used. The repetitive controller used ten times more operations per control cycle than Convergent Control. The exact figure is dependent on the operating point, since the filter lengths depend on the disturbance period. Note that the figures given are very rough indications of the relative efforts required. As the available computational power is continuously increasing, the author does not see it as a crucial factor, if the particular algorithm is beneficial for the purpose. In practice, other functionalities and code surveillance consume a major portion of the computational power, rather than the actual algorithms. Nevertheless, the figures can be considered as indications of the overall simplicity or complexity of the different algorithms.

The current work provides an identification method for rotors, explains and compares different active control methods, and illustrates the implementation issues of the methods. In addition to the scientific contributions listed in Section

1.5, this thesis has practical implications. In the author's view, the significance of this thesis is in the completed practical implementations of the systems. The automatic compensation of the disturbance during identification, understanding the different roles of feedback and feedforward (or repetitive) controllers, and the feature of the repetitive control with respect the feedforward control methods have been dealt with in the work. In the author's knowledge, the present work is the first to study repetitive control in rotor vibration control.

7.1 Future work

Currently, research is directed towards active control of electrical machine vibrations using the machine's internal forces (the ACRVEM project). For that purpose, Convergent Control will be the first method to be investigated. The repetitive control method may also be particularly useful, if periodic electromechanical excitations occur at unpredictable frequencies. Then, the repetitive controller must be implemented with a higher order algorithm than that used in the current work. Moreover, the forthcoming test environment probably poses new challenges for active control in the form of non-linear force generation.

In its current form, the repetitive control method was not in a normalised form as Convergent Control and the normalised adaptive FIR method were. The feature is advantageous when optimising the feedback gain and the convergence rate over the operating range. Implementing this feature on the repetitive control is one subject for further consideration.

The behaviour of the adaptive FIR filter with several harmonics raised some questions. It is interesting to study further why the algorithm did not succeed to damp the second harmonic and what actually is the best way to normalise the algorithm. The author suggests that the coefficient update should be normalised regarding all the eigenvalues, not just the largest. However, according to the preliminary tests a modified algorithm did not solve the convergence problems of the adaptive FIR filter with the LMS algorithms observed in this work.

As it is known and also shown in this work, the damping a point in a structure may mean amplification at another point of the structure. This fact leads to

interesting optimisation problems that are certainly worth of studying and relevant in practical applications.

Furthermore, the stability condition derived for basic repetitive control algorithm was conservative and no analytical stability condition was derived for repetitive control with interpolation and DC removal. An effort is to study more precise and less conservative stability boundaries for the algorithms developed and to include modelling errors in the analysis.

References

Albertos, P. & Sala, A. 2002. *Iterative identification and control*. Springer-Verlag London. 309 p. ISBN 1-85233-509-2.

Bao, C., Sas, P. & van Brussel, H. 1993. Comparison of two on line identification algorithms for active noise control. *Proc. of the Second Recent Advances in Active Control of Sound and Vibration*. Pp. 38–51.

Betschon, F. & Schöb, R. 1998. On-line-adapted vibration control. *Sixth International Symposium on Magnetic Bearings.* Massachusetts, USA. Pp. 362–371.

Burrows, C.R. & Sahinkaya, M.N. 1983. Vibration control of multi-mode rotor-bearing systems. *Proc. of the Royal Society of London.* Series A, Mathematical and Physical Sciences, Vol. 386, No. 1790, pp. 77–94

Carme, C. 1999. The third principle of active control: the feed forback. *Proc. of Active 99*. Fort Lauderdale. USA. 12 p.

Chen, K. & Longman, R.W. 2002. *Stability issues using FIR filtering in repetitive control*. Advances in the Astronautical Sciences, Vol. 206, pp. 1321–1339.

Cheung, L.Y., Dunn, R.W., Daniels, A.R. & Berry, T. 1994. Active vibration control of rotor systems. *Proc. of Intl. Conf. on Control, Control '94*. IEEE. Coventry, UK. Vol. 2. Pp. 1157–1163.

Childs, D. 1993. *Turbomachinery Rotordynamics: Phenomena, Modeling, and Analysis*. John Wiley & Sons, Inc. 496 p. ISBN 0-471-53840-X.

Clark, R.L. 1999. Adaptive structures: compensators by design. *Proc. of Active 99*. Fort Lauderdale. USA. 10 p.

Couche, J. & Fuller, C. 1999. Active control of power train and road noise in the cabin of a sport utility vehicle with advanced speakers. *Proc. of Active 99*. Fort Lauderdale. USA. 12 p.

Craig, R.R. & Bampton, M.C. 1968. *Coupling of substructures for dynamic analyses*. AIAA Journal. American Institute of Aeronautics and Astronautics, Vol. 6, No. 7, pp. 1313–1319.

Daley, S., Hätönen, J. & Tammi, K. 2006. Instantaneous harmonic vibration control of a flexible rotor. *Proc. of Active 2006. Adelaide* 18–20 September 2006. 8 p.

Ehmann, C., Alizadeh, A. & Nordmann, R. 2003. *Schwingungsdämpfung aktiv gelagerter Rotoren mit robuster Regelung, in Schwingungen in rotierenden Maschinen*. Feb. 2003, Darmstadt.

Elliot, S.J., Stothers, I.M. & Nelson, P.A. 1987. *A multiple error LMS algorithm and its application to the active control of sound and vibration*, IEEE Transactions on Acoustics, Speech and Signal Processing, Vol. 35, pp. 1423–1434.

Elliot, S.J. 2001. *Signal processing for active control*. Academic Press. London. 511 p. ISBN 0-12-237085-6.

Eriksson, L.J., Laak, T.A. & Allie, M.C. 1999. On-line secondary path modeling for FIR and IIR adaptive control in the presence of acoustic feedback, *Proc. of Active 1999.* Virginia Polytechnic institute and State University, Blacksburg, USA. Pp. 949–960.

Ewins, D.J. 2000. Modal testing: theory, practice and application. Research Studies Press. Baldock England. 562 p. ISBN 0-86380-218-4.

Fehren, H., Gebauer-Teichmann, A., Gnauert, U., Grabow, F., Siebald, H., Wenzel, M. & Wimmel, R. 2000. Active vibration reduction for rotating rolls. *Seventh International Congress on Sound and Vibration*. Garmich-Partenkirchen. Pp. 379–386.

Forte, P., Paterno, M. & Rustighi, E. 2004. *A magnetorheological fluid damper for rotor applications*. International Journal of Rotating Machinery, Vol. 10, No. 3, pp. 174–182.

Francis, B.A. & Wonham, W.M. 1975. *The internal model principle for linear multivariable regulators*. Appl. Mathematics & Optimization, Vol. 2, No. 2, pp. 170–194.

Fuller, C.R., Elliot, S.J. & Nelson, P.A. 1996. *Active control of vibration*. Academic Press. London. 332 p. ISBN 0-12-269440-6.

Fung, R., Huang, J., Chien, C. & Wang, Y. 2000. *Design and application of continuous time controller for rotation mechanisms*. International Journal of Mechanical Sciences, Vol. 42, pp. 1805–1819.

Gasch, R., Nordmann, R. & Pfutzner, H. 2002. *Rotordynamik*. Springer-Verlag. Berlin. 705 p. ISBN 3-540-41240-9.

Gawronski, W. 1996. *Balanced control of flexible stuctures*. Springer-Verlag. London. 262 p. ISBN 3-540-76017-2.

Genta, G. 1999. *Vibration of structures and machines*. Springer-Verlag. New York. 591 p. ISBN 0-387-98506-9.

Genta, G. 2005. *Dynamics of rotating systems*. Springer-Verlag. New York. 664 p. ISBN 0-387-20936-0.

Glad, T. & Ljung, L. 2000. *Control theory*. Taylor & Francis. London. 467 p. ISBN 0-7484-0878-9.

Hall, S.R. & Wereley, N.M. 1989. Linear control issues in the higher harmonic control of helicopter vibrations. *Proc. of 45th Annu. Forum Amer. Helicopter Soc*. Boston, USA. Pp. 955–971.

Hansen, C.H. & Snyder, S.D. 1997. *Active control of noise and vibration*. E & FN Spon, London, UK. 1267 p. ISBN 0-419-19390-1.

Herzog, R., Bühler, P., Gähler, C. & Larsonneur, R. 1996. *Unbalance compensation using genralized notch filters in the multivariable feedback of magnetic bearings*. IEEE Tracsactions on Control Systems Technology, Vol. 4, No. 5, pp. 580–586.

Heylen, W., Lammens, S. & Sas, P. 1999. *Modal analysis theory and testing*. Katholieke Universiteit. Leuven. ISBN 90-73802-61-X.

Hillerström, G. & Sternby, J. 1994. Repetitive control using low order models. *Proc. of American Control Conference.* Vol. 2. Pp. 1873–1878. ISBN 0-7803-1783-1.

Hillerström, G. 1996. *Active suppression of vibrations – a repetitive control approach.* IEEE Transactions on Control Systems Technology, Vol. 4, No. 1, pp. 72–78.

Hirschmanner, M., Steinschaden, N. & Springer, H. 2002. Adaptive control of a rotor excited by destabilizing cross-coupling forces. *Proc. of Sixth International Conf. on Rotor Dynamics*. Sydney, Australia. Vol. I. Pp. 38–45.

Hjalmarsson, H. & Ljung, L. 1993. A discussion of "unknown-but-bounded" disturbances in system identification. *Proc. of 32nd Decision and Control Conf, IEEE.* Pp. 535–536.

Hynninen, A. 2002. *Sähkögeneraattorin roottorin ja sen laakeroinnin värähtely-tekninen mallintaminen mitoituslaskelmissa* [Modelling of the rotor and its bearings in vibration based dimensioning of an electric generator]. Espoo: Helsinki University of Technology. 97 p. Master's Thesis. In Finnish.

Hätönen, J. 2004. *Issues of algebra and optimality in iterative learning control*. University of Oulu. 155 p. Doctoral dissertation. ISBN 951-42-7351-6.

Hätönen, J.J., Freeman, C.T., Owens, D.H., Lewin, P.L. & Rogers, E. 2004. Robustness analysis of a gradient-based repetitive control algorithm. *Proc. of 43rd IEEE Conference on Decision and Control.* Atlantis, Paradise Island, Bahamas. Pp. 1301–1306.

Hätönen, J., Daley, S. & Tammi, K. 2006. Instantaneous Harmonic Control – Convergence Analysis and Experimental Verification. *Under preparation for the Proc. of Thirteenth International Congress on Sound and Vibration (ICSV13),* Vienna. International Institute of Acoustics and Vibration. 8 p.

Inoue, T., Nakano, M., Kubo, T., Matsumoto, S. & Baba, H. 1981. High accuracy control of a proton synchrotron magnet power supply. *Proc. of the 8th IFAC World Congress*. Vol. XX. Kyoto, Japan. Pp. 216–221.

Ioannou, P.A. & Sun, J. 1996. *Robust adaptive control*. Prentice-Hall, Inc. USA. 825 p. ISBN 0-13-439100-4.

Ishimatsu, T., Shimomachi, T. & Taguchi, N. 1991. Active vibration control of flexible rotor using electromagnetic damper. *Intl. Conf. on Industrial Electronics, Control and Instrumentation*. IEEE. Vol. 1. Kobe, Japan. Pp. 437–441.

ISO 1940-1:2003/Cor 1:2005. Mechanical vibration. Balance quality requirements for rotors in a constant (rigid) state. Part 1 and part 2.

Jeffcott, H.H. 1919. *The lateral vibration of loaded shafts in the neighbourhood of a whirling Speed. – The effect of want of balance*. London, Edinburgh and Dublin Philosophical Magazine and Journal of Science, Vol. 6:27, pp. 304–314.

Järviluoma, M. & Valkonen, A. 2001. *Test equipment and controller for active rotor vibration damping*. Progress report. VTT Automation. Oulu. 38 p.

Järviluoma, M. & Valkonen, A. 2002. *Test equipment and controller for active rotor vibration damping: set-up, methods, results*. Progress report. VTT Automation. Oulu. 53 p.

Kataja, J. 1999. *Applications of adaptive algorithms for active noise control*. Tampere University of Technology. 99 p. Master's thesis.

Kempf, C., Messner, W., Tomizuka, M. & Horowitz, R. 1993. *Comparison of four discrete-time repetitive control algorithms*. IEEE Control Systems Magazine, Vol. 13, pp. 48–54.

Klinge, P. 2002. *Modysol manuaali* [Modysol manual]. Espoo. VTT Research Report BTUO57-021002. 20 p. In Finnish.

Knopf, E. & Nordmann, R. 1998. Active magnetic bearings for the accurate force measurement in rotating machinery. *The Fourth International Conference on Motion and Vibration Control*. ETH Zurich.

Knospe, C.R., Hope, R.W., Tamer, S.M. & Fedigan, S.J. 1996. *Robustness of adaptive unbalance control of rotors with magnetic bearings*. Journal of Vibration and Control, Vol. 2, pp. 33–52.

Knospe, C.R., Fedigan, S.J., Hope, R.W. & Williams, R.D. 1997. *A multitasking DSP implementation of adaptive magnetic bearing control*. Transactions on Control Systems Technology, Vol. 5, No. 2, pp. 230–238.

Krämer, E. 1993. *Dynamics of rotors and foundations*. Springer-Verlag. Germany. 383 p. ISBN 3-540-55725-3.

Kuo, S. E. & Morgan, D.R. 1996. *Active noise control systems Algorithms and DSP implementations*, John Wiley & Sons, USA. 389 p. ISBN 0-471-13424-4.

Lantto, E. 1999. *Robust control of magnetic bearings in subcritical machines*. Acta Polytechnica Scandinavica. The Finnish Academy of Technology. Espoo. 143 p. Doctoral dissertation. ISBN 592-5148-80-7.

Maciejowski, J.M. 2002. *Predictive control*. Pearson Education Limited, Edinburgh Gate. Pp. 56–61.

Medvedev, A. & Hillerström, G. 1993. On perfect disturbance rejection. *Proc. of 32nd Conference on Decision and Control.* Vol. 2. Pp. 1324–1329. ISBN 0-7803-1298-8.

Meirovitch, L. 1997. *Principles and techniques of vibration*. Prentice-Hall. New Jersey. 694 p. ISBN 0-02380141-7.

Meurers, T. & Veres, S.M. 2002. Implementation aspects for FSF-based feedback control with secondary path estimation. *Proc. of Active 2002*, ISVR, Southampton, UK. Pp. 1327–1338.

Moore, S., Lai, J. & Shanknar, K. 2005. ARMAX modal parameter estimation using random and periodic excitation. *1st International Operational Modal Analysis Conf*. Copenhagen, Denmark. 8 p.

Nelson, F.C. 2002. A review of the origins and current status of rotor dynamics. *Proc. of IFToMM Conf.* Sydney, Australia. 7 p.

Nordmann, R. & Aenis, M. 2004. *Fault diagnosis in a centrifugal pump using active magnetic bearings*. International Journal of Rotating Machinery, Vol. 10, No. 3, pp. 183–191.

Preumont, A. 2002. *Vibration control of active structures*. Kluwer Academic Publishers. Netherlands. 364 p. ISBN 1-4020-0925-9.

Proakis, J.G. & Manolakis, D.G. 1996. *Digital signal processing*. 3rd edition. Prentice-Hall, USA. 248 p. ISBN 0-12-394289-9.

Przybyłowicz, P.M. 2004. *Active stabilisation of a rigid rotor by piezoelectrically controlled mobile journal bearing system*. Australian Journal of Mechanical Engineering, Vol. 1, No. 2, pp. 123–127.

Qui, J., Tani, J. & Kwon, T. 2001. Control of synchronous vibration of a rotor system with active gas bearing. *Proc. of the Eight International Congress on Sound and Vibration*. Hong Kong. China. 8 p.

Ren, W. & Kumar, P.R. 1989. Adaptive active noise control: structures, algorithms and convergence analysis. *Proc. of Inter-Noise 89.* Vol. 1. Newport Beach, California, USA. Pp. 435–440.

Sahinkaya, M.N., Cole, M.O.T. & Burrows, C.R. 2002. On the use of Scroeder phased harmonic sequences in multi-frequency vibration control of flexible rotor/magnetic bearing systems. *Proc. of the Eight International Symposiums on Magnetic Bearings*. Mito. Japan. Aug. 26–28, 2002. Pp. 217–222.

Schweitzer, G., Bleurer, H. & Traxler, A. 1994. *Active magnetic bearings*. Hochschulverlag AG. ETH Zurich. 244 p. ISBN 3-7281-2132-0.

Schweitzer, G. 2002. Active magnetic bearings – chances and limitations. *Proc. of 6th International IFToMM Conf. on Rotor Dynamics*, Sydney, Australia. 14 p.

Siebald, H., Fehren, H., Gnauert, U., Kohlrautz, D., Wenzel, M. & Hader, P. 2005. Verschleissminimierung an Papierenkalandern durch Aktives Vibrations Minderungssystem. *Adaptronic Congress*, Göttingen. May 31 – June 1. 2005. 317 p.

Sievers, L.A. & von Flotow, A.H. 1988. Linear control design for active vibration isolation of narrow band disturbances. *Proc. of 27th Decision and Control Conf.* Vol. 2. IEEE. Pp. 1032–1037

Smith, C., Takeuchi, K. & Tomizuka, M. 1999. Cost Effective Repetitive Controllers for Data Storage Devices. *Proc. of the 14th IFAC World Congress*, Beijing, China, July 1999.

Sun, J.C., Wang, X.G. & Xi, F.J. 2000. Sliding mode active vibration control of circular saws. *International Conference on Control Applications*. IEEE. Pp. 953–958.

Sun, L., Krodkiewski, J.M. & Cen, Y. 1998. *Self-tuning adaptive control of forced vibration in rotor systems using an active journal bearing*. Journal of Sound and Vibration, Vol. 213, No. 1. pp. 1–14.

Tammi, K. 2003a. *Mass unbalance compensation of rotor with adaptive finite-impulse-response filter and Convergent Control.* VTT Industrial Systems, Espoo. Research report BTUO57-031122. 23 p.

Tammi, K. 2003b. *Active vibration control of rotor in desktop test environment*. VTT Publications 498. Espoo. 82 p. ISBN 951-38-6225-9; 951-38-6226-7. http://virtual.vtt.fi/inf/pdf/publications/2003/P498.pdf.

Tammi, K. 2003c. Active vibration control of rotor using magnetic actuator. *Proc. of Tenth International Congress on Sound and Vibration (ICSV10)*, Stockholm. International Institute of Acoustics and Vibration. Pp. 315–322.

Tammi, K. 2003d. Test environment for active vibration control of rotor. *Workshop on Smart Materials and Structures (SMART'03)*, Jadwisin 2–5 Sept, 2003, Poland. AMAS Conference Proceedings. Pp. 223–231. ISSN 1730-1521.

Tammi, K., Hynninen, A. & Klinge, P. 2004. An active vibration control study for an electrical machine. *Proc. of Seventh International Conference on Computational Structures Technology (CST2004)*, Lisbon, 7–9 Sept. 2004. Civil-Comp Press. 8 p.

Tammi, K. 2005. Combined feedback-feedforward control for rotor vibrations. *Proc. of Twelfth International Congress on Sound and Vibration (ICSV12),* Lisbon. International Institute of Acoustics and Vibration. 8 p.

Tammi, K., Hätönen, J. & Daley, S. 2006a. Active Vibration Control of a Rotor Using a Novel Adaptive Repetitive Control Algorithm. *Proc. Thirteenth International Congress on Sound and Vibration (ICSV13)*, Vienna. International Institute of Acoustics and Vibration. 8 p.

Tammi, K., Hätönen, J. & Daley, S. 2006b. Novel adaptive repetitive algorithm for active vibration control of a variable-speed rotor. *Proc. of Eighth International Conference on Motion and Vibration Control* (MOVIC 2006), Daejeon, Korea. Pp. 386–381.

Tomizuka, M., Tsao, T.-C. & Chew, K.K. 1989. *Analysis and synthesis of discrete-time repetitive controllers*. ASME Journal of Dynamic Systems, Measurement and Control, Vol. 111, pp. 353–358.

Treichler, J.R., Johnson, C.R. & Larimore, M.G. 2001. *Theory and design of adaptive filters*. Prentice Hall, Inc. USA. 350 p. ISBN 0-13-040265-6.

Utku, S. 1998. *Theory of adaptive structures*. CRC Press. USA. 269 p. ISBN 0-8493-7431-6.

Vance, J.M. 1987. *Rotordynamics of turbomachinery*. John Wiley & Sons, Inc. USA. 388 p. ISBN 0-471-80258-1.

Van Der Poel, T., Van Dijk, J., Jonker, J. & Soemers, H. 2006. Control design for hard mount vibration isolation in high-precision machinery. *Proc. Thirteenth International Congress on Sound and Vibration (ICSV13)*, Vienna. International Institute of Acoustics and Vibration. 8 p.

Wang, J. & Meng, G. 2002. Instability of a cantilever rotor supported on MR fluid damper and sliding bearing. *Sixth International Conf. on Rotor Dynamics. Vol. 2. IFToMM.* Sydney. Pp. 615–620. ISBN 0-7334-1962-3.

Widrow, B. & Stearns, S.D. 1987. *Adaptive signal processing*. Prentice-Hall, Englewood Cliffs. New Jersey. 474 p. ISBN 0-13-004029-0.

Zhao, H., Zhao, L. & Jiang, W. 2000. Simulation and experimental research on unbalance vibration control of AMB system. *Seventh International Symposium on Magnetic Bearings.* Zurich. Aug. 23–25, 2000. Pp. 573–578.

Zhu, C., Robb, D.A. & Ewins, D.J. 2002. Dynamics of an over-hung rotor with a disc-type magneto-rheological fluid damper. *Proc. of IFToMM Conf.* Sydney, Australia. 8 p.

Åström, K.J. & Wittenmark, B. 1990. *Computer controlled systems*. Prentice-Hall, Inc. USA. 543 p. ISBN 0-13-168600-3.

Åström, K.J. & Wittenmark, B. 1995. *Adaptive control*. Addison-Wesley Publishing Company, Inc. USA. 574 p. ISBN 0-201-55866-1.

Appendix A: Quality grades for balancing

Table A1 shows typical balancing quality grades for rotors in different applications. The grades, also referred as the *G values*, represent the product of the maximum eccentricity and the maximum speed of the rotor. A smaller grade indicates a smaller unbalance.

Table A1. Quality grades recommended for different types of rotors (ISO 1940 standard, Genta 1999).

Quality grade [mm/s]	**Rotor type**
40	Car wheels, wheel rims, drive shafts Crankshaft/drives of engines of cars, trucks and locomotives
16	Drive shafts (propeller shafts, cardan shafts) with special requirements Parts of agricultural machinery Individual components of engines for car, truck and locomotives
6.3	Parts of process plant machines Paper machinery rolls; print rolls Fans Assembled aircraft gas turbine rotors
2.5	Gas and steam turbines, including marine main turbines Rigid turbo-generator rotors Turbo-compressors
1	Tape recorder and phonograph drives Grinding machine drives Small electric armatures with special requirements

Appendix B: Positive real systems

Positive realness has been mentioned as a stability requirement for adaptive algorithms presented in this thesis. This appendix briefly defines concept of positive realness and shows some characteristics of positive real functions.

A transfer function $G(\imath\omega)$ is said to be positive real if $Re(G(\imath\omega)) \geq 0$ for all frequencies ω.

In other words, all the function values lie in the right half of the complex plane, or the system phase remains within ±90° for all ω. The condition is relatively demanding, since practical systems usually are not positive real (*e.g.* the phase change of one oscillator is 180°). However, positive realness has been used as the sufficient stability condition for the algorithms presented. This is because a positive real system remains stable even with infinite feedback gain. This can be explained by the fact that the Nyquist plot of a positive real system does not encircle the critical point (–1, i 0) regardless the gain K (Figure B1).

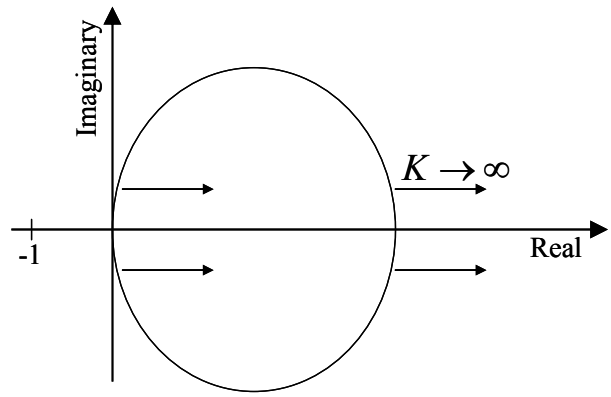

Figure B1. The Nyquist plot of a positive real system.

Appendix C: System models and other filters used in the experimental work

This appendix is to list the system models and the filters implemented in the control unit. Other parameters, such as convergence coefficients, leak coefficients *etc*, may vary depending on the test performed. Those parameters are listed in corresponding sections of this thesis.

C.1 Collocated layout

The Convergent Control algorithm used the inverse of the system model (one complex number for each speed of rotation). This number was computed according to

$$\begin{aligned} \mathrm{Re}(G_m^{-1}) &= 4.66662\text{-}0.00007392\omega^2 \\ \mathrm{Im}(G_m^{-1}) &= 0.02604\omega \\ \omega &= 2\pi f_{rot} \end{aligned} \tag{C1}$$

where f_{rot} is the speed of rotation. The adaptive FIR with the LMS algorithm the following discrete-time system model

$$\begin{aligned} G_m(q) &= \frac{8.778e\text{-}07q + 7.772e\text{-}07}{q^2\text{-}1.639q + 0.6945} \\ T_S &= 0.001024\mathrm{s} \end{aligned} \tag{C2}$$

The models of the algorithms were identical in X and Y directions.

C.2 Non-collocated layout

The Convergent Control algorithm used the inverse of the system model (one complex number for each speed of rotation). For the non-collocated layout, different models were used in X and Y directions. The complex numbers were computed according to

$$
\begin{aligned}
\mathrm{Re}(G_{mX}^{-1}) &= \text{-}9.1474e\text{-}09\omega^3+6.4417e\text{-}06\omega^2\text{-}0.00065708\omega\text{-}0.12424 \\
\mathrm{Im}(G_{mX}^{-1}) &= \text{-}1.2539e\text{-}09\omega^3+4.8746e\text{-}06\omega^2\text{-}0.0017162\omega+0.060949 \\
\mathrm{Re}(G_{mY}^{-1}) &= \text{-}7.2578e\text{-}09\omega^3+5.5643e\text{-}06\omega^2\text{-}0.00054461\omega\text{-}0.12972 \\
\mathrm{Im}(G_{mX}^{-1}) &= 7.3158e\text{-}10\omega^3 +2.9350e\text{-}06\omega^2\text{-}0.0011704\omega+0.035471 \\
\omega &= 2\pi f_{rot}
\end{aligned}
\tag{C3}
$$

The adaptive FIR filter used the following discrete-time model in X and Y directions

$$
\begin{aligned}
G_{mX}(q) &= \\
&\frac{\text{-}0.103q^5+0.1477q^4\text{-}0.2721q^3\text{-}0.304q^2\text{-}0.2746q\text{-}0.2011}{q^6\text{-}1.146q^5\text{-}0.2194q^4+0.2998q^3+0.2771q^2+0.09995q\text{-}0.1516} \\
G_{mX}(q) &= \\
&\frac{\text{-}0.05135q^5+0.07378q^4\text{-}0.4104q^3\text{-}0.2271q^2\text{-}0.1885q\text{-}0.1638}{q^6\text{-}1.259q^5\text{-}0.06012q^4 + 0.3054q^3+0.2501q^2\text{-}0.05055q\text{-}0.03226} \\
T_S &= 0.001024\text{s}
\end{aligned}
\tag{C4}
$$

Note that (C4) is the plant model from the actuator to the rotor midpoint. The repetitive control method used a FIR model for the system. The length of the FIR was dependent on the delay filter order (*N*). The system models were the following

$$
\begin{aligned}
G_{mX}(q) &= \sum_{i=0}^{N} c_X(i)q^i,\ C_X = \begin{bmatrix} c_X(0) & \cdots & c_X(35) \end{bmatrix} \\
G_{mY}(q) &= \sum_{i=0}^{N} c_Y(i)q^i,\ C_Y = \begin{bmatrix} c_Y(0) & \cdots & c_Y(35) \end{bmatrix} \\
N &\le 35 \\
T_S &= 0.001024\text{s}
\end{aligned}
\tag{C5}
$$

where C_X = [0.0, 0.0, –0.0560, –0.0480, –0.1266, –0.4410, –0.8733, –1.2833, –1.5114, –1.5032, –1.3150, –0.9904, –0.5603, 0.0754, 0.4055, 0.8250, 1.1349, 1.3060, 1.3285, 1.2093, 0.9709, 0.6489, 0.2860, –0.0727, –0.3859, –0.6200, –0.7534, –0.7775, –0.6970, –0.5286, –0.2985, –0.0380, 0.2199, 0.4448, 0.6121]

and C_Y = [0.0, 0.0, –0.0279, –0.0270, –0.2144, –0.6257, –1.0540, –1.4106, –1.5794, –1.5240, –1.3010, –0.9502, –0.5099, –0.0253, 0.4533, 0.8737, 1.1938, 1.3860, 1.4381, 1.3525, 1.1453, 0.8442, 0.4851, 0.1081, –0.2473, –0.5460, –0.7608, –0.8746, –0.8818, –0.7881, –0.6090, –0.3683, –0.0946, 0.1818, 0.4320]

The *Q filter* used had the following pulse transfer function

$$Q(q) = \sum_{i=0}^{14} c_Q(i) q^{7-i}, \; C_Q = \begin{bmatrix} c_Q(0) & \cdots & c_Q(14) \end{bmatrix} \qquad T_S = 0.001024\text{s} \tag{C6}$$

where C_Q=[–0.0037, 0.0, 0.0161, 0.0, –0.0678, 0.0, 0.3024, 0.4977, 0.3024, 0.0, –0.0678, 0.0, 0.0161, 0.0, –0.0037]. The *Q filters* were identical in X and Y directions.

Series title, number and
report code of publication

VTT Publications 634
VTT-PUBS-634

Author(s)
Tammi, Kari

Title

Active Control of Radial Rotor Vibrations

Identification, feedback, feedforward, and repetitive control methods

Abstract

Active vibration control methods for rotors were studied in order to develop solutions to enhance machines' dynamic behaviour, durability, and operating range. The aim of the thesis was to develop identification and control methods for active vibration control of a rotor. The identification method developed in the thesis improved run-time rotor identification by compensating rotation-related disturbances before the actual identification procedure. The control system design comprised an inner feedback loop and an outer loop for compensation for harmonic excitations due to mass unbalance and other rotation-related excitations. The feedback loop was shown to be essential in terms of providing favourable conditions for the other compensation algorithm in the outer loop. For the outer loop, three algorithms were tested: two feedforward control methods and a repetitive control method. The algorithms were validated and compared using an experimental set-up. Concerning the feedforward methods, the Convergent Control algorithm was found to be a more effective and simpler algorithm for the purpose than the adaptive FIR filter with the LMS algorithm. The adaptive gradient-based repetitive control, developed in this thesis, was found to have a poorer performance than the feedforward control methods, but to provide benefits for applications where excitation frequencies are not as predictable as in the current application.

ISBN
978-951-38-7007-2 (soft back ed.)
978-951-38-7008-9 (URL: http://www.vtt.fi/publications/index.jsp)

Series title and ISSN	Project number
VTT Publications 1235-0621 (soft back ed.) 1455-0849 (URL: http://www.vtt.fi/publications/index.jsp)	5143

Date	Language	Pages
April 2007	English, Finnish abstr.	151 p. + app. 5 p.

Name of project	Commissioned by
ARCVEM	Academy of Finland, VTT

Keywords	Publisher
dynamic rotor systems, radial vibrations, rotors, control methods, active control, vibrations, identification, feedback control, feedforward control, repetitive control	VTT P.O.Box 1000, FI-02044 VTT, Finland Phone internat. +358 20 722 4404 Fax +358 20 722 4374

Julkaisun sarja, numero ja raporttikoodi

VTT Publications 634
VTT-PUBS-634

Tekijä(t)
Tammi, Kari

Nimeke

Roottorin radiaalivärähtelyjen aktiivinen hallinta

Tiivistelmä

Aktiivisia roottorivärähtelyjen hallintamenetelmiä tutkittiin koneiden dynaamisen käyttäytymisen ja kestävyyden parantamiseksi sekä käyttöalueen laajentamiseksi. Väitöskirjan tavoite oli kehittää identifiointi- ja säätömenetelmiä roottorin aktiivisen värähtelynhallinnan tarkoituksiin. Kehitetty identifiointimenetelmä paransi roottorin käynninaikaista mallinnusta kompensoimalla pyörimisestä johtuvat häiriöt ennen varsinaista identifiointia. Kehitetty säätöjärjestelmä perustui sisempään takaisinkytkentäsilmukkaan ja ulompaan silmukkaan. Takaisinkytkentäsilmukalla osoitettiin olevan merkittävä rooli systeemin muokkaamisessa suotuisaksi ulomman silmukan säätöä silmällä pitäen. Ulommassa silmukassa testattiin kahta myötäkytkettyä säätömenetelmää ja yhtä oppivaa säätömenetelmää. Algoritmien toimivuutta vertailtiin koelaitteistolla. Myötäkytketyistä menetelmistä taajuustason algoritmi todettiin tehokkaammaksi ja yksinkertaisemmaksi kuin adaptiiviseen FIR-suotimeen perustuva LMS-algoritmi. Työssä kehitetty adaptiivinen oppiva algoritmi todettiin suorituskyvyltään huonommaksi kuin myötäkytketyt algoritmit. Toisaalta kyseisestä oppivasta algoritmista löydettiin etuja sovelluksiin, joissa herätetaajuudet eivät ole yhtä ennustettavia kuin tutkitussa tapauksessa.

ISBN
978-951-38-7007-2 (nid.)
978-951-38-7008-9 (URL: http://www.vtt.fi/publications/index.jsp)

Avainnimeke ja ISSN	Projektinumero
VTT Publications 1235-0621 (nid.) 1455-0849 (URL: http://www.vtt.fi/publications/index.jsp)	5143

Julkaisuaika	Kieli	Sivuja
Huhtikuu 2007	Englanti, suom. kiel. tiiv.	151 s. + liitt. 5 s.

Projektin nimi	Toimeksiantaja(t)
ARCVEM	Suomen Akatemia, VTT

Avainsanat	Julkaisija
dynamic rotor systems, radial vibrations, rotors, control methods, active control, vibrations, identification, feedback control, feedforward control, repetitive control	VTT PL 1000, 02044 VTT Puh. 020 722 4404 Faksi 020 722 4374

VTT PUBLICATIONS

617 Leskinen, Sonja. Mobile Solutions and the Construction Industry. Is it a working combination? 2006. 93 p. + app. 2 p.

618 Salo, Outi. Enabling Software Process Improvement in Agile Software Development Teams and Organisations. 2006. 15049 p. + app. 96 p.

619 Hienonen, Risto, Keskinen, Jari & Koivuluoma, Timo. Reliability of materials for the thermal management of electronics. 113 p. + app. 31 p.

620 Talja, Heli. Asiantuntijaorganisaatio muutoksessa. 2006. 250 s. + liitt. 37 s.

621 Kutila, Matti. Methods for Machine Vision Based Driver Monitoring Applications. 2006. 82 p. + app. 79 p.

622 Pesonen, Pekka. Innovaatiojohtaminen ja sen vaikutuksia metsäteollisuudessa. 2006. 110 s. + liitt. 15 s.

623 Hienonen, Risto & Lahtinen, Reima. Korroosio ja ilmastolliset vaikutukset elektroniikassa. 2007. 243 s. + liitt. 172 s.

624 Leviäkangas, Pekka. Private finance of transport infrastructure projects. Value and risk analysis of a Finnish shadow toll road project. 2007. 238 p. + app. 22 p.

625 Kynkäänniemi, Tanja. Product Roadmapping in Collaboration. 2007. 112 p. + app. 7 p.

626 Hienonen, Risto & Lahtinen, Reima. Corrosion and climatic effects in electronics. 2007. 242 p. + app. 173 p.

627 Reiman, Teemu. Assessing Organizational Culture in Complex Sociotechnical Systems. Methodological Evidence from Studies in Nuclear Power Plant Maintenance Organizations. 2007. 136 p. + app. 155 p.

628 Kolari, Kari. Damage mechanics model for brittle failure of transversely isotropic solids. Finite element implementation. 2007. 195 p. + app. 7 p.

629 Communications Technologies. VTT's Research Programme 2002-2006. Final Report. Ed. by Markku Sipilä. 2007. 354 p.

630 Solehmainen, Kimmo. Fabrication of microphotonic waveguide components on silicon. 2007. 68 p. + app. 35 p.

631 Törrö, Maaretta. Global intellectual capital brokering. Facilitating the emergence of innovations through network mediation. 106 p. + app. 2 p.

632 Lanne, Marinka. Yhteistyö yritysturvallisuuden hallinnassa. Tutkimus sisäisen yhteistyön tarpeesta ja roolista suurten organisaatioiden turvallisuustoiminnassa. 2007. 118 s. + liitt. 81 s.

633 Oedewald, Pia & Reiman, Teemu. Special characteristics of safety critical organizations. Work psychological perspective. 2007. 114 p. + app. 9 p.

634 Tammi, Kari. Active control of radial rotor vibrations. Identification, feedback, feedforward, and repetitive control methods. Espoo 20076. 151 p. + app. 5 p.

Julkaisu on saatavana
VTT
PL 1000
02044 VTT
Puh. 020 722 4404
Faksi 020 722 4374

Publikationen distribueras av
VTT
PB 1000
02044 VTT
Tel. 020 722 4404
Fax 020 722 4374

This publication is available from
VTT
P.O. Box 1000
FI-02044 VTT, Finland
Phone internat. + 358 20 722 4404
Fax + 358 20 722 4374

ISBN 978-951-38-7007-2 (soft back ed.)
ISSN 1235-0621 (soft back ed.)
ISBN 978-951-38-7008-9 (URL: http://www.vtt.fi/publications/index.jsp)
ISSN 1455-0849 (URL: http://www.vtt.fi/publications/index.jsp)